OLEFIN METATHESES IN METAL COORDINATION SPHERES: DEVELOPMENT OF GYROSCOPE-LIKE *TRANS*-SPANNING BIS(PYRIDINE) COMPLEXES AND ORGANOMETALLIC II-ADDUCTS OF CONJUGATED POLYMERS

A Dissertation

by

PAUL DAVID ZEITS

Submitted to the Office of Graduate Studies of
Texas A&M University
in partial fulfillment of the requirements for the degree of

DOCTOR OF PHILOSOPHY

December 2011

Major Subject: Chemistry

Olefin Metatheses in Metal Coordination Spheres: Development of Gyroscope-like *trans*-Spanning Bis(pyridine) Complexes and Organometallic π-Adducts of Conjugated Polymers

OLEFIN METATHESES IN METAL COORDINATION SPHERES: DEVELOPMENT OF GYROSCOPE-LIKE *TRANS*-SPANNING BIS(PYRIDINE) COMPLEXES AND ORGANOMETALLIC Π-ADDUCTS OF CONJUGATED POLYMERS

A Dissertation

by

PAUL DAVID ZEITS

Submitted to the Office of Graduate Studies of
Texas A&M University
in partial fulfillment of the requirements for the degree of

DOCTOR OF PHILOSOPHY

Approved by:

Chair of Committee,	John Gladysz
Committee Members,	Donald Darensbourg
	François Gabbaï
	Jaime Grunlan
Head of Department,	David Russell

December 2011

Major Subject: Chemistry

ABSTRACT

Olefin Metatheses in Metal Coordination Spheres: Development of Gyroscope-like *trans*-Spanning Bis(pyridine) Complexes and Organometallic π-Adducts of Conjugated Polymers.

(December 2011)

Paul David Zeits, B.S., Michigan State University

Chair of Advisory Committee: Dr. John A. Gladysz

The olefin metathesis reaction has become one of the most powerful carbon-carbon bond forming reaction in synthetic chemistry. This work has expanded the utility of olefin metathesis in metal coordination spheres in three major directions (1) the synthesis and characterization of *trans*-spanning bis(pyridine)$PtCl_2$ complexes, (2) the development of regioregular CpIr π-adducts of polyacetylene (PA), and (3) the development of regioregular Cp*Ru and Cp*Ir π-adducts of poly(phenylene-vinylene) (PPV).

Chapter I gives a brief overview of olefin metathesis and previous applications to organometallic substrates.

Chapter II details the synthesis of pyridine ligands containing alkenyl substituents, 2-$NC_5H_4(CH_2O(CH_2)_nCH{=}CH_2)$ (*n* = 1, 2), 3-$NC_5H_4(CH_2O(CH_2)_nCH{=}CH_2)$ (*n* = 1-5, 8, 9), and 3,5-$NC_5H_3(p\text{-}C_6H_4O(CH_2)_7CH{=}CH_2)_2$. Metalation of the new ligands with $PtCl_2$ affords the corresponding *trans*-bis(pyridine)dichloroplatinum complexes, *trans*-$PtCl_2$(2-$NC_5H_4(CH_2O(CH_2)_nCH{=}CH_2))_2$ (*n* = 1, 2), *trans*-$PtCl_2$(3-

$NC_5H_4(CH_2O(CH_2)_nCH{=}CH_2))_2$ (n = 1-5, 8, 9), and *trans*-$PtCl_2(3,5\text{-}NC_5H_3(p\text{-}C_6H_4O(CH_2)_7CH{=}CH_2))_2$. Ring-closing metatheses with Grubbs′ first generation catalyst followed by hydrogenations with Pd/C afford the title complexes *trans*-$PtCl_2[2,2'\text{-}(NC_5H_4(CH_2O(CH_2)_{2n+2}OCH_2)H_4C_5N)]$ (n = 1, 2), *trans*-$PtCl_2[3,3'\text{-}(NC_5H_4(CH_2O(CH_2)_{2n+2}OCH_2)H_4C_5N)]$ (n = 4, 8, 9), and *trans*-$PtCl_2[3,5,3',5'\text{-}(NC_5H_3(p\text{-}C_6H_4O(CH_2)_{12}O\text{-}p\text{-}C_6H_4)_2H_3C_5N)]$. Reactions with methylmagnesium bromide afford *trans*-$PtCl(CH_3)(3\text{-}NC_5H_4(CH_2O(CH_2)_nCH{=}CH_2))_2$ (n = 2, 8) and *trans*-$PtCl(CH_3)[3,3'\text{-}(NC_5H_4(CH_2O(CH_2)_nOCH_2)H_4C_5N)]$ (n = 10, 18), which feature dipolar rotators. Low temperature NMR spectra in the latter remained facile on the NMR time scale in $CDFCl_2$ at −120 °C.

Chapter III focuses on the application of ROMP with organometallic monomers to form metal π-adducts of polyacetylene. The new complex (η^4-benzene)Cp*Ir has been synthesized, crystallographically characterized, and evaluated in the ROMP reaction. Monomers (η^4-benzene)CpIr, [(η^6-COT)CpRu][PF_6], and (η^4-COT)$Fe(CO)_3$ were also evaluated in the ROMP reaction. ROMP of (η^4-benzene)CpIr with Grubbs′ first generation catalyst afforded the conductive regioregular polymer CpIr-PA.

Chapter IV focuses on the synthesis of the divinyl benzene complexes $[Cp^*Ir(C_6H_4(CH{=}CH_2)_2)][BF_4]_2$ and $[Cp^*Ru(C_6H_4(CH{=}CH_2)_2)][OTf]$ and their polymerization *via* ADMET to afford PPV systems. Treatment of divinyl benzene complexes with Grubbs′ second generation catalyst afforded the conductive regioregular polymers $[Cp^*Ir\text{-}PPV][BF_4]_{2n}$ and $[Cp^*Ru\text{-}PPV][OTf]_n$. The photophysical properties of the new π-metal adducts of PPV exhibit blue-shifts relative to typical PPVs and retain strong UV absorption.

TABLE OF CONTENTS

CHAPTER Page

LIST OF FIGURES

FIGURE Page

FIGURE Page

FIGURE Page

LIST OF SCHEMES

SCHEME Page

SCHEME Page

SCHEME Page

LIST OF TABLES

NOMENCLATURE

δ	chemical shift in ppm
λ	wavelength
$\{^1H\}$	proton decoupled
br	broad
COT	cyclooctatetraene
Cp	cyclopentadienyl
Cp*	1,2,3,4,5-pentamethylcyclopentadienyl
d	doublet (NMR), days
dme	1,2-dimethoxyethane
DMSO	dimethylsulfoxide
DP	degree of polymerization
ESI	electrospray ionization
h	hour
i	iso
IR	infrared
m	multiplet (NMR), medium (IR)
m	meta
Me	methyl
MEH-PPV	poly(2-methoxy-5-(2′-ethyl-hexyloxy)-*p*-phenylene-vinylene)
min	minutes
n	normal, number of units
NMR	nuclear magnetic resonance
Np	neopentyl

o	ortho
p	para
PA	polyacetylene
PBP	poly(*n*-butylphenylene)
PHP	poly(*n*-hexylphenylene)
ppm	parts per million
PPP	poly(*p*-phenylene)
PPV	poly(phenylene-vinylene)
R	alkyl group
s	singlet (NMR), strong (IR)
sept	septet (NMR)
t	triplet (NMR)
t	tertiary
TMS	trimethylsilyl
UV	ultraviolet
Vis	visible
vs	very strong (IR)
v/v	volume/volume
w	weak (IR)

CHAPTER I

INTRODUCTION

Olefin metathesis has become one of the most widely applicable carbon-carbon bond forming reactions to date.[1] At the outset, olefin metathesis spawned from Ziegler-Natta chemistry and involved ill defined catalytic systems.[2] However, the versatility of olefin metathesis has been realized and driven through the development of highly active, functional group tolerant, single site catalysts. The tremendous utility of olefin metathesis garnered the 2005 Nobel Prize in Chemistry presented to Yves Chauvin, Robert H. Grubbs, and Richard R. Schrock.

Metathesis comes from the Greek word μεταθεσιζ, μετα (meta = change) and θεσιζ (tithemi = place). Olefin metathesis effectively breaks two carbon-carbon double bonds, rearranges the ends, and forms two new double bonds (Scheme 1.1). There are four general categories of olefin metathesis (Scheme 1.2). The first, cross metathesis, involves two alkenes undergoing an intermolecular transformation to produce a statistical distribution of new olefins. The second, ring-opening metathesis polymerization (ROMP), involves the opening of a cyclic olefin to produce a polymeric compound. The third, ring-closing metathesis, enables the formation of cyclic molecules. The fourth, acyclic diene metathesis polymerization (ADMET), is related to cross metathesis but forms a polymer instead of small molecules.

This dissertation follows the style of the *Journal of the American Chemical Society*.

Scheme 1.1. General example of olefin metathesis.

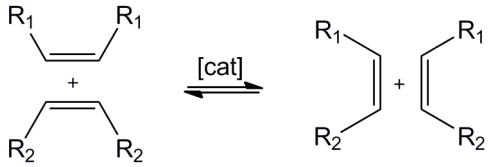

Scheme 1.2. Types of olefin metathesis reactions.

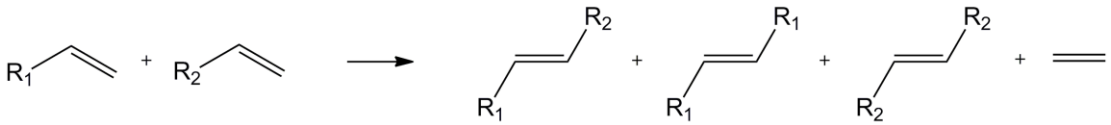

Cross Metathesis

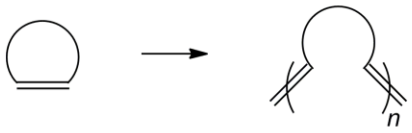

Ring-Opening Metathesis Polymerization (ROMP)

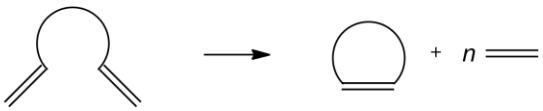

Ring-Closing Metathesis

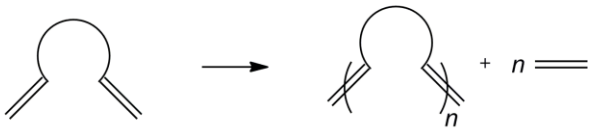

Acyclic Diene Metathesis Polymerizatin (ADMET)

This dissertation makes use of five different olefin metathesis catalysts, Grubbs′ first generation, Grubbs′ second generation, Grubbs′ third generation, Schrock′s catalyst, and a tungsten derivative of Schrock′s catalyst, **I-V**, respectively (Figure 1.1). Although a plethora of olefin metathesis catalysts exist, most are derivatives of these five.

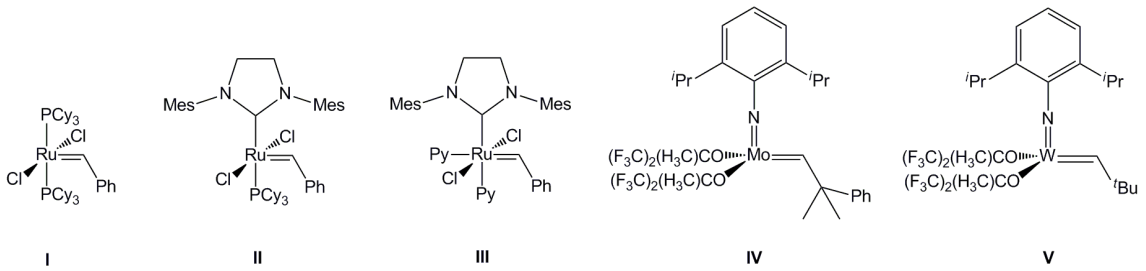

Figure 1.1. Single site olefin metathesis catalysts used in this dissertation; Grubbs′ 1 (**I**), Grubbs′ 2 (**II**), Grubbs′ 3 **(III**), Schrock′s (**IV**), and Schrock′s tungsten (**V**).

Over the last decade, the Gladysz group has been involved with olefin metathesis in metal coordination spheres.[3-5] This concept dates back to 1984 when Rudler achieved cross metathesis and ring-closing metathesis with tungsten complexes (Scheme 1.3).[6] Since then, examples of all four general categories of olefin metathesis (*vide supra*) have been accomplished in a metal coordination sphere. Selected cases will be discussed further.

Scheme 1.3. Olefin metathesis in a metal coordination sphere from Rudler.

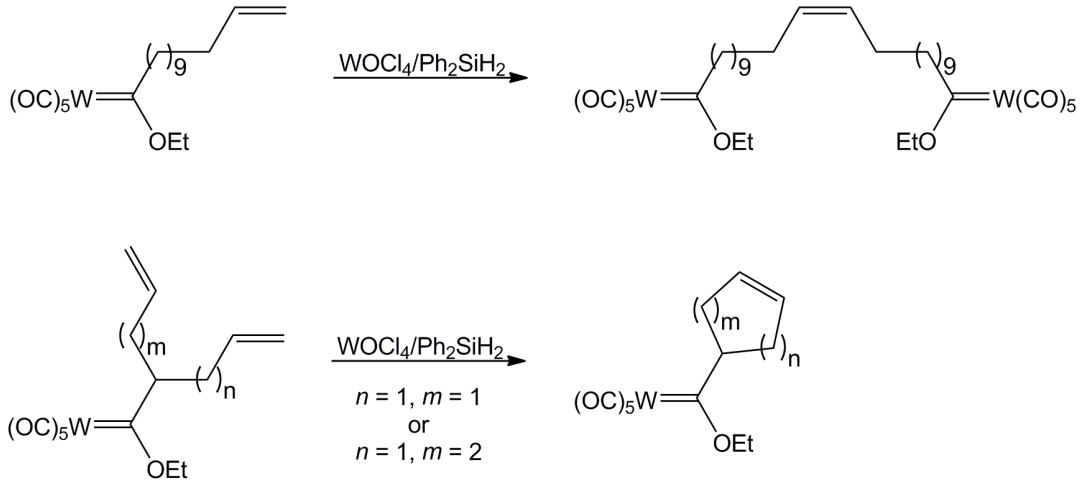

In 2001, Kawai and coworkers used a Schrock-type catalyst to achieve cross metathesis with vinylarenes and vinylferrocene (Scheme 1.4).[7] By varying the reaction

conditions, they were able to achieve selectivities for the heterodimer of >99%. Typical of cross metathesis, the production and removal of ethylene helps drive this equilibrium reaction to completion.

Scheme 1.4. Cross metathesis of vinylferrocene with vinylarenes.

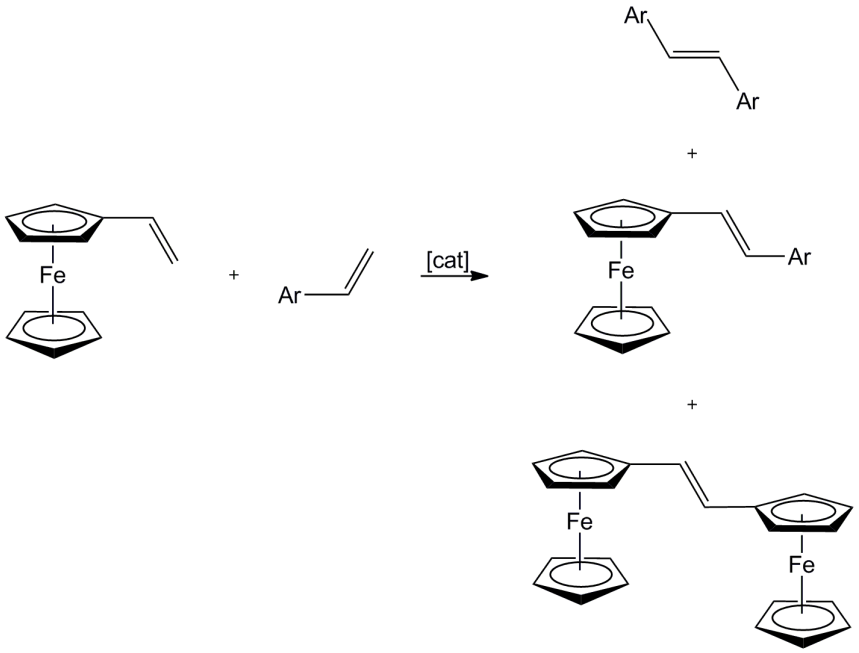

ROMP has also been achieved using a variety of cyclic ferrocenes. Scheme 1.5 shows the successful ROMP of 1,1′-divinylferrocene from the Tilley group.[8] Typical of ROMP, this reaction is driven by the relief of ring strain in the monomer. The polymer thus formed is obtained as an intractable orange powder.

Scheme 1.5. ROMP of 1,1′-divinylferrocene.

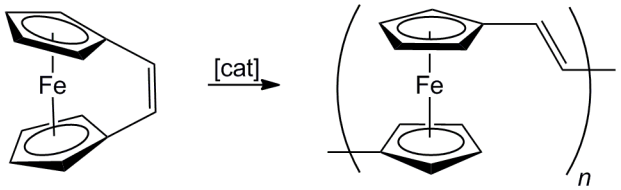

Lee and co-workers were able to solve the solubility issues by introducing an alkyl substituent onto the backbone of the ring (Scheme 1.6).[9] In this example, the *t*-butyl substituent effectively enhanced solubility to enable production of a polymer with a weight average molecular weight of ≥ 300,000.

Scheme 1.6. ROMP of 1,1′-(1-*t*-butyl-1,3-butadienylene)ferrocene.

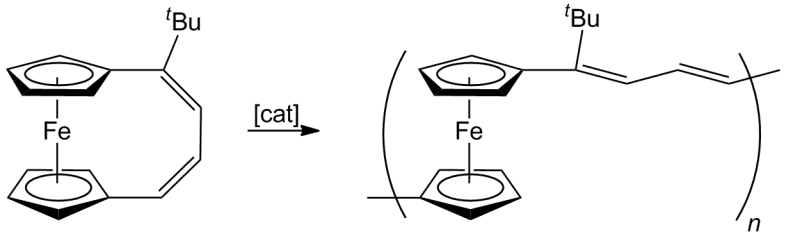

The Gladysz group has shown a diverse range of ring-closing metathesis including intra and interligand reactions (Scheme 1.7).[3] Both examples in Scheme 1.7 utilize the production and removal of ethylene to drive the reaction to completion. While ADMET is also possible, it can be avoided by using dilute reaction mixtures.

Scheme 1.7. Ring-closing metathesis of $[(\eta^5\text{-}C_5H_5)Re(NO)(PPh_3)(S(CH_2CH{=}CH_2)_2)][OTf]$ and *cis*-$[(Cl)_2Pt(P(Ph_2)(CH_2)_6CH{=}CH_2)_2]$.

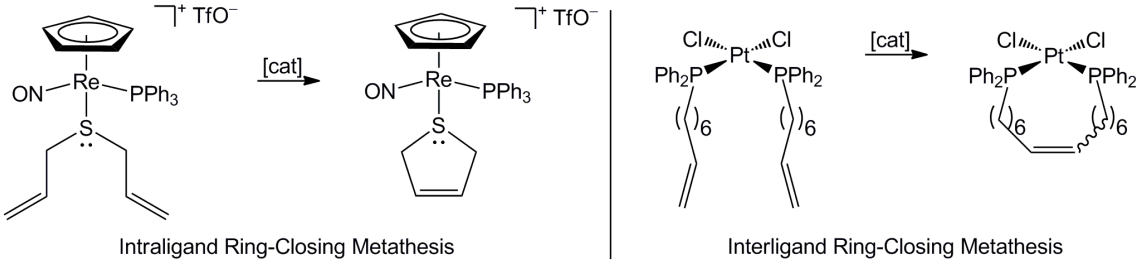

In a recent example of ADMET, Tyler and coworkers have been able to utilize a molybdenum dimer (Scheme 1.8).[10] As usual, this example employs the production and

removal of ethylene to drive the reaction. Alternatively, ring-closing metathesis is accomplished under dilute reaction conditions.

Scheme 1.8. ADMET of $[(\eta^5\text{-}C_5H_4(CH_2)_8CH{=}CH_2)Mo(CO)_3]_2$ (top) and ring-closing metathesis (bottom).

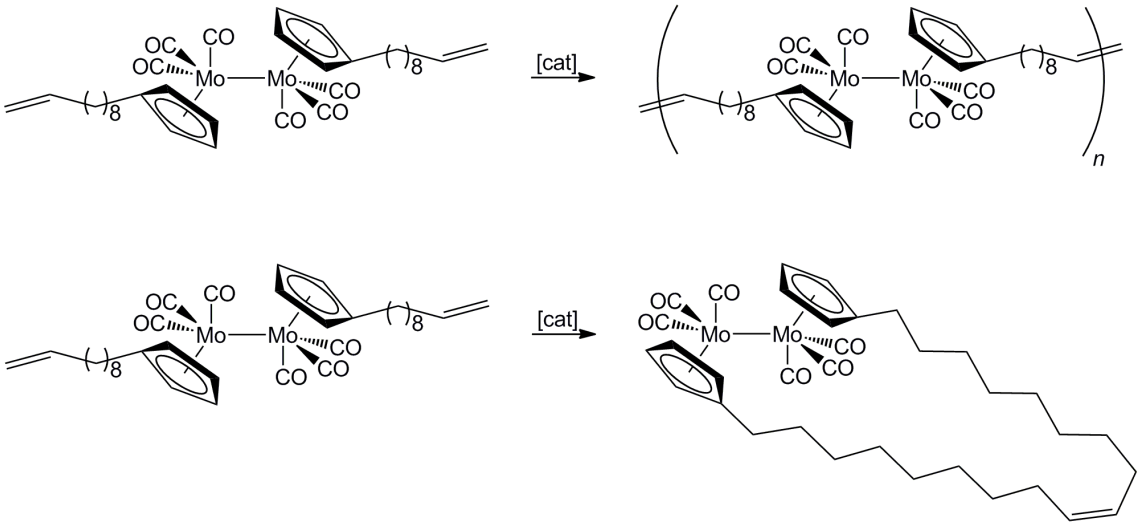

Each chapter of this dissertation is concerned with a different type of olefin metathesis in a metal coordination sphere. In all cases, new molecular devices or designer materials are the goal.

Chapter II focuses on ring-closing metathesis of pyridine based platinum(II) complexes. This work falls under the general concept of molecular machines or, more specifically, molecular rotors.[11] The Gladysz group has carried out considerable work directed at molecular gyroscopes using phosphine ligands.[5] This chapter focuses on a less explored approach using pyridine ligands, and their application to molecular gyroscopes. Pyridines are of interest for several reasons, including their unique symmetry properties and their ability to be functionalized.

Chapter III focuses on ROMP of cyclooctatetraene and benzene complexes in which one or more double bonds are not coordinated to the metal center. Since these ligands are completely conjugated, the resulting polymer backbones are also completely conjugated. These reactions form a new class of polyacetylene (PA) in which the polymer backbone has repeat units of organometallic π-adducts. The physical and chemical aspects of this new class of polymers are investigated.

Chapter IV focuses on ADMET of divinylbenzene metal complexes. ADMET of the pendant vinyl groups forms poly(phenylene-vinylene) (PPV) in which the phenylene unit is an organometallic arene complex. Additionally, these monomers are cationic complexes. Thus, this type of polymerization forms a conjugated polymer that is also a polyelectrolyte. The physical and chemical aspects of these polymers are investigated.

CHAPTER II

GYROSCOPE-LIKE COMPLEXES WITH *TRANS*-SPANNING BIS(PYRIDINE) LIGANDS

INTRODUCTION

Macroscopic machines with rotating components play significant roles in our everyday lives, from the cars or bicycles that get us to work to the turbines that generate power for our homes. In the last few years there has been an increasing effort to mimic these types of devices on the molecular level.[12] These "molecular rotors" are classified as having a rotator and a stator. Since motion is relative to the observer, the rotator is defined as having the smaller moment of inertia and the stator is defined as having the larger moment of inertia. Several examples of molecular rotors include rope-skipping rotors, molecular turnstiles, and molecular gyroscopes (Figure 2.1).[5,13,14]

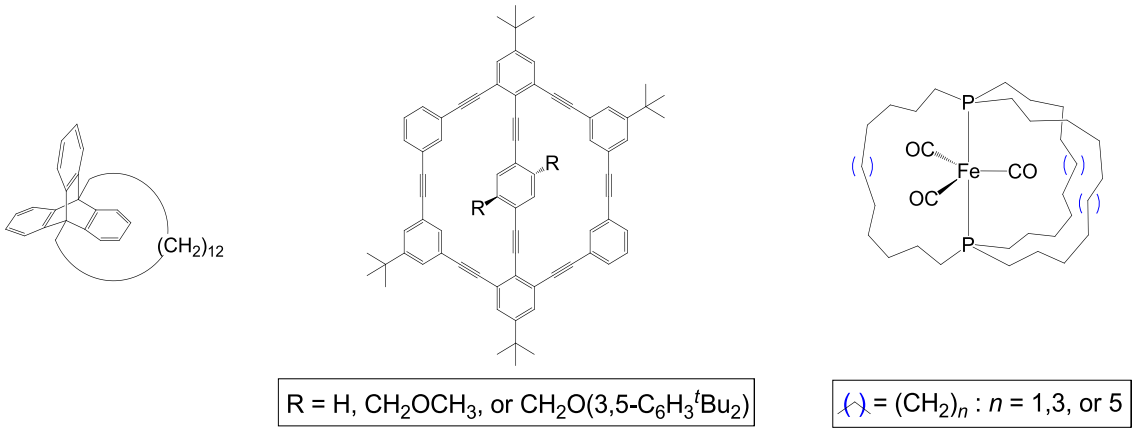

Figure 2.1. Vögtle′s rope-skipping rotor (left), Bedard and Moore′s molecular turnstile (middle), and Gladysz′s molecular gyroscope (right).

In this work, all of the molecular rotors consist of a central rotator encased within a stator whose extremities constitute a macrocycle. This type of complex has been coined a "molecular gyroscope". The term molecular gyroscope suggests the potential for the rotator to rapidly rotate within the stator cage. In Vögtle′s rope-skipping rotor (Figure 2.1, left) the triptycyl rotator shows two sets of aromatic signals in the ^{1}H NMR. This suggests that the rotator is not rapidly rotating on the NMR time scale. With Bedard and Moore′s molecular turnstile (Figure 2.1, middle), the facility of rotation of the center spindle depends on the R group. When R = H, rotation is rapid on the NMR time scale. When R = $CH_2O(3,5\text{-}C_6H_3\text{-}t\text{-}Bu_2)$, rotation is stopped. In the case of Gladysz′s molecular gyroscopes (Figure 2.1 right), the cage can be expanded with adjustments in the size of the ligand to allow for more facile rotation of the rotator.

The Gladysz group has utilized ring closing metathesis in a metal coordination sphere to form molecular gyroscopes (Scheme 2.1).[3,5,15] These molecular gyroscopes feature a symmetrically substituted (ML_y) or unsymmetrically substituted ($ML_yL'_{y'}$) rotator encased by two axial ligands connected by a number of spokes.

Scheme 2.1. Representative examples of ring closing olefin metathesis/hydrogenation to form molecular gyroscopes.

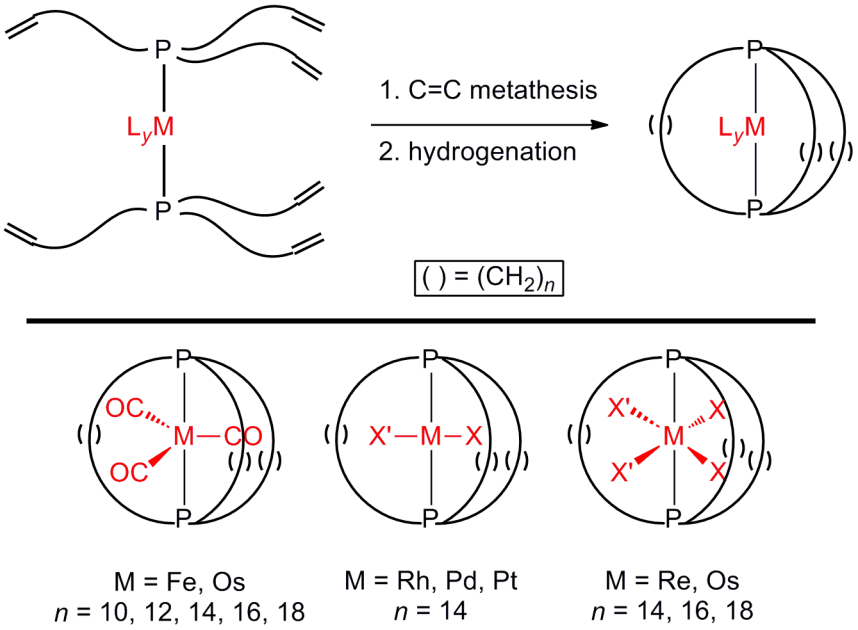

Trigonal bipyramidal iron complexes were found to be of particular interest because the geometry at the metal center had the same three-fold symmetry as the phosphine ligands. This leads to a configuration that is considered to be pre-organized for three-fold intramolecular ring-closing metathesis (Figure 2.2-a). This pre-organization is believed to lead to higher yields than the symmetry mismatched configuration of the square planar or octahedral analogs. As seen in Figure 2.2, pseudo-Newman projections can be used to depict this concept by looking down the axis of the *trans* ligands. Blue substituents (R) are in good proximity for olefin metathesis. This leaves the green substituents (R) in an unfavorable position for intramolecular olefin metathesis.

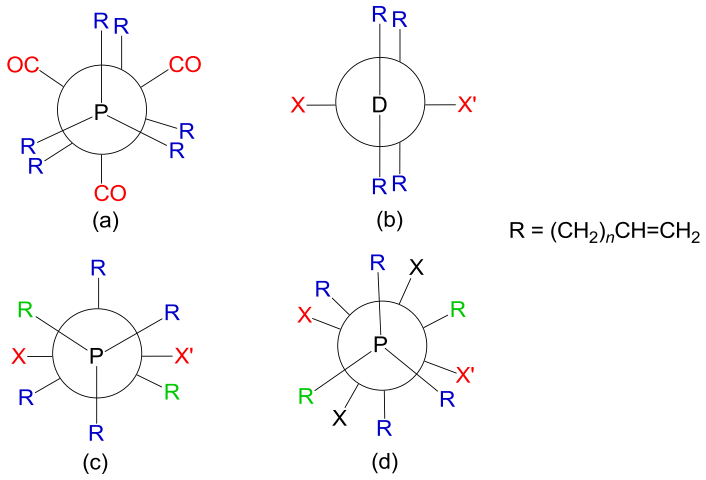

Figure 2.2. Newman-type projections for (a) trigonal bipyramidal *trans*-bis(phosphine) complex, (b) square planar *trans*-bis(DR_2) complex, (c) square planar *trans*-bis(phosphine) complex, and (d) octahedral *trans*-bis(phosphine) complex.

Ligands in which the metal-donor atom linkage defines a two-fold symmetry axis would be optimal for two-fold ring-closing metathesis of square planar complexes, as shown in Figure 2.2-b. Some work has been done with thioether ligands.[3] However, the SR_2 ligands are pyramidal, and therefore the metal sulfur linkage lies in a mirror plane, but not a symmetry axis. Alternatively, certain types of planar aromatic heterocycles, such as pyridine, should give alkene containing ligands that would adopt a pre-organized conformation.

Lambert was the first to use the two-fold symmetric pyridine in combination with a square planar complex (Scheme 2.2).[16] Lambert′s open chain complex (**VI**) should possess a pre-organized configuration (see Figure 2.2-b), similar to that of the trigonal bipyramidal iron complexes. Two-fold ring-closing metathesis of **VI** is readily accomplished with Grubbs′ first generation catalyst (**I**; Figure 1.1) to give Lambert′s gyroscope (**VII**) in 80% yield. The *E*/*Z* nature of the double bonds in **VII** was not described. However, an X-ray crystal structure showed two *Z* CH=CH linkages. Lambert

left the field of chemistry about a year later. Subsequently, the Gladysz group has picked up the investigation of pyridine based gyroscopes.

Scheme 2.2. Synthesis of Lambert′s complex.

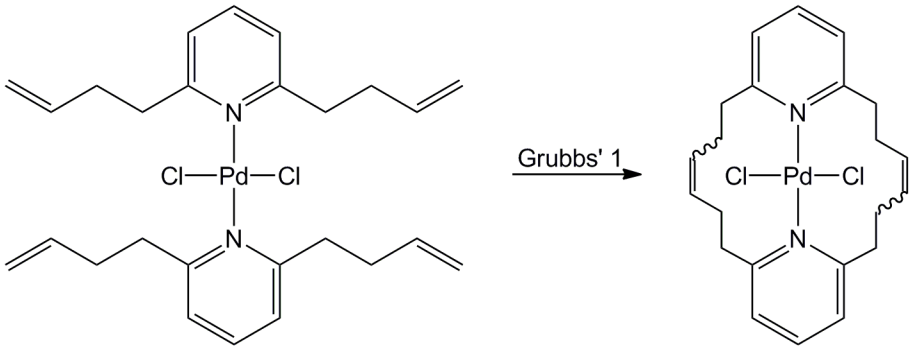

VI **VII**

Pyridine ligands are also of interest since they possess a motif that makes them modifiable, particularly with respect to substituents. Comparable attributes are lacking in their phosphine based counterparts. Introducing thiol or thioacetyl substituents on the pyridine would have potential applications with mechanically controllable break (MCB) junctions.[17] Weber and coworkers have shown that MCB junctions can be used to connect gold electrodes by a single molecule.[17b,c] Furthermore, compounds similar to Lambert′s can have dipolar rotators functioning as an on/off switch when oriented in an external field. This concept is similar to the function of molecular compasses.[18]

With slight modifications of pyridine based molecular rotors, applications in single molecule wires could be sought (Figure 2.3). Contrary to their phosphine based predecessors, the pyridine ligands are completely conjugated. This attribute would facilitate the transmittal of charge from one ligand, through the metal center, and out the opposite ligand. Additionally, introducing a dipolar rotor at the metal center could create

an on/off switch. By orienting the dipolar rotor in an external field, conjugation at the metal center could be turned on or off.

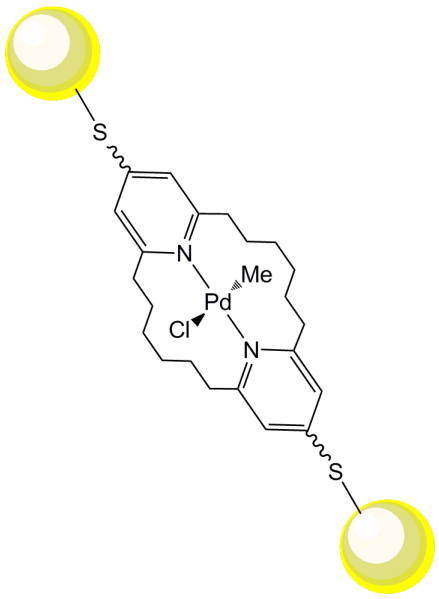

Figure 2.3. Hypothetical *trans*-spanning bis(pyridine) molecular gyroscope connecting two gold electrodes.

Earlier work conducted in the Gladysz group in Erlangen has expanded upon Lambert′s complex and also started a small library of other pyridine based gyroscopes.[19] At the outset of this project, the carbon-carbon double bonds in the spokes of **VII** were hydrogenated with Adams′ catalyst to give **VIII** in 62% yield (Scheme 2.3).[19] Since a mixture of *E* and *Z* isomers are normally formed through olefin metathesis, hydrogenation facilitates isolation and characterization of the gyroscope.

Scheme 2.3. Hydrogenation of Lambert′s gyroscope with Adams′ catalyst.

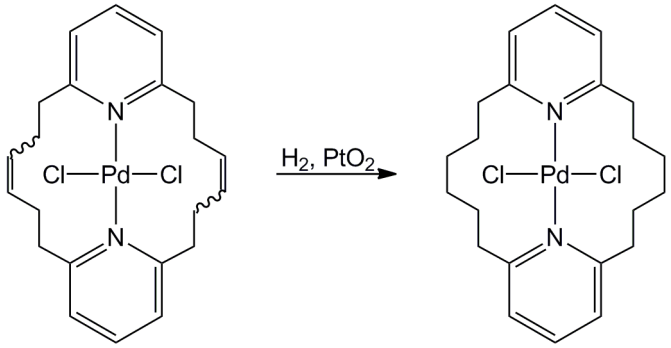

VII **VIII**

To gauge the suitability of structures of the type **VIII** as a gyroscope, Rachiero performed an X-ray crystallographic study. The crystal structure of **VIII** is shown in Figure 2.4. While there is an intrinsic barrier to rotation around any chemical bond, the concept of molecular gyroscopes seeks to encase the rotator with little to no additional hindrance imposed by the cage. One way of conceptualizing this objective is to compare the radius of the rotator with the bridge height (horizontal clearance) of the cage. If the bridge height is larger than the rotator radius, there is theoretically enough free space for the rotator to pass through the macrocycle. If the bridge height is smaller than the radius of the rotator, it may still be possible for the rotator to pass through the macrocycle, but at a distinct energetic cost. In complex **VIII**, the radius of the rotator would be the Pd-Cl bond distance plus the van der Waals radius (VDWR) of chlorine. The bridge height is then defined as the distance from the metal center to the remote carbon atoms of the spokes minus the VDWR of carbon.[20] These are taken as the two carbon atoms closest to the plane of the rotator in each spoke. Taking the palladium to chloride distance (2.313 Å) and adding the VDWR of chloride (1.75 Å) gives a rotator radius of 4.06 Å. The bridge height is then determined to be 2.58 Å by subtracting the VDWR of carbon (1.70 Å) from the shortest palladium to remote carbon distance (4.282 Å). This simple

calculation, along with the space filling model, suggests that there will not be enough room for facile $PdCl_2$ rotation in **VIII**.

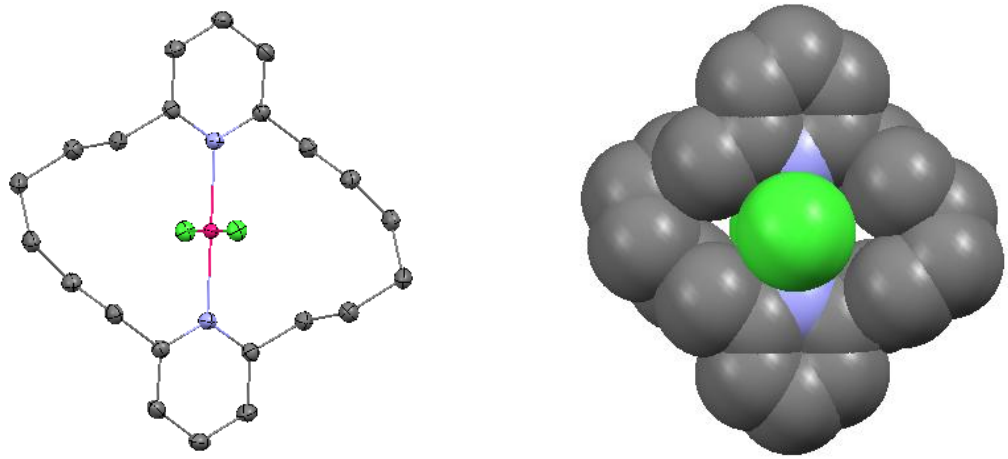

Figure 2.4. X-ray crystal structure of **VIII**; thermal ellipsoid plot (left) and space filling model (right).

Additionally, it is important to evaluate the top-bottom (vertical) clearance of the bis(pyridine) cage (Figure 2.5). For clarity, Figure 2.5 shows several perspectives of **VIII** with the methylene carbon atoms removed, except for those directly bound to the pyridine ligands. The top-bottom clearance is then defined as the distance between *ortho*-methylene carbon atoms minus two times the VDWR of carbon. This analysis gives a top-bottom clearance in **VIII** of only 0.58 Å. Additionally, the centroid between methylene carbon atoms is 2.465 Å from the palladium center. This is comparable to the Pd-Cl bond distance of 2.313 Å, which means the chloride would pass almost directly between the methylene carbon atoms during rotation. Given the van der Waals diameter of chlorine (3.50 Å) and the small van der Waals gap (0.58 Å), the top-bottom clearance will impart a significant hindrance to rotation, to the first approximation. As seen in Figure 2.5 (middle), the pyridine ligands are nearly coplanar. For a further, visual

approximation of the impact of top-bottom clearance, the *ortho*-methylene carbon atoms and chloride ligands can be represented by space filling spheres (Figure 2.5 right). Looking down the pyridine plane shows a narrow gap between methylene carbon atoms as compared to the chloride ligand diameter.

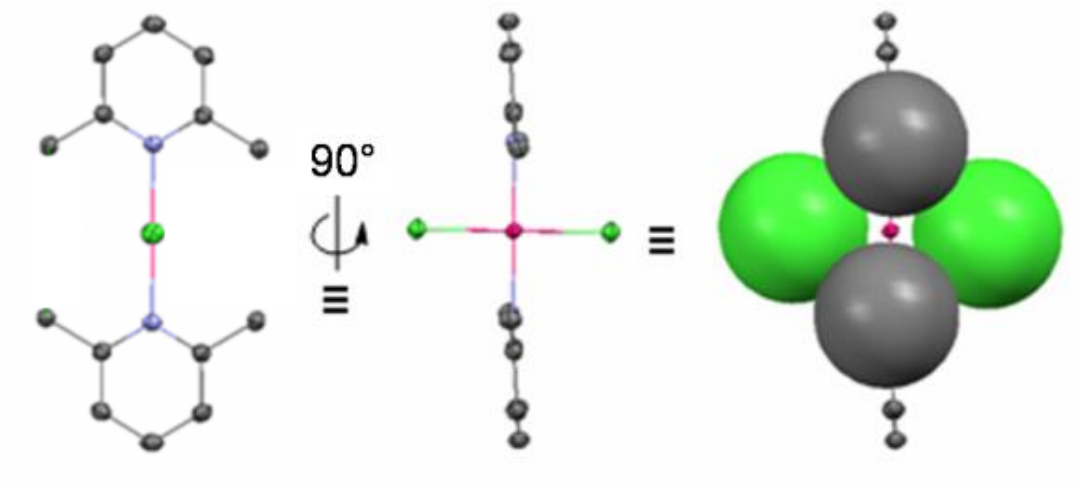

Figure 2.5. Top-bottom clearance analysis of **VIII**; relative distances viewed through the Cl-Pd-Cl axis (left), view down the pyridine plane (middle), and an analogous view with chlorine and methylene carbon atoms at VDWR (right).

In solution, comparing the rotator radius to the bridge height combined with a top-bottom clearance analysis will suffice. However, in the realm of the solid state, it is important that the gyroscope or compass cages pack in such a manner as to avoid close intermolecular contacts with the rotator. This concept is realized by finding the closest intermolecular contact to the metal center and comparing it to the radius of the rotator (Figure 2.6). The closest intermolecular contact of **VIII** is found by taking the distance to the closest atom (carbon, 5.290 Å) and subtracting the VDWR of carbon to give a clearance of 3.59 Å. Comparing this value to the rotator radius of 4.06 Å suggests crystal packing would increase the barrier to rotation in the solid state.

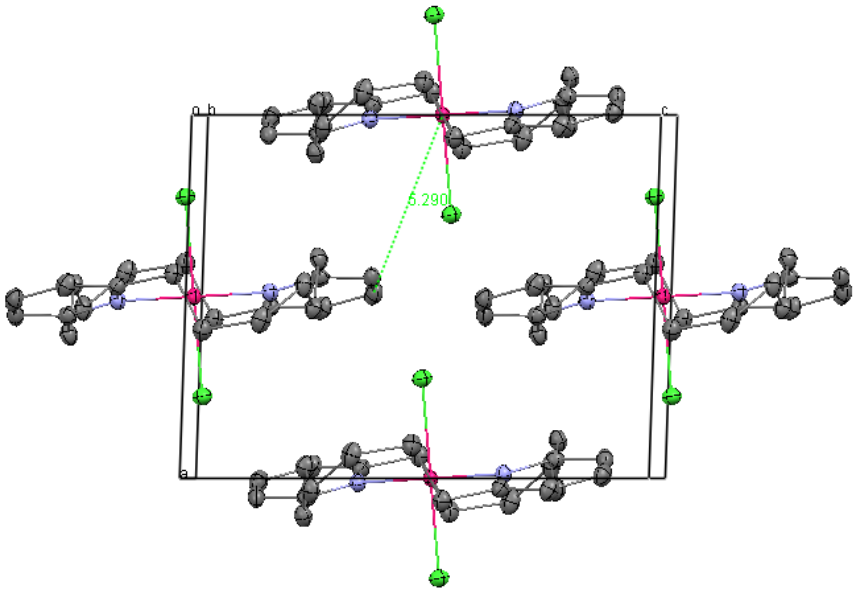

Figure 2.6. Crystal packing of **VIII** showing the closest intermolecular contact to palladium.

Rachiero then set out to develop new pyridine based molecular gyroscopes. The first ligands involved 2,6-disubstituted pyridines. As shown in Scheme 2.4, reaction of **IX** with the alcohols $HO(CH_2)_nCH{=}CH_2$ (n = 1, **a**; 2, **b**; 3, **c**; 4, **d**) in the presence of the quaternary ammonium salt $[C_6H_5CH_2N(CH_3)_3][Cl]$ (20 mol%) gave the diethers 2,6-$NC_5H_3(CH_2O(CH_2)_nCH{=}CH_2)_2$ in 45-55% yields.[19,21]

Scheme 2.4. Rachiero′s syntheses of 2,6-$NC_5H_3(CH_2O(CH_2)_nCH{=}CH_2)_2$.

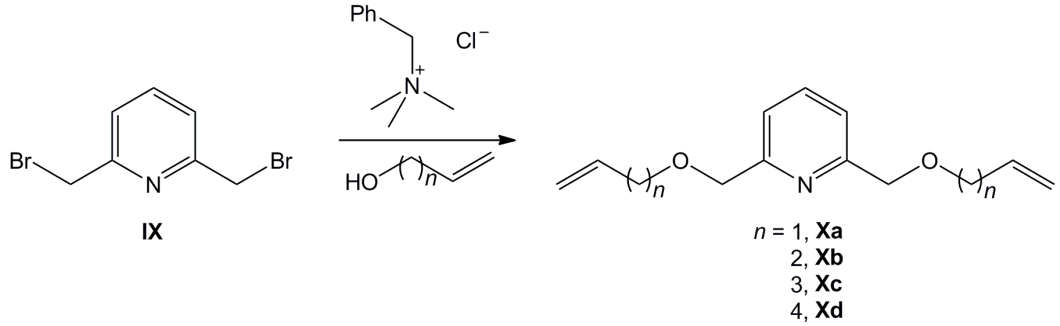

The next step in the gyroscope synthesis involved metalation of the pyridine ligands to form the open chain platinum complexes (Scheme 2.5). In the case of the smallest ligand, **Xa**, the open chain complex (**XIa**) is formed in 88% yield. However, as the ligands become bigger, metalation becomes less favorable. Metalation to form open chain complex **XIb** only proceeds in 26% yield, while the larger ligands show no reaction.

Scheme 2.5. Rachiero's syntheses of the platinum complexes (2,6-$NC_5H_3(CH_2O(CH_2)_nCH{=}CH_2)_2)_2PtCl_2$.

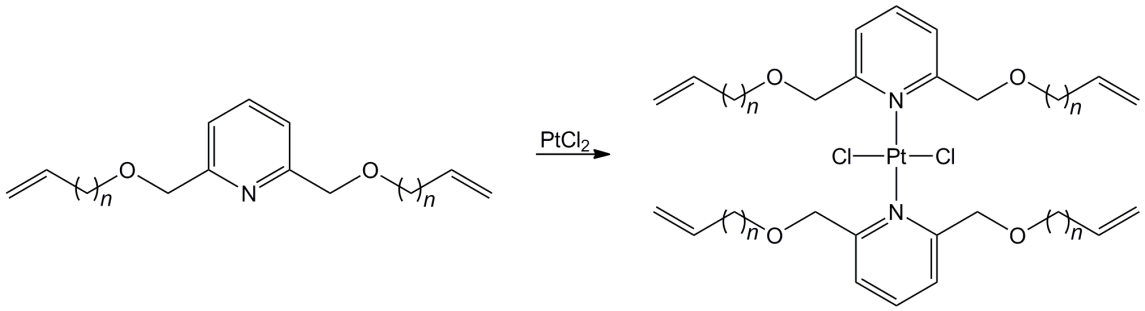

n = 1, **Xa**
2, **Xb**
3, **Xc**
4, **Xd**

n = 1, *trans*-**XIa**
2, *trans*-**XIb**

Following preparation of the open chain complexes *trans*-**XIa** and *trans*-**XIb**, two-fold ring-closing metathesis and hydrogenation was performed. As outlined in Scheme 2.6, this formed the two spoke gyroscopes *trans*-**XIIa** and *trans*-**XIIb** in 10% and 22% yields, respectively.

Scheme 2.6. Rachiero′s syntheses of *trans*-**XIIa,b**.

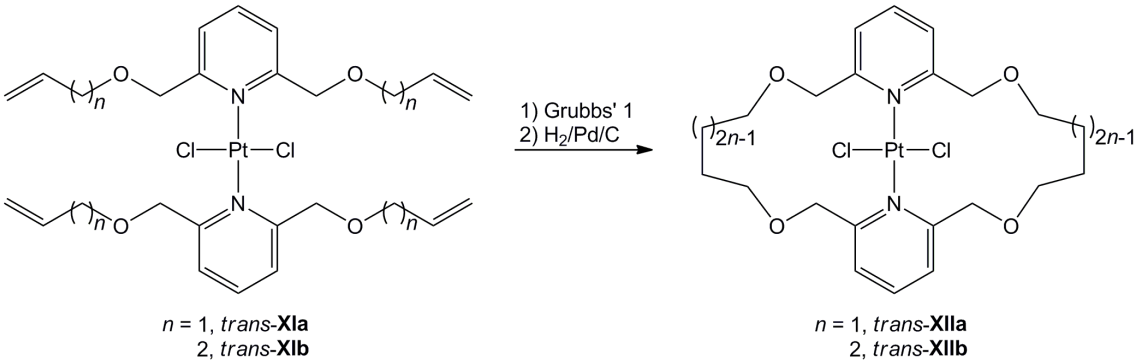

The X-ray crystal structures of *trans*-**XIIa** and *trans*-**XIIb** have been determined (Figure 2.7). Complex *trans*-**XIIa** has a rotator radius of 4.06 Å and a bridge height of 2.49 Å, suggesting the macrocyclic cage is too sterically encumbering to allow facile rotation. Complex *trans*-**XIIb** has a rotator radius of 4.06 Å and a bridge height of 4.38 Å, suggesting that, apart from the issue of top-bottom clearance (Figure 2.5), rotation would be possible within the macrocyclic cage.

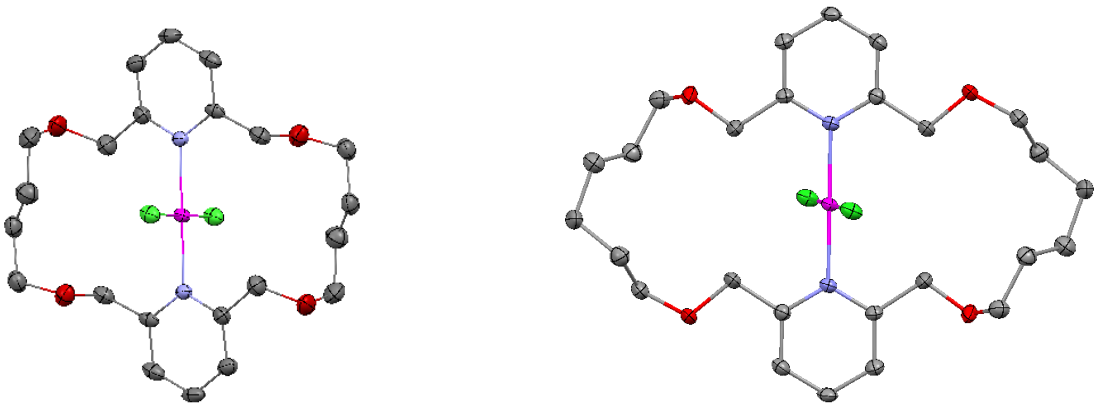

Figure 2.7. Thermal ellipsoid plots of *trans*-**XIIa** (left) and *trans*-**XIIb** (right). The three disordered atoms in *trans*-**XIIb** are depicted in their dominant conformations.

Although the bridge height of *trans*-**XIIa** is smaller than that of *trans*-**XIIb**, the closest intermolecular contact is larger (3.13 Å vs. 2.89 Å). However, neither distance is conducive to facile rotation in the crystal lattice.

For a visual approximation, space filling models of *trans*-**XIIa** and *trans*-**XIIb** are shown in Figure 2.8. This depiction shows that there is considerably more room for rotation in *trans*-**XIIb** in the lateral dimension.

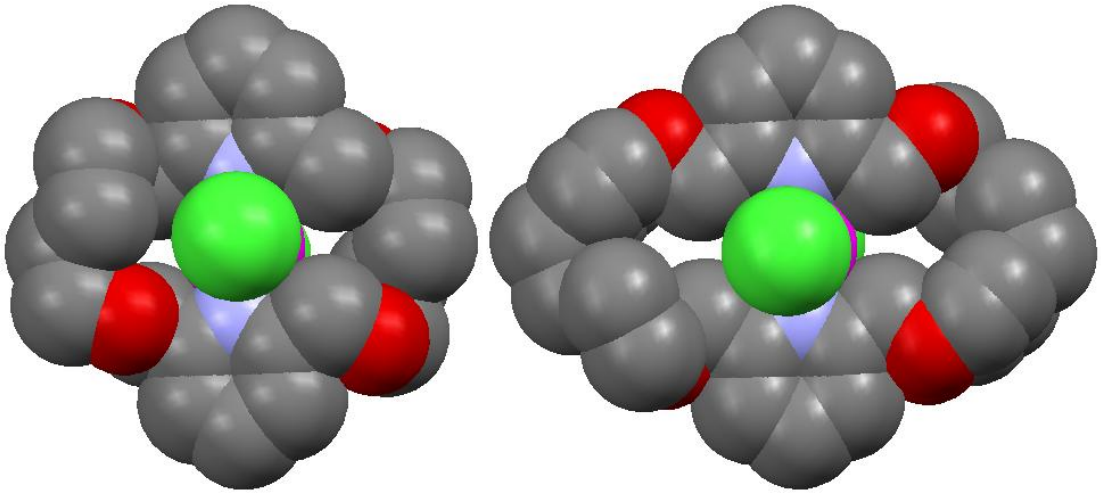

Figure 2.8. Space filling models of *trans*-**XIIa** (left) and *trans*-**XIIb** (right).

The next step in pyridine based gyroscope chemistry would be to introduce a dipolar rotator. This desymmetrization would allow rotation to be probed by standard ^{1}H NMR spectroscopy (Figure 2.9). Protons H_1 and $H_{1'}$ are enantiotopic and will have the same chemical shift. Protons H_1 and H_2 are diastereotopic and will have a different chemical shift. If rotation is rapid on the NMR time scale, H_2 exchanges with $H_{1'}$, which is enantiotopic with H_1.

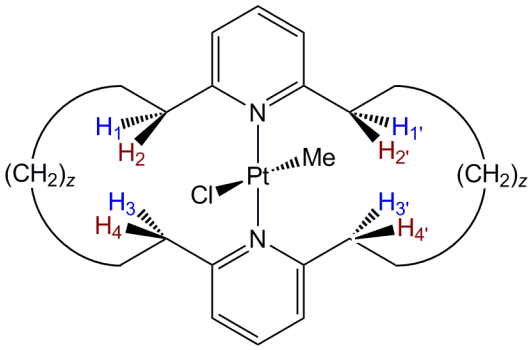

Figure 2.9. Desymmetrized pyridine complex with diagnostic protons labeled.

Desymmetrization reactions were carried out by Rachiero on *trans*-**XIa** using standard synthetic techniques.[22] Unfortunately, suitable conditions could not be found. Presumably, the steric hindrance imposed by 2,6-disubstitution on pyridine prohibits access to the platinum center.

To circumvent the problem of proximal substitution, Rachiero designed 3,5-disubstituted pyridines to reduce the steric hindrance at the platinum center. The synthesis of his 3,5-diester pyridines is shown in Scheme 2.7.

Scheme 2.7. Rachiero′s syntheses of 3,5-diester pyridines.

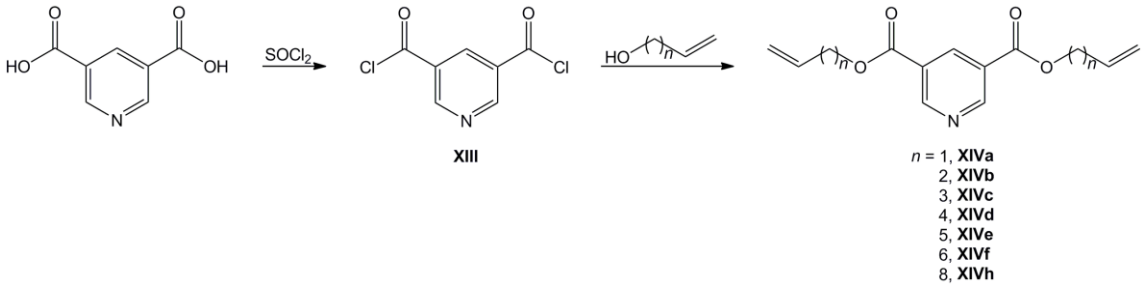

Moving the substituents further from the nitrogen donor greatly facilitates metalation. Rachiero was able to synthesize *trans*-platinum complexes with ligands **XIV** in 41-90% yields (Scheme 2.8).

Scheme 2.8. Rachiero′s metalations of 3,5-diester pyridines with $PtCl_2$.

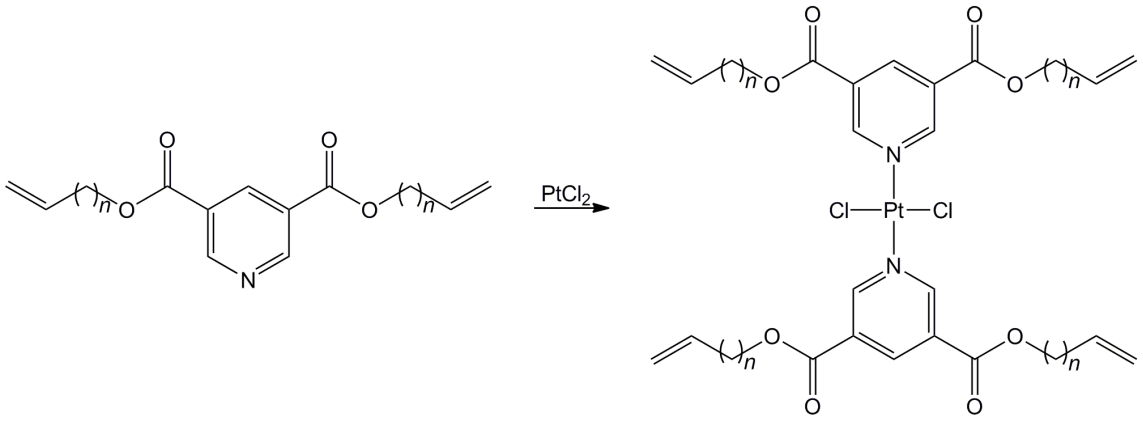

n = 1, **XIVa**
3, **XIVc**
4, **XIVd**
5, **XIVe**
6, **XIVf**
8, **XIVh**

n = 1, *trans*-**XVa**
3, *trans*-**XVc**
4, *trans*-**XVd**
5, *trans*-**XVe**
6, *trans*-**XVf**
8, *trans*-**XVh**

Rachiero then performed two-fold ring-closing metatheses and hydrogenations of the complexes *trans*-**XVd-f**,**h** (Scheme 2.9). The highest yield was achieved with *trans*-**XVIe** (45%). Complexes *trans*-**XVId**,**f**,**h** were isolated with yields of <20%.

Scheme 2.9. Rachiero′s syntheses of *trans*-**XVId-f**,**h**.

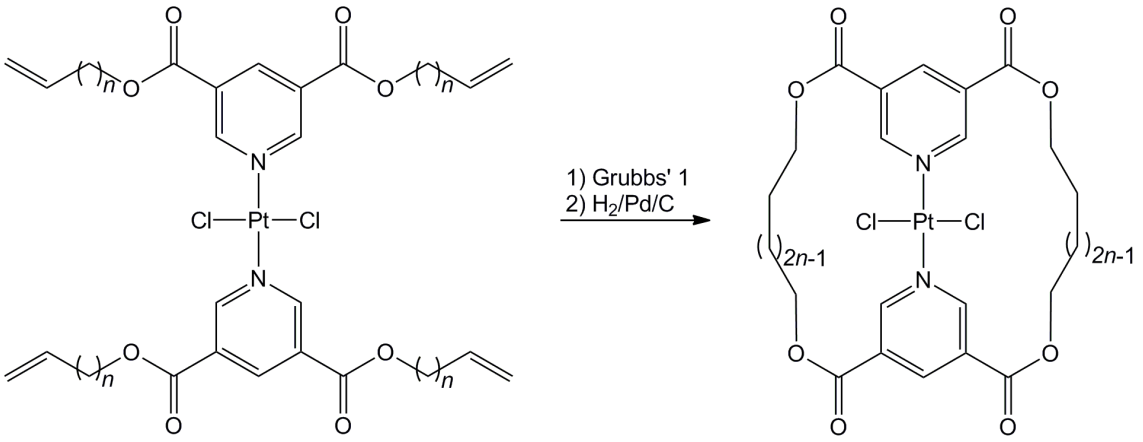

n = 4, *trans*-**XVd**
5, *trans*-**XVe**
6, *trans*-**XVf**
8, *trans*-**XVh**

n = 4, *trans*-**XVId**
5, *trans*-**XVIe**
6, *trans*-**XVIf**
8, *trans*-**XVIh**

The X-ray crystal structure of *trans*-**XVIe** was determined (Figure 2.10). The radius of the rotator was found to be 4.04 Å and the bridge height was found to be 7.66 Å, indicating that ample room for rotation within the macrocyclic cage exists. This is clearly seen in the space filling model. Additionally, the top-bottom clearance improved dramatically when substitution shifts to the 3-position on pyridine. In the case of *trans*-**XVIe**, the *ortho*-hydrogen atoms are of interest, imparting a top-bottom clearance of 1.57 Å. This top-bottom clearance is considerably larger than 2-substituted pyridines and should provide for more facile rotation. However, the closest intermolecular contact was found to be 3.21 Å, indicating that rotation in the crystal lattice would be hindered.

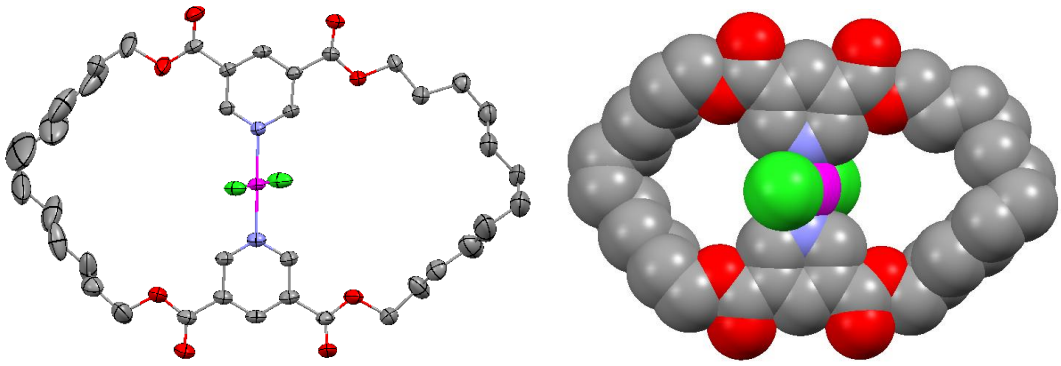

Figure 2.10. X-ray crystal structure of *trans*-**XVIe**, thermal ellipsoid plot (left) and space filling model (right). The three disordered atoms are depicted in their dominant conformations.

Desymmetrization of platinum complexes bearing 3,5-diester pyridine ligands is not so straight forward. As a model desymmetrization reaction, Rachiero was able to exchange one chloride ligand in *trans*-**XVc** with a phenylacetylide ligand (Scheme 2.10). This reaction was carried out in the presence of CuI using CH_2Cl_2/*i*-Pr_2NH (10:1 v/v) as solvent.[23] The complex *trans*-**XVII** has been a big asset for proof of principle. By tying the sterics back, the metal center is more readily accessible for substitution reactions.

However, with the ester functionality of the ligands, simple carbon (R^-) nucleophiles typical of salt metathesis reactions cannot be used. Furthermore, the phenylacetylide ligand is >8 Å in length and would be detrimental to facile rotation of the rotator in all but the largest macrocycles.

Scheme 2.10. Desymmetrization of *trans*-**XVc**.

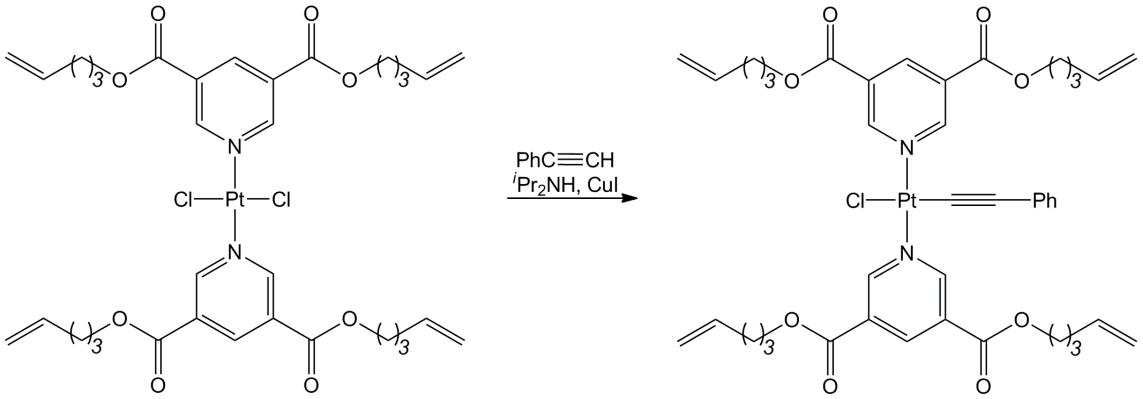

trans-**XVc** *trans*-**XVII**

RESULTS

In order to expand on the results of Rachiero (*vide supra*), new pyridine ligands with reduced steric hindrance were sought. The first new ligand targeted featured an ether moiety with substitution in the 2-position (Scheme 2.11). Both **1a** and **1b** have been synthesized previously by a Williamson ether synthesis from 2-pyridinemethanol and the corresponding alkenyl chloride.[24,25] In this study, it was found that a Williamson ether synthesis starting from 2-(chloromethyl)pyridine hydrochloride was advantageous. Not only are the yields higher, but longer chain alkenyl alcohols are cheaper than the corresponding halides.

Scheme 2.11. Syntheses of monoether ligands 2-$NC_5H_4(CH_2O(CH_2)_nCH{=}CH_2)$.

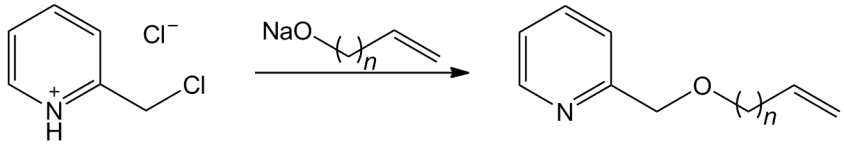

n = 1, **1a** (61%)
2, **1b** (59%)

Metalation of **1a** and **1b** with $PtCl_2$ in refluxing benzene proved possible, but gave low yields (Scheme 2.12). In accord with the trends in Scheme 2.6 above, this suggests the importance of steric effects. Complexes *trans*-**2a**,**b**, and all other new compounds below, were characterized by NMR, IR, and in most cases microanalyses, as summarized in the experimental section. In particular, the sp^2 ^1H and ^{13}C NMR signals of the free and coordinated pyridines could be assigned on the basis of well established chemical shift trends.[26,27]

Scheme 2.12. Syntheses of *trans*-**2a** and *trans*-**2b**.

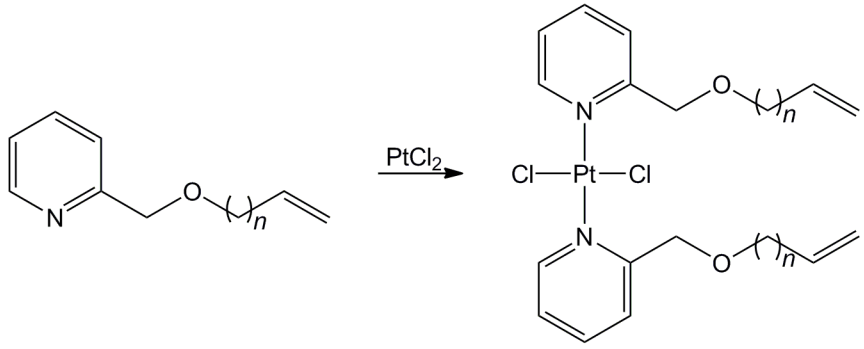

n = 1, **1a**
2, **1b**

n = 1, *trans*-**2a** (40%)
2, *trans*-**2b** (12%)

Interestingly, *trans*-**2a** and *trans*-**2b** exist as atropisomers as shown in Scheme 2.13. The two rotamers of *trans*-**2a** are observable by ^1H NMR in a 1:1 ratio. A variable temperature NMR study was performed and coalescence of the NCC$\underline{H_2}$O ^1H signals was

observed between 35 ˚C and 40 ˚C in $CDCl_3$. The T_c value was extrapolated as 311 K, giving a $\Delta G^{\ddagger}(T_c)$ value of 16.6 kcal/mol. It has previously been reported that the 2-methylpyridine analog of *trans*-**2a**,**b** gave a 65:35 mixture of atropisomers, and similar phenomena have been found for closely related complexes.[26] The ^1H NMR spectra of *trans*-**2b** were also recorded over a range of temperatures in $CDCl_3$ (−50 to +50 ˚C). However, only line broadening was observed. The ^{13}C NMR spectra of *trans*-**2a** and *trans*-**2b** also showed line broadening.

Scheme 2.13. Atropisomers of *trans*-**2a,b**.

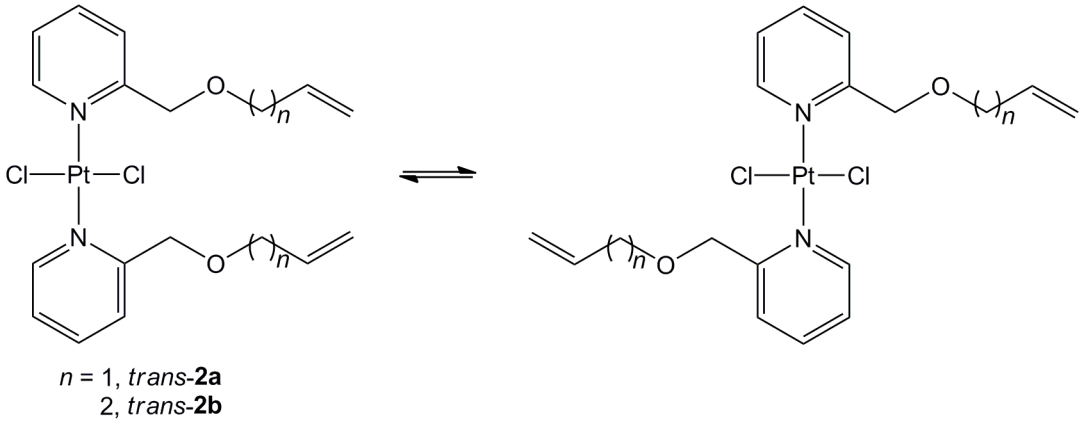

n = 1, *trans*-**2a**
2, *trans*-**2b**

Subsequent ring-closing metathesis and hydrogenation was facile to give the rope-skipping rotors shown in Scheme 2.14. The ^1H and ^{13}C NMR spectra confirmed the absence of olefinic signals.

Scheme 2.14. Syntheses of *trans*-**3a** and *trans*-**3b**.

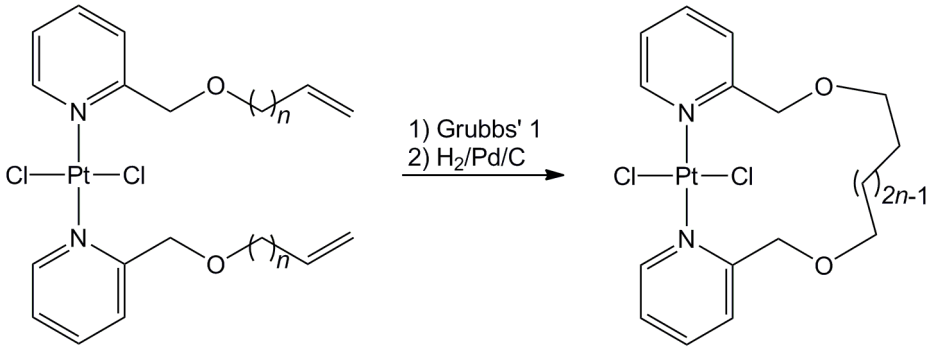

n = 1, *trans*-**2a**
2, *trans*-**2b**

n = 1, *trans*-**3a** (63%)
2, *trans*-**3b** (79%)

Single crystals of *trans*-**3b** suitable for X-ray diffraction studies were grown from a CH_2Cl_2/ethyl acetate (1:2 v/v) solution at room temperature. Two independent molecules were found in the unit cell. One of them exhibited an anti $O\underline{C}H_2\underline{C}H_2\underline{C}H_2\underline{C}H_2$ linkage and a gauche $OCH_2CH_2\underline{C}H_2\underline{C}H_2\underline{C}H_2\underline{C}H_2$ linkage. The linkage conformations in the other molecule were reversed. Key bond lengths and angles are summarized in Table 2.1.

Table 2.1. Key bond lengths (Å) and angles (°) in crystallographically characterized complexes.

	***trans*-3b(1)**[a]	***trans*-3b(2)**[a]	***trans*-6d(1)**[a]	***trans*-6d(2)**[a]	***trans*-6h ·CH_2Cl_2**
bond lengths					
M-Cl1	2.310(2)	2.319(3)	2.297(3)	2.299(3)	2.297(3)
M-Cl2	2.321(3)	2.309(3)	2.297(3)	2.311(3)	2.295(3)
M-N1	2.049(7)	2.000(8)	2.012(7)	2.021(7)	2.016(9)
M-N2	2.039(7)	2.012(8)	2.012(7)	2.021(7)	2.015(10)
bond angles					
N1-M-N2	178.5(4)	178.1(4)	177.5(3)	178.5(4)	178.3(3)
Cl1-M-Cl2	179.04(12)	179.27(13)	177.63(9)	177.63(9)	178.70(11)
Cl1-M-N1	89.4(2)	90.4(2)	90.75(17)	89.50(17)	89.5(2)
Cl2-M-N2	90.2(2)	89.7(2)	89.29(17)	90.52(17)	90.3(3)
Cl1-M-N2	89.8(2)	90.4(2)	90.74(17)	90.52(17)	90.5(3)
Cl2-M-N1	90.5(2)	89.4(2)	89.30(16)	89.50(17)	89.7(2)

[a] Values for the two independent molecules of *trans*-**3b** and *trans*-**6d** in the unit cell.

Multiple views of the X-ray crystal structure and packing diagrams are depicted in Figures 2.11-2.13. Geometrical parameters pertinent to molecular rotors are discussed here. The bridge height and radius of the rotator are quite similar to those of *trans*-**XIIb** (3.39 Å and 4.07 Å, respectively). The closest intermolecular contact was found to be 2.63 Å. This structural analysis suggests that facile rotation in the crystal lattice will be hindered.

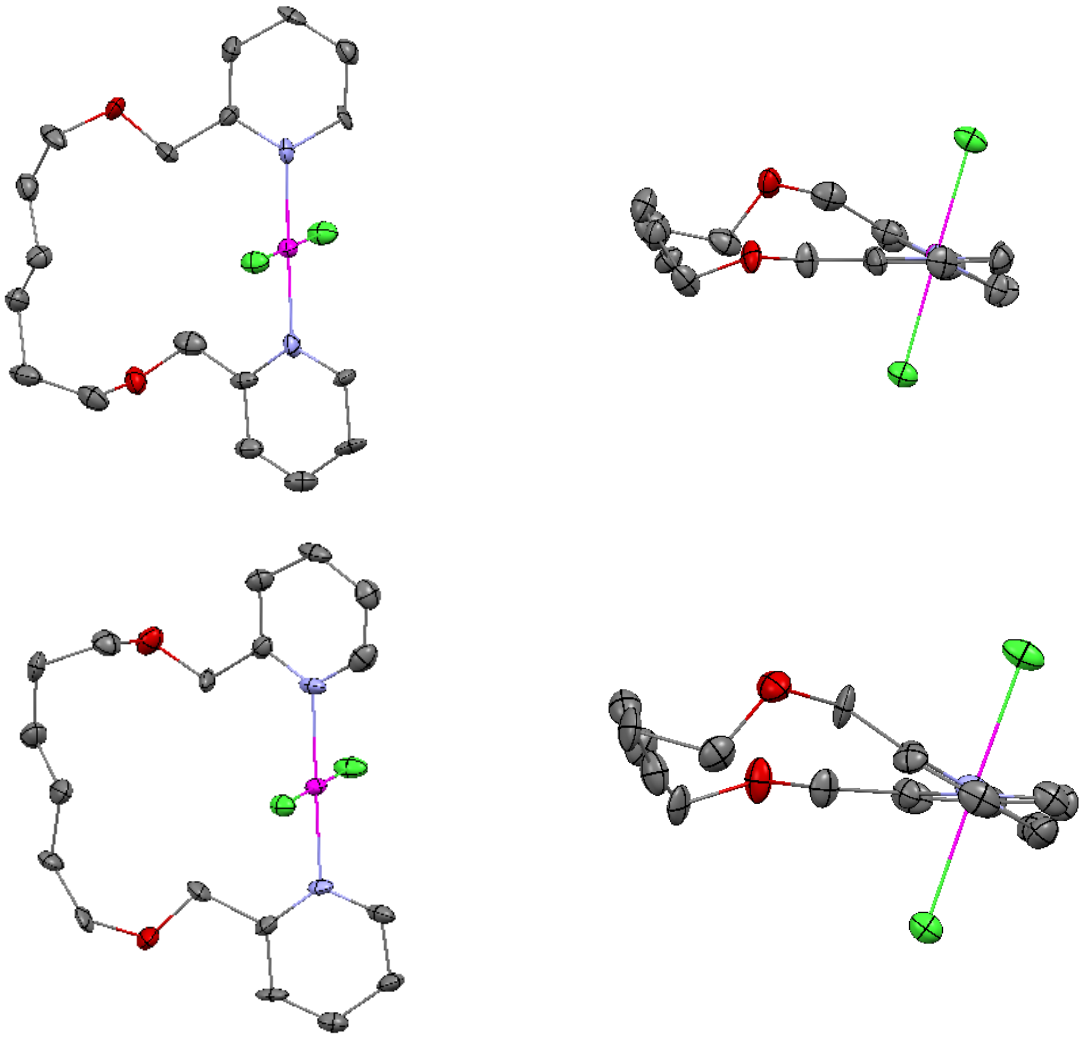

Figure 2.11. Thermal ellipsoid plots (50% probability) of the two independent molecules of *trans*-**3b**: side view (left) and view along the N-Pt-N axis (right).

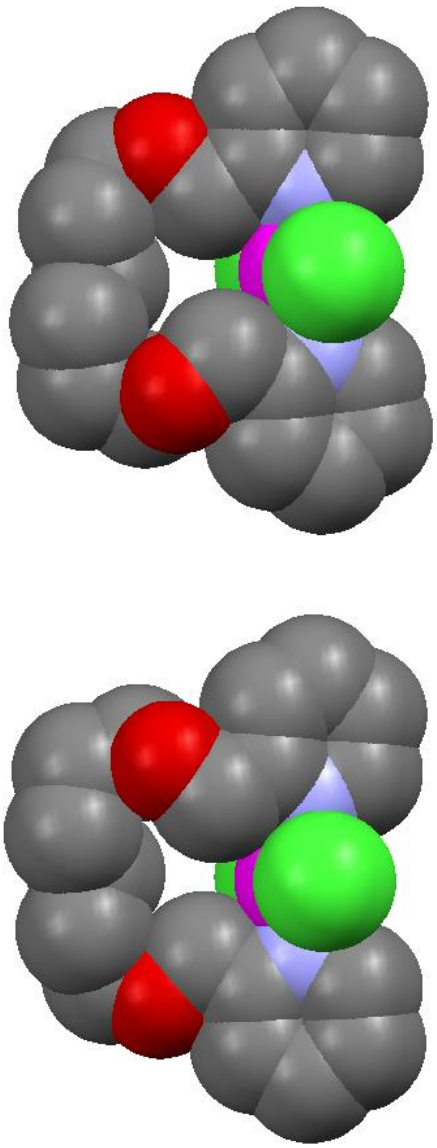

Figure 2.12. Space filling models of the two independent molecules of *trans*-**3b**.

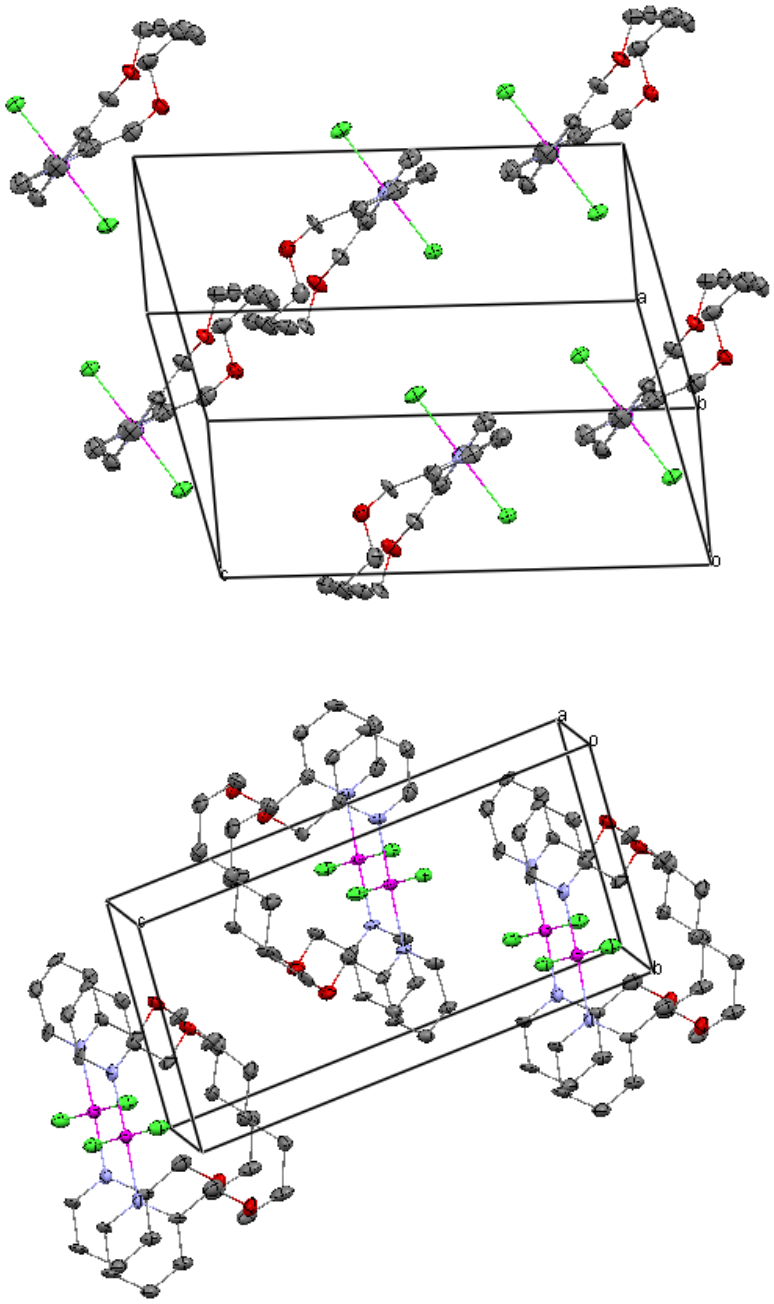

Figure 2.13. Thermal ellipsoid plots (50% probability) of the crystal packing in *trans*-**3b**: view down the N-Pt-N channels (top) and side view (bottom).

From the space filling model, it is evident that these rope-skipping rotors have a metal center that is more accessible than gyroscopes of the type **XII**. However, reaction of *trans*-**3a** and *trans*-**3b** with methylmagnesium bromide (2.5 equivalents, ether, room temperature) did not allow for chloride substitution. In both reactions, pure starting material was recovered in >95% yield.

Next, pyridine ligands with substituents in the 3-position were evaluated. The new 3-substituted pyridines, **4a-i** depicted in Scheme 2.15, were prepared using a Williamson ether synthesis, analogous to ligands **2**.

Scheme 2.15. Syntheses of monoether ligands 3-$NC_5H_4(CH_2O(CH_2)_nCH{=}CH_2)$.

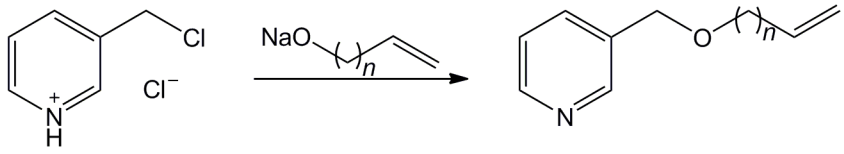

n = 1, **4a** (84%)
2, **4b** (92%)
3, **4c** (70%)
4, **4d** (48%)
5, **4e** (81%)
8, **4h** (84%)
9, **4i** (80%)

With the steric hindrance about the donor nitrogen diminished or "tied back", the metalation of **4** proved very facile (Scheme 2.16). In some cases (*n* = 2 or 8), *cis* and *trans* products were obtained in a nearly 1:1 ratio. These isomers were readily separated on a silica column.

Scheme 2.16. Metalation of ligands **4**.

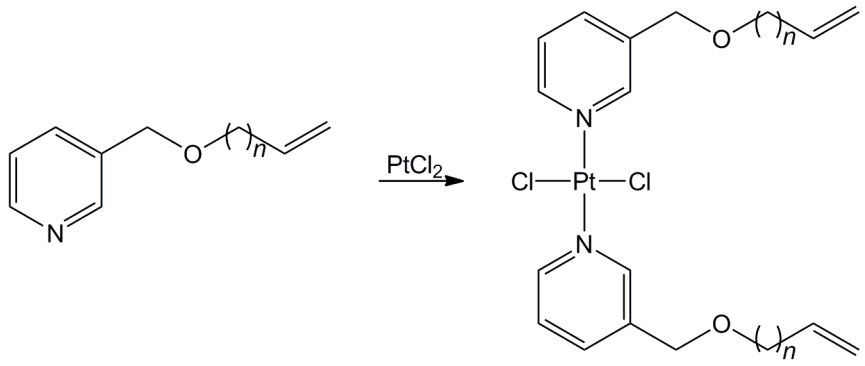

n = 1, **4a**
2, **4b**
3, **4c**
4, **4d**
5, **4e**
8, **4h**
9, **4i**

n = 1, *trans*-**5a** (84%)
2, *trans*-**5b** (49%)
3, *trans*-**5c** (70%)
4, *trans*-**5d** (48%)
5, *trans*-**5e** (81%)
8, *trans*-**5h** (46%)
9, *trans*-**5i** (80%)

Subsequent ring-closing metatheses and hydrogenations proved facile (Scheme 2.17). When $n = 4$, the lower limit of macrocycle formation was observed. When $n = 3$, Grubbs′ first generation catalyst loadings of up to 10 mol% and refluxing in dichloromethane for three days did not show any evidence of olefin metathesis in the ^{1}H NMR spectrum.

Scheme 2.17. Ring-closing metatheses/hydrogenations of *trans*-**5d-h**.

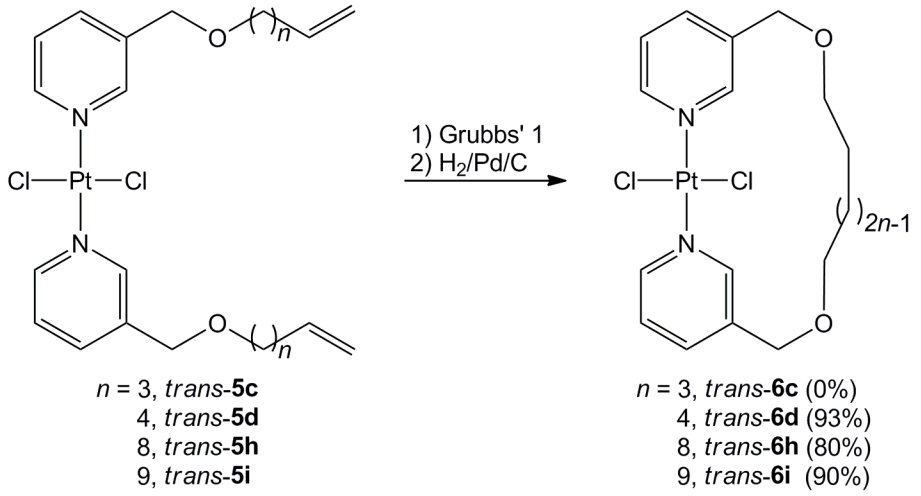

Single crystals of *trans*-**6d** suitable for X-ray diffraction studies were grown from a CH_2Cl_2/ethyl acetate (1:2 v/v) solution at room temperature. Two independent molecules were found in the unit cell. Key bond lengths and angles are summarized in Table 2.1 above. The $OCH_2\underline{C}H_2\underline{C}H_2$ carbon atoms (C8 and C9) were disordered over two positions and refined to 59-62:41-38 occupancies, as described in the experimental section.

Multiple views of the X-ray crystal structure and packing diagrams are depicted in Figures 2.14-2.16. Only the dominant conformation of the disordered molecule is depicted. Geometrical parameters pertinent to molecular rotors are presented here. A rotator radius of 4.05 Å and a bridge height of 5.43 Å are calculated for *trans*-**6d** indicating that rotation within the macrocyclic cage is possible. However, the closest intermolecular contact in *trans*-**6d** is 3.52 Å, indicating that rotation in the crystal lattice will be hindered.

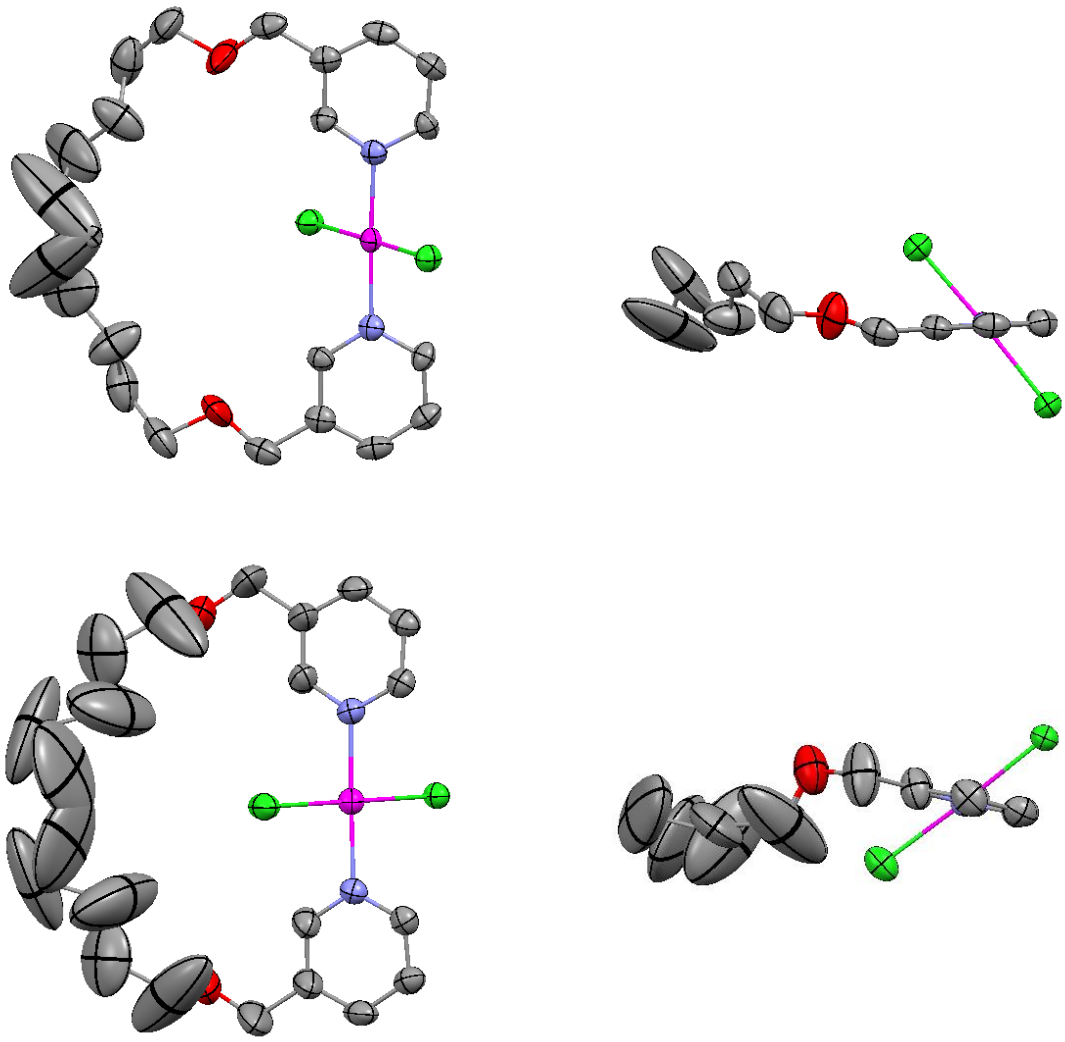

Figure 2.14. Thermal ellipsoid plots (50% probability) of the two independent molecules of *trans*-**6d**: side view (left) and view along the N-Pt-N axis (right). The two disordered atoms are depicted in their dominant conformations.

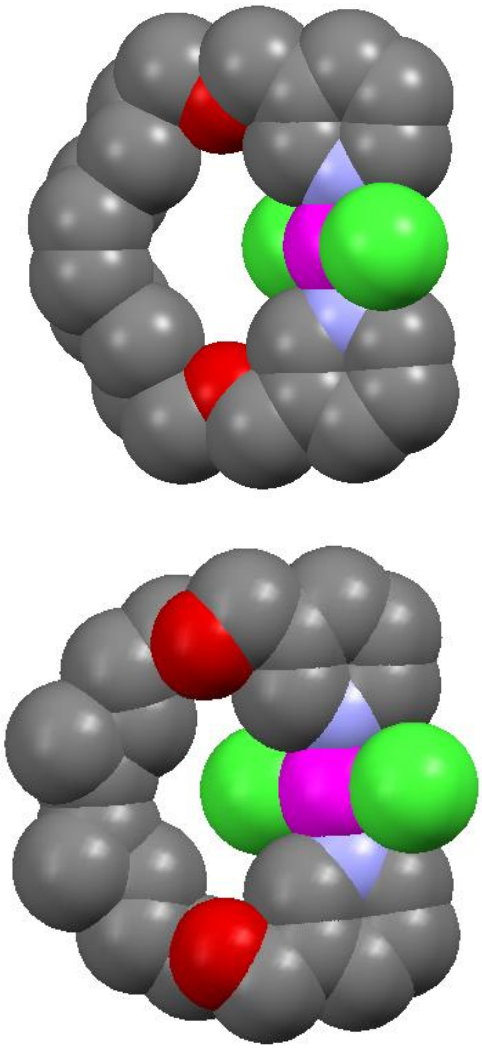

Figure 2.15. Space filling models of the two independent molecules of *trans*-**6d**; the two disordered atoms are depicted in their dominant conformations.

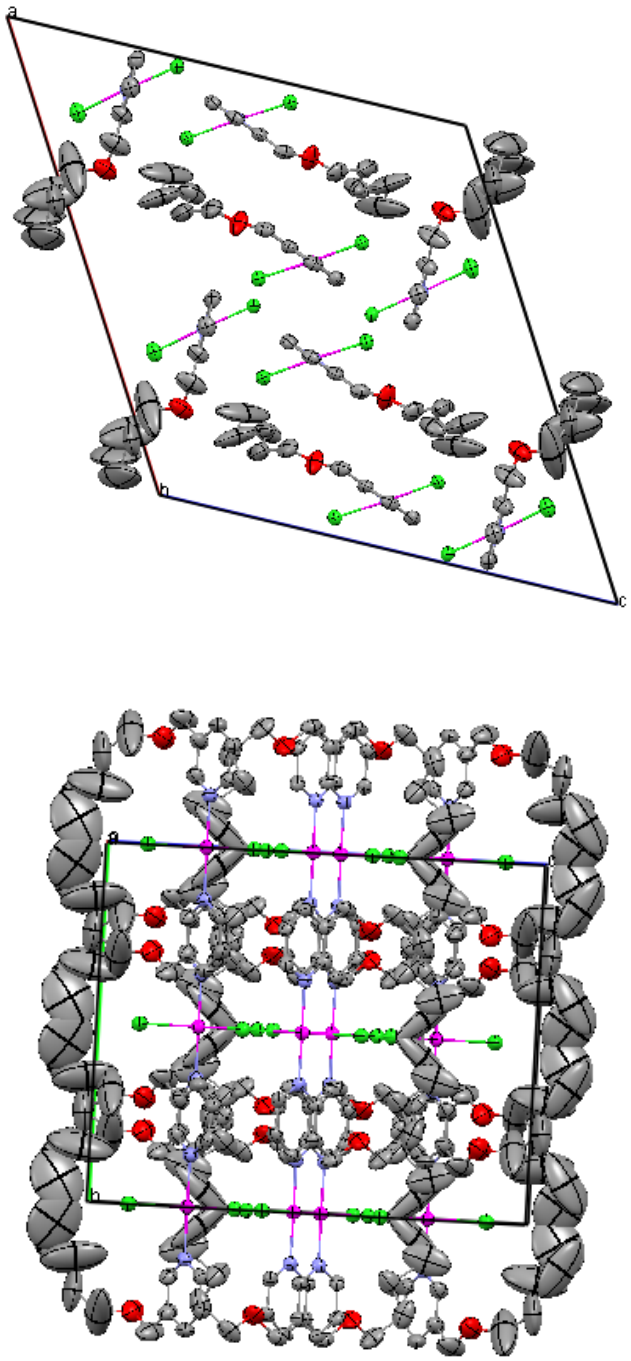

Figure 2.16. Thermal ellipsoid plots (50% probability) of the crystal packing in *trans*-**6d**: view down the N-Pt-N channels (top) and side view (bottom).

Single crystals of *trans*-**6h**·CH_2Cl_2 suitable for X-ray diffraction studies were grown from a CH_2Cl_2/ethyl acetate (1:2 v/v) solution at room temperature. Key metrical parameters are given in Table 2.1 above, and multiple views of the X-ray crystal structure and packing diagrams are depicted in Figures 2.17-2.19. In the case of *trans*-**6h**·CH_2Cl_2, a very large bridge height of 7.57 Å was calculated. In fact, the bridge height is so large that it readily accommodates a dichloromethane molecule within the macrocycle, as seen in the X-ray crystal structure. The bridge height of 7.57 Å is much larger than the rotator radius of 4.05 Å, indicating that rotation within the macrocyclic cage is possible, in the absence of the solvate. The closest intermolecular contact in *trans*-**6h**·CH_2Cl_2 was found to be 3.73 Å. Although this distance is shorter than the radius of the rotator, it is longer than the closest intermolecular contact observed with the two-spoke bis(pyridine)platinum gyroscopes (*vide supra*). Of course, the solvate presents additional hindrance in the lattice.

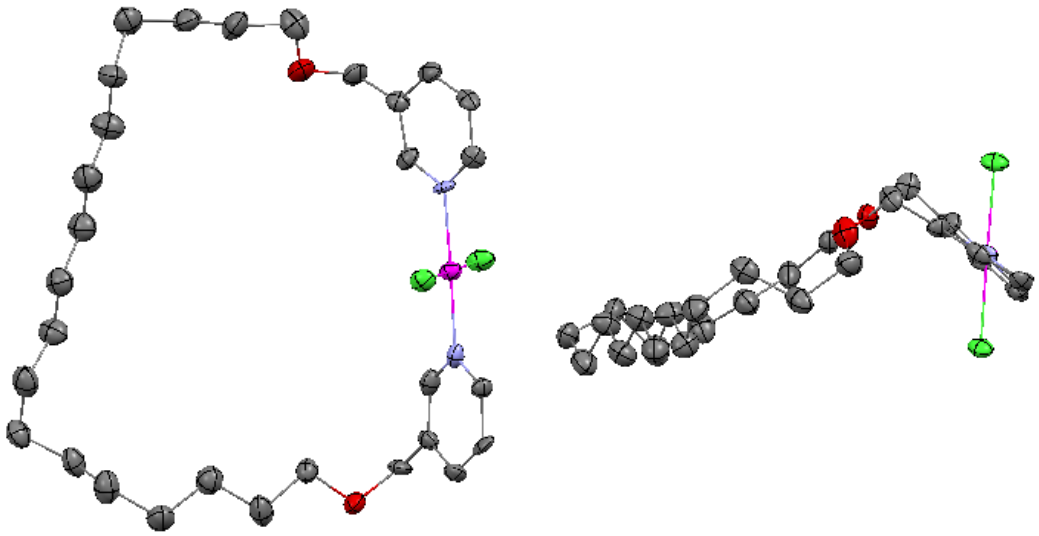

Figure 2.17. Thermal ellipsoid plots (50% probability) of *trans*-**6h**·CH_2Cl_2: side view (left) and view along the N-Pt-N axis (right). The solvent molecule has been removed for clarity.

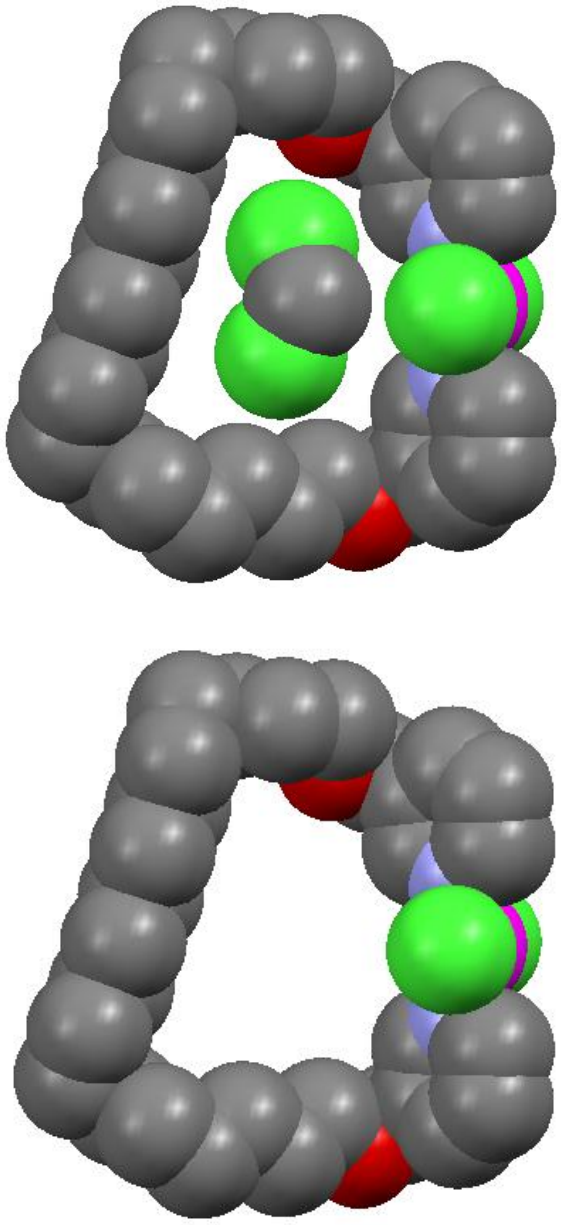

Figure 2.18. Space filling models of *trans*-**6h**·CH_2Cl_2;with solvate (top) and solvate removed (bottom).

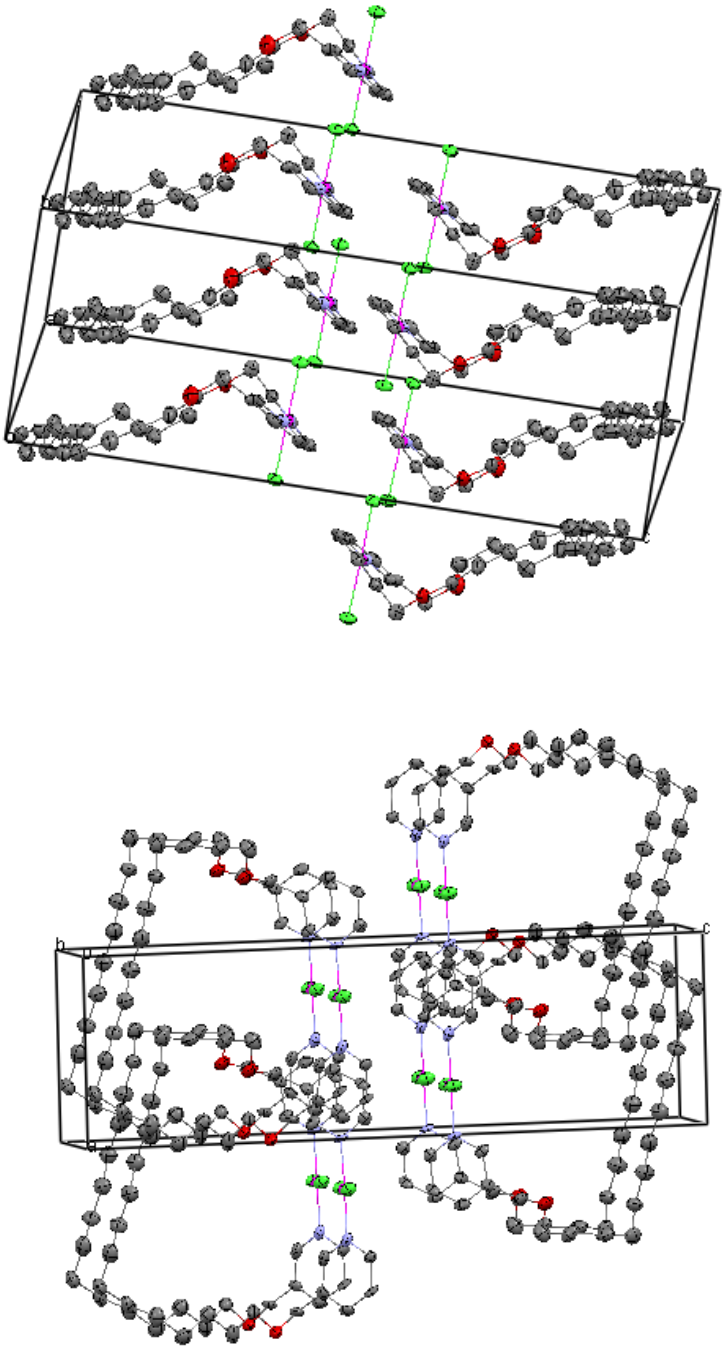

Figure 2.19. Thermal ellipsoid plots (50% probability) of the crystal packing in *trans*-**6h**·CH_2Cl_2: view down the N-Pt-N channels (top) and side view (bottom). The solvent molecule has been removed for clarity.

In the sterically less encumbered 3-substituted pyridine complexes, desymmetrization was attempted by reaction with methylmagnesium bromide (Scheme 2.18). For model reactions, desymmetrization was first attempted on the open chain complexes *trans*-**5b** and *trans*-**5h**. Chloride substitution proved facile to give *trans*-**7b** and *trans*-**7h**. Monosubstitution is as expected and has been described in the literature.[22c]

Scheme 2.18. Syntheses of *trans*-**7b** and *trans*-**7h**.

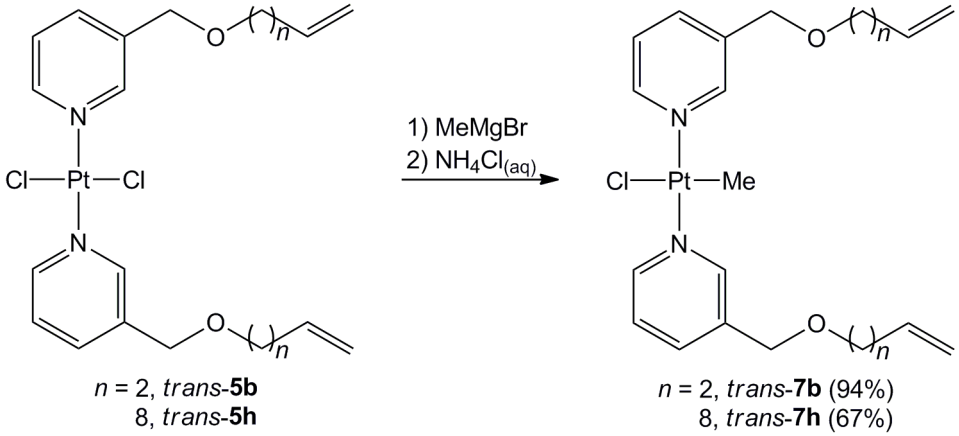

Following the promising substitution results on open chain complexes, methylation was attempted on the rope-skipping rotors *trans*-**7b** and *trans*-**7h**. Both complexes readily exchanged a chloride ligand for a methyl ligand to produce the dipolar rope-skipping rotors *trans*-**8d** and *trans*-**8h** (Scheme 2.19).

Scheme 2.19. Syntheses of *trans*-**8d** and *trans*-**8h**.

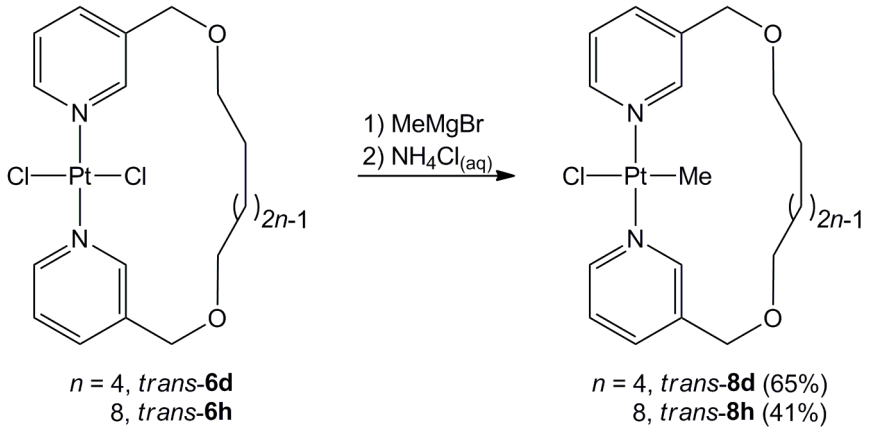

Upon desymmetrization, the methylene protons in *trans*-**8d** and *trans*-**8h** become diastereotopic. At room temperature in $CDCl_3$ *trans*-**8d** and *trans*-**8h** exhibit only one set of ^1H NMR signals for the methylene protons. Spectra of *trans*-**8d** were recorded at low temperature in $CDCl_2F$.[28] Upon cooling to −120 ˚C, no decoalescence was observed. This suggests that rotation is approaching a minimum level of friction in solution.

Additionally, a 3,5-disubstituted pyridine with phenylene spacers was investigated. Phenylene spacers have been employed in phosphine based molecular gyroscopes to access the so-called giant gyroscopes.[3c] The initial step to pyridine ligands with phenylene spacers involved a Kumada coupling with 3,5-dichloropyridine. While several catalysts exist for Kumada coupling reactions, standard palladium and nickel catalysts were evaluated.[29,30] For a model reaction, the coupling of phenylmagnesium bromide with 3,5-dichloropyridine was tested (Scheme 2.20). With a 0.5 mol% loading of **XVIII**, a 90.1% yield was achieved compared to a 91.4% yield with **XIX** (1.0 mol%). Given the comparable yields, **XIX** was used in further reactions since it is significantly cheaper.

Scheme 2.20. Synthesis of 3,5-diphenylpyridine as a model reaction for Scheme 2.21.

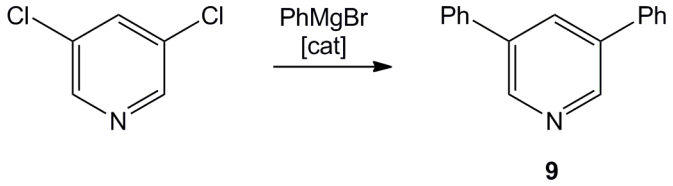

9

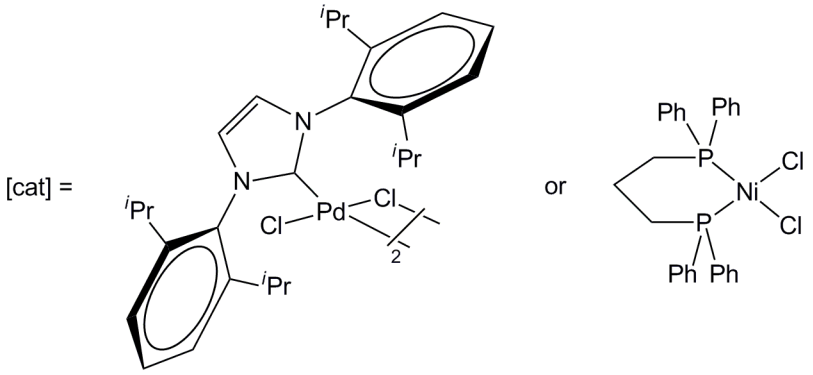

XVIII **XIX**

The synthesis of giant pyridine ligands with phenylene spacers is shown in Scheme 2.21 and follows literature precedent.[31] The first step involves a Kumada coupling between *p*-anisolemagnesium bromide and 3,5-dichloropyridine using the advantageous **XIX** (1 mol%) to produce the substitution product **10** in 73% yield. Next, **10** was deprotected with BBr_3 to give the bis(phenol) **11** in 66% yield. Finally, the alkenyl groups were installed by a Williamson ether synthesis to give the new ligand **12** in 32% yield.

Scheme 2.21. Synthesis of a 2,5-disubstituted pyridine ligand with phenylene spacers (**12**).

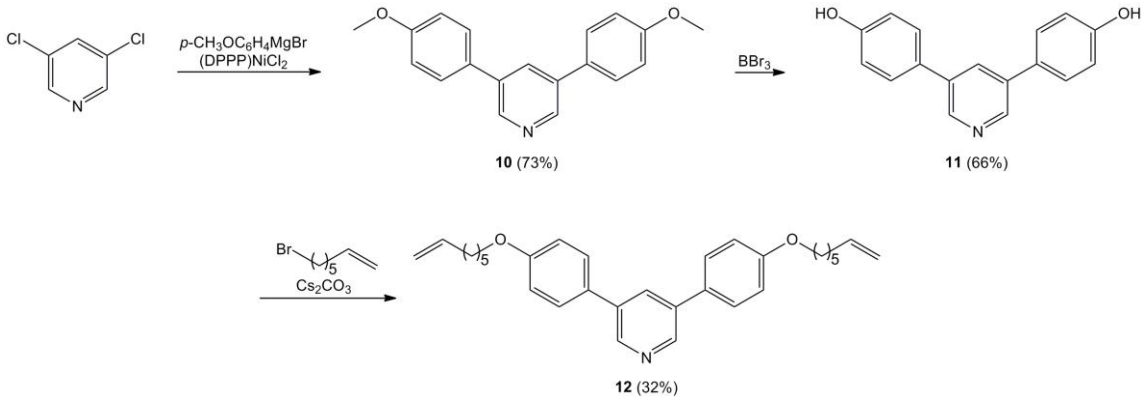

Following the standard metalation procedure (*vide supra*), **12** and $PtCl_2$ were reacted in refluxing benzene to afford *trans*-**13** (Scheme 2.22).

Scheme 2.22. Synthesis of *trans*-**13**.

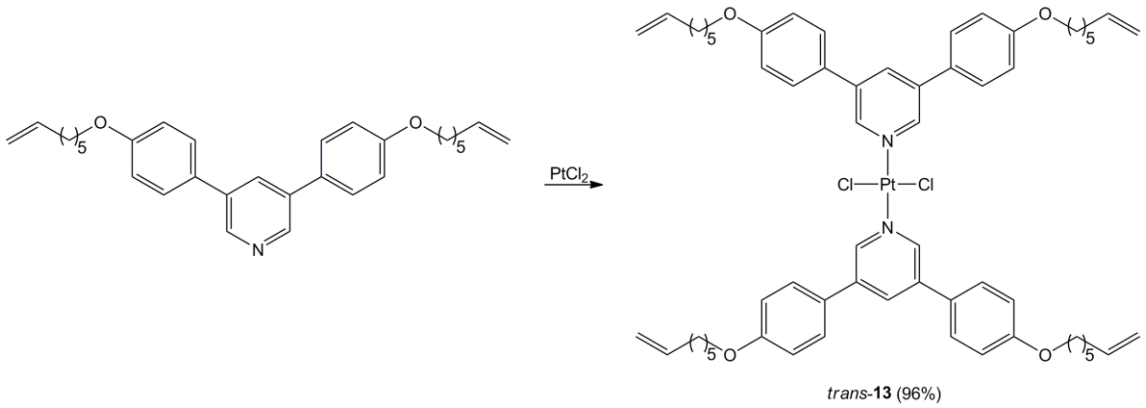

Subsequently, two-fold ring-closing metathesis and hydrogenation afforded the giant pyridine gyroscope *trans*-**14** as a yellow solid in 49% yield after workup (Scheme 2.23). Unfortunately, attempts to grow single crystals have not yet been successful.

Scheme 2.23. Synthesis of *trans*-**14**.

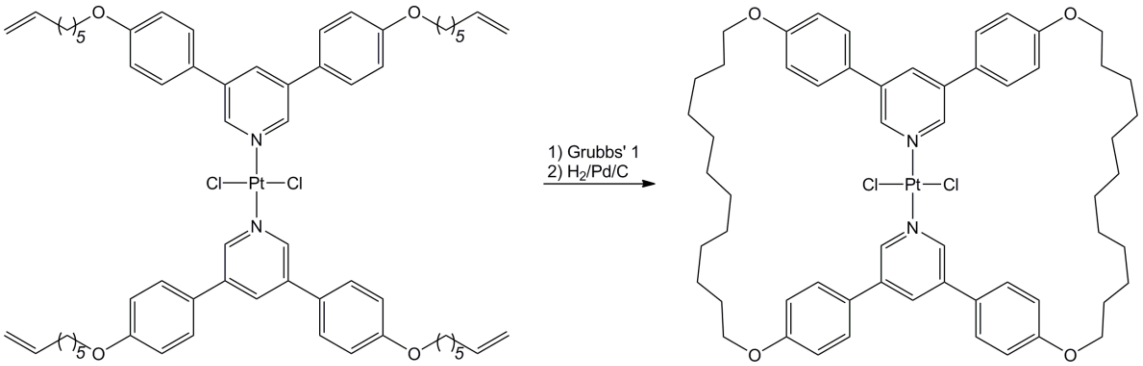

DISCUSSION

The preceding studies establish that gyroscope-like complexes with *trans*-spanning bis(pyridine) ligands are generally available *via* ring-closing metatheses of a variety of suitable square planar platinum precursors. These feature 2-, 3-, 2,6-, and 3,5-mono or disubstituted pyridine ligands with $CH_2O(CH_2)_nCH{=}CH_2$ (n = 1,2,4,8,9), $CO_2(CH_2)_nCH{=}CH_2$ (n = 4-6,8), and $C_6H_4O(CH_2)_nCH{=}CH_2$ (n = 5) substituents (Schemes 2.6, 2.9, 2.14, 2.17, and 2.23). This in depth investigation provides much needed perspective regarding an early fragmentary report by Lambert involving a $PdCl_2$ system (Scheme 2.2). Interestingly, singly bridged *trans*-bis(pyridine) complexes undergo ring-closing metathesis/hydrogenation in considerably higher yields than their doubly bridged counterparts (Schemes 2.6, 2.9, and 2.23 vs. Schemes 2.14 and 2.17). Curiously, the new rope-skipping rotors described here involve a shorter reaction time for hydrogenation. When the hydrogenation steps were run for longer periods, yields were found to be severely diminished.

The bond lengths and angles about the platinum in the newly crystallographically characterized complexes are compared in Table 2.1 above. Only very slight deviations from idealized square planar geometries are evident. Bond angles between *cis* ligands

range from 89.29° to 90.75°. Bond angles between *trans* ligands range from 177.5° to 179.27°. The largest discrepancies from idealized square planar geometry are seen with *trans*-**6d**(1). Not surprisingly, as shown above, *trans*-**6d** was the lower limit for macrocycle formation. The Pt-N bond lengths are in good general agreement, ranging from 2.000 Å to 2.049 Å. The Pt-Cl bond lengths are also in good general agreement, ranging from 2.295 Å to 2.321 Å. Very similar values were found for the five related complexes structurally characterized by Rachiero (Figures 2.4, 2.7, and 2.10).[19]

Additionally, as shown in Scheme 2.23, the giant pyridine gyroscope *trans*-**14** was synthesized in the highest yield reported for a doubly bridged *trans*-bis(pyridine) complex. While the X-ray crystal structure of *trans*-**14** has not been obtained, the facile purification by chromatography strongly suggests the product is not oligomeric or polymeric.

Table 2.2 focuses in on the metrical properties associated with the rotators, their ligand environments, and their nearest neighbors, both for the compounds in this study and earlier work. As expected, the radii of the $PtCl_2$ rotators are identical within experimental error. Bridge heights scale with the size of the macrocycle and range from 2.49 Å for 13 atoms in *ortho*-substituted *trans*-**XIIa** to 7.66 Å for 23 atoms in *meta*-substituted *trans*-**XVIe**. Additionally, *trans*-**6h**·CH_2Cl_2 has a similarly large bridge height of 7.57 Å. The macrocycle in *trans*-**6h**·CH_2Cl_2 contains 29 atoms with *meta*-substitution.

Table 2.2. Data relevant to rotator rotation in crystalline complexes; all values are given in Å.

Molecule	Rotator Radius	Bridge Height	Top-Bottom Clearance[c]	Closest Intermolecular Contact[d]
VIII	4.06	2.58	0.58[a]	3.59
***trans*-XIIa**	4.06	2.49	0.63[a]	3.13
***trans*-XIIb**	4.06	4.38	0.45[a]	2.89
***trans*-XVIe**	4.04	7.66	1.40[b]	3.21
***trans*-3b**	4.07	3.39	0.87[a]	2.63
***trans*-6d**	4.05	5.43	1.36[b]	3.52
***trans*-6h·CH_2Cl_2**	4.05	7.57	1.43[b]	3.73

[a] *Ortho*-substitution. [b] *Meta*-substitution. [c] See Figure 2.5. [d] See Figure 2.6.

As expected, top-bottom clearance strongly correlates with substitution pattern. The *ortho* bridged systems are very congested (0.45-0.87 Å clearance) and are unlikely to support rotation of any type. In this context, it is worth noting that the *ortho*-substituted atropisomers of *trans*-**2a**,**b** (Scheme 2.13) do interconvert. However, as shown in Scheme 2.24, this requires rotation about only a single platinum-nitrogen bond, and a single unfavorable chlorine/*ortho*-carbon steric interaction. In the gyroscope-like complexes, there are a minimum of two such interactions in the transition state for rotation. With *meta* substituted pyridine ligands, all exhibit much greater top-bottom clearance (1.36-1.43 Å), much closer to the VDWR of chlorine (1.75 Å).

Scheme 2.24. Steric consequences of rotation about a single platinum-nitrogen bond.

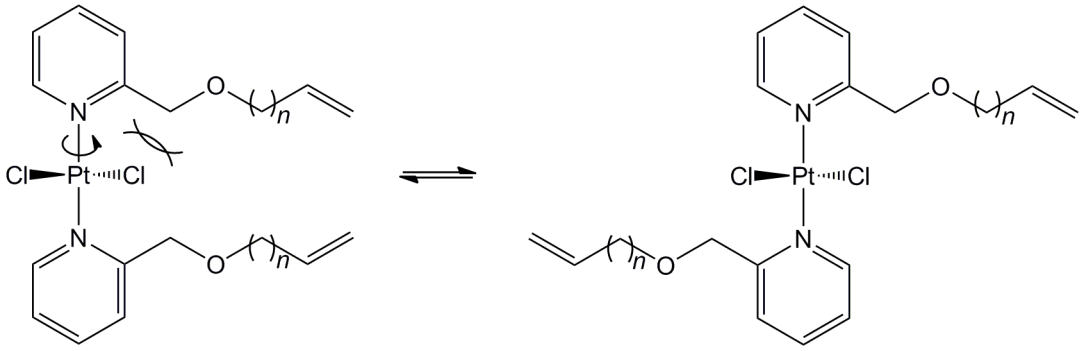

n = 1, *trans*-**2a**
2, *trans*-**2b**

As noted above, the largest intermolecular contact involving the $PtCl_2$ rotator is observed in the single spoke complex *trans*-**6h**·CH_2Cl_2 (3.73 Å). This is quite close to the radius of the rotator (4.05 Å), and if it were not for the solvate molecule within the macrocycle might enable some solid state rotation at a temperature below the melting point (131-134 °C). However, such phenomena would be unlikely in the other complexes.

From the solid sate structural analysis, *trans*-**6h**·CH_2Cl_2 would be the best model for further development of MCB junctions and molecular compasses. This complex exhibits a large bridge height, large top-bottom clearance, and a beneficial close contact distance. Furthermore, introducing a dipole at this metal center is facile. The only disadvantage is the diminished steric protection of the rotator, especially relative to the diphosphine based gyroscopes in Scheme 2.1.

As noted earlier, one advantage of the pyridine-based gyroscopes over diphosphine-based gyroscopes is the availability of a functionalizable *para* (4-) position. Thus, one could envision anchoring a system to a surface as shown in Scheme 2.25. This type of thioacetate functionality has been used extensively in MCB junctions.[17] This

sequence would involve the $AcSC_6H_4C{\equiv}C$ substituted molecular rotor **XXI**, which could be synthesized by bromination of *trans*-**6h** followed by a Sonogashira coupling. This would constitute a fascinating direction for future research. The rotator could be rendered dipolar by a monosubstitution reaction, either before or after the surface immobilizing step.

Scheme 2.25. Possible functionalization of *trans*-**6h** for applications with MCB junctions.

CONCLUSION

A variety of alkene containing pyridines have been synthesized and elaborated into novel *trans*-bis(pyridine)platinum complexes. Subsequently, these complexes have undergone ring-closing metatheses and hydrogenations to afford new single spoke molecular rotors featuring macrocycles of 13, 15, 21, 29, and 31 atoms, as well as a giant two spoke molecular rotor featuring a macrocycle of 29 atoms. The syntheses of the

single spoke molecular rotors proceed much more readily than their two spoke counterparts.

It has also been shown that systems with 3-substituted pyridine ligands exhibit much less congestion about the metal center. Substitution reactions become facile, allowing the rotator to be desymmetrized – i.e., the exchange of a single chloride ligand for a methyl ligand. Even with the smallest 3-substituted macrocycle, rotation of the resulting chloride methyl complex remains rapid on the NMR time scale to −120 ˚C.

EXPERIMENTAL

General

All reactions were carried out in an inert atmosphere using standard Schlenk and vacuum line techniques. All workups were carried out in air. Chemicals were treated as follows: benzene and pentane were distilled from Na/benzophenone; ethyl acetate, hexanes, petroleum ether, and dichloromethane for chromatography were used as received; all other solvents were purified using a Glass Contour solvent purification system; $CDCl_3$ (Cambridge Isotope Laboratories), DMSO-d_6 (Aldrich), silica (Acros, 60 A), sodium (J.T. Baker, A.C.S. reagent), allyl alcohol (Alfa Aesar, 98%), 3-buten-1-ol (TCI, 95%), 4-penten-1-ol (TCI, 98%), 5-hexen-1-ol (TCI, 95%), 6-hepten-1-ol (TCI, 95%), 9-decen-1-ol (TCI, 95%), 10-undecen-1-ol (TCI, 95%), 3-(chloromethyl)pyridine hydrochloride (Alfa Aesar, 97%), 2-(chloromethyl)pyridine hydrochloride (TCI, 98%), platinum(II) chloride (ABCR, 99.9%), 3,5-dichloropyridine (TCI, 98%), 4-bromoanisole (Alfa Aesar, 99%), BBr_3 (Aldrich, 1.0 M in CH_2Cl_2), Cs_2CO_3 (Alfa Aesar, 99.9%), 7-bromo-1-heptene (Aldrich, 97%), Pd/C (Acros, 10%), methylmagnesium bromide (Acros, 3.0 M in ether; titration vs. I_2 gave 2.94 M),[32] phenylmagnesium bromide (Aldrich, 1.0 M in THF), magnesium (Alfa Aesar, 99.8%), NH_4Cl (Mallinckrodt, 99.5%), dichloro(di-μ-chloro)bis[1,3-bis(2,6-di-isopropylphenyl)imadazol-2-ylidene]di-

palladium(II) (**XVIII**; Strem, 97%), and (DPPP)$NiCl_2$ (**XIX**; Strem, 99%) were used as received.

NMR spectra were recorded on a Varian NMRS 500 MHz spectrometer at ambient probe temperatures and referenced as follows: ^1H: residual internal $CHCl_3$ (δ, 7.26 ppm) or DMSO-d_5 (δ, 2.50 ppm); ^{13}C: internal $CDCl_3$ (δ, 77.23 ppm). The ^1H and ^{13}C NMR signals of the free and coordinated nitrogen donor ligands were assigned based literature generalizations.[26,27] IR spectra were recorded using a Shimadzu IRAffinity-1 spectrometer with a Pike MIRacle ATR system (diamond/ZnSe crystal). Melting points were recorded with a Stanford Research Systems (SRS) MPA100 (Opti-Melt) automated melting point system. Microanalyses were conducted by Atlantic Microlab.

General Procedures

Syntheses of Ligands 1a-b and 4a-i

A Schlenk flask was charged with sodium (2.5-3.0 equivalents) and then the ω-alken-1-ol (*ca*. 20 equivalents). The mixture was heated (oil bath) with stirring until all of the sodium dissolved, and cooled to room temperature. Then 2- or 3-(chloromethyl)pyridine hydrochloride (1 equivalent, ~2 g) was added and the mixture heated for 12-16 h. The excess alcohol was removed at the reaction temperature by oil pump vacuum. Water and dichloromethane were added to the residue. The phases were separated and the aqueous phase extracted with dichloromethane (2 × 50 mL). The dichloromethane layers were then combined and dried ($MgSO_4$). The solvent was removed by oil pump vacuum. The residue was passed through a silica column (8 × 1.5 cm) eluted with ethyl acetate (300 mL). Solvent removal by oil pump vacuum afforded spectroscopically pure ligand as a yellow to brown oil.

Syntheses of Metal Complexes

A round bottom flask was charged with a suspension of $PtCl_2$ (*ca.* 1 g) in benzene (50 mL) and fitted with a condensor. Then the nitrogen donor ligand (2.1 equivalents) was added with stirring. The mixture was refluxed (oil bath) 14 h and the solvent removed by oil pump vacuum. The residue was chromatographed on a silica column (32 × 2.5 cm) eluted with 1:4 v/v ethyl acetate/dichloromethane. In some cases, two bands were obtained (*trans* isomer followed by *cis* isomer).

Syntheses of Macrocycles

A round bottom flask was charged with a 0.0019-0.0021 M dichloromethane solution of the metal complex and fitted with a condenser. Grubbs′ first generation catalyst (*ca.* 4 mol% per new C=C bond formed) in dichloromethane (5 mL) was added by syringe with stirring. The mixture was then refluxed (oil bath) while maintaining a flow of nitrogen orthogonal to the top of the condenser. After 18 h, a ^1H NMR spectrum of an aliquot usually showed the reaction to be complete. In the cases of *trans*-**3b**, *trans*-**6i**, and *trans*-**14**, a second charge of Grubbs′ first generation catalyst in dichloromethane (5 mL) was used with an additional 24 h of refluxing. The solvent was then removed by oil pump vacuum and the residue passed through a silica column (15.5 × 1.5 cm) eluted with 1:4 v/v ethyl acetate/dichloromethane. The solvent was removed by oil pump vacuum. A three neck flask was charged with this residue, Pd/C (10% w/w, 5.00 mol%), toluene (30 mL), and ethanol (30 mL), and was fitted with a glass stopper, a stopcock attached to a H_2 balloon, and a septum. The headspace was then evacuated and the H_2 from the balloon introduced. After 23 h, chloroform (40 mL) was added and the mixture filtered through a celite column (5 × 2 cm). The column was washed with chloroform (2 × 40 mL). The solvent was removed from the filtrate by oil pump vacuum and the residue passed through a silica column (29 × 1.5 cm) eluted with 1:4 v/v ethyl

acetate/dichloromethane. In the case of *trans*-**14**, the hydrogenation procedure was repeated twice.

Methylations

A round bottom flask was charged with dichloroplatinum complex (1 mmol) and ether (15 mL) in an argon filled glove box. Then methylmagnesium bromide (2.5-3.0 equivalents of a *ca*. 2.94 M solution in ether) was added with stirring. After 2 h, saturated aqueous NH_4Cl (5 mL) was added. The mixture was diluted with water (45 ml) and ether (35 mL) and the phases separated. The water layer was extracted with ether (2 × 50 mL). The ether layers were combined and dried ($MgSO_4$). The solvent was then removed by oil pump vacuum. The residue was chromatographed on a silica column (39 × 2.5 cm) eluted with 1:4 v/v ethyl acetate/dichloromethane.

2-$NC_5H_4(CH_2OCH_2CH{=}CH_2)$ (1a)

Allyl alcohol (15.6510 g, 269.473 mmol), sodium (0.8942 g, 36.94 mmol), and 2-(chloromethyl)pyridine hydrochloride (2.4870 g, 15.161 mmol) were combined as described above (ligand synthesis; sodium dissolved and reaction conducted at 80 °C for 12 h). This gave **1a** (1.3682 g, 9.1776 mmol, 61%) as a brown oil.

^{1}H NMR ($CDCl_3$): δ 8.54 (m, 1H, *o*-*H*C_{6pyr}), 7.68 (m, 1H, *p*-*H*C_{4pyr}), 7.45 (m, 1H, *m*-*H*C_{3pyr}), 7.17 (m, 1H, *m*-*H*C_{5pyr}), 6.01-5.92 (ddt, 1H, $^3J_{HH}$*trans* = 17.3 Hz, $^3J_{HH}$*cis* = 10.3 Hz, $^3J_{HH}$ = 5.5 Hz, C*H*=), 5.35-5.19 (m, 2H, =CH_2), 4.64 (s, 2H, CH_2O), 4.11 (m, 2H, OCH_2CH). ^{13}C{^{1}H} NMR ($CDCl_3$): δ 158.7 (*o*-C_{2pyr}), 149.2 (*o*-C_{6pyr}), 136.8 (*C*H=), 134.6 (*p*-C_{pyr}), 122.5 (*m*-C_{3pyr}), 121.5 (*m*-C_{5pyr}), 117.5 (=*C*H_2), 73.1 (*C*H_2O), 72.0 (O*C*H_2CH). These data agreed with those previously reported.[24]

IR (cm^{-1}, neat oil): 3076 (w), 2859 (w), 1717 (m), 1591 (m), 1306 (m), 1244 (m), 1107 (s), 1084 (s), 993 (s), 926 (s), 758 (s).

2-$NC_5H_4(CH_2O(CH_2)_2CH=CH_2)$ (1b)

3-Buten-1-ol (14.0023 g, 194.188 mmol), sodium (0.6338 g, 27.57 mmol) and 2-(chloromethyl)pyridine hydrochloride (1.9507 g, 11.892 mmol) were combined as described above (ligand synthesis; sodium dissolved and reaction conducted at 80 °C for 12 h). This gave **1b** (1.8179 g, 11.138 mmol, 59%) as a yellow oil.

^{1}H NMR ($CDCl_3$): δ 8.53 (m, 1H, *o*-HC_{6pyr}), 7.68 (m, 1H, *p*-HC_{4pyr}), 7.44 (m, 1H, *m*-HC_{3pyr}), 7.17 (m, 1H, *m*-HC_{5pyr}), 5.90-5.81 (ddt, 1H, $^3J_{HH}$*trans* = 17.1 Hz, $^3J_{HH}$*cis* = 10.1 Hz, $^3J_{HH}$ = 6.9 Hz, C*H*=), 5.14-5.03 (m, 2H, =CH_2), 4.64 (s, 2H, CH_2O), 3.62 (t, 2H, $^3J_{HH}$ = 6.9 Hz, OCH_2CH_2), 2.41 (m, 2H, OCH_2CH_2). ^{13}C{^{1}H} NMR ($CDCl_3$): δ 158.9 (*o*-C_{2pyr}), 149.2 (*o*-C_{6pyr}), 136.9 (*C*H=), 135.3 (*p*-C_{4pyr}), 122.5 (*m*-C_{3pyr}), 121.5 (*m*-C_{5pyr}), 116.7 (=*C*H_2), 73.9 (*C*H_2O), 70.6 (O*C*H_2CH_2), 34.4 (*C*H_2CH=). These data agreed with those previously reported.[25]

IR (cm^{-1}, neat oil): 2907 (w), 2859 (m), 1717 (m), 1591 (m), 1435 (s), 1121 (s), 1088 (s), 993 (s), 914 (s), 756 (s).

***trans*-$PtCl_2$(2-$NC_5H_4(CH_2OCH_2CH=CH_2))_2$ (*trans*-2a)**

$PtCl_2$ (0.8468 g, 3.183 mmol) and **1a** (1.2956 g, 8.6841 mmol) were combined as described above (syntheses of metal complexes). This gave *trans*-**2a** (0.7258 g, 1.286 mmol, 40%) as a light yellow solid and a mixture of atropisomers (*ca*. 50:50).

^{1}H NMR ($CDCl_3$): δ 8.92 (m, 2H, *o*-HC_{6pyr}), 7.77 (m, 2H, *m*-HC_{5pyr}), 7.69 (m, 2H, *p*-HC_{pyr}), 7.24 (m, 2H, *m*-HC_{5pyr}), 6.13-5.98 (m, 2H, C*H*=), 5.65 and 5.63 (2s, 4H, atropisomers CH_2O), 5.50-5.26 (m, 4H, =CH_2), 4.27 (m, 4H, OCH_2CH).

m.p. 160-162 ˚C.

IR (cm^{-1}, powder film): 3073 (w), 2868 (w), 2837 (w), 1611 (m), 1483 (m), 1431 (m), 1340 (m), 1123 (s), 1094 (s), 926 (m), 768 (s), 719 (s).

Elemental Analysis: calculated: C, 38.31%; H, 3.93%; N, 4.96%.

found: C, 38.35%; H, 3.93%; N, 4.97%.

^{1}H VT-NMR ($CDCl_3$), $NC_5H_4CH_2O$ signal: −50 ˚C, 5.605 and 5.584 (Δ = 6.2 Hz); −30 ˚C, 5.617 and 5.597 (Δ = 6.0 Hz); −10 ˚C, 5.624 and 5.606 (Δ = 5.9 Hz); 0 ˚C, 5.631 and 5.613 (Δ = 5.4 Hz); 10 ˚C, 5.638 and 5.620 (Δ = 5.2 Hz); 30 ˚C, 5.650 and 5.636 (Δ = 4.1 Hz); 35 ˚C, 5.650 and 5.642 (Δ = 3.0 Hz); 40 ˚C, 5.648 (Δ = 0 Hz).

Based upon the visual appearance of the spectra at 35 ˚C and 40 ˚C, the coalescence temperature (T_c) could be extrapolated as 311 K. The free energy of activation at the coalescence temperature was calculated to be 16.6 kcal/mol as follows:[33]

$\Delta G^{\ddagger} = RT_c[\ln(k_B/h) - \ln(k/T_c)]$

R is the gas constant (1.987×10^{-3} kcal/mol·K), k_B is the Boltzmann constant (3.300×10^{-27} kcal/K), h is the Planck constant (1.584×10^{-37} kcal·s), and $k = \pi\delta\upsilon/\sqrt{2}$, with δυ taken as the peak separation at 223 K (6.2 Hz).

***trans*-$PtCl_2(2\text{-}NC_5H_4(CH_2O(CH_2)_2CH{=}CH_2))_2$ (II) (*trans*-2b)**

$PtCl_2$ (1.1470 g, 4.3120 mmol) and **1b** (1.4989 g, 9.1833 mmol) were combined as described above (syntheses of metal complexes). This gave *trans*-**2b** (0.3065 g, 0.5174 mmol, 12.0%) as a light yellow solid. The broadened CH_2O ^{1}H NMR signal suggested a mixture of atropisomers.

^{1}H NMR ($CDCl_3$): δ 8.92 (m, 2H, *o*-HC_{6pyr}), 7.77 (m, 2H, *m*-HC_{5pyr}), 7.67 (m, 2H, *p*-HC_{pyr}), 7.24 (m, 2H, *m*-HC_{5pyr}), 5.96-5.87 (m, 2H, C*H*=), 5.64 (br s, 4H, CH_2O), 5.20-5.09 (m, 4H, =CH_2), 3.80 (t, 4H, $^3J_{HH}$ = 6.4 Hz, OCH_2CH_2), 2.50 (m, 4H, OCH_2CH_2).

m.p. 188-191 ˚C, decomposition.

IR (cm^{-1}, powder film): 2164 (w), 2012 (w), 1981 (w), 1611 (w), 1477 (w), 1439 (w), 1356 (m), 1130 (s), 1099 (s), 1001 (m), 924 (m), 773 (s), 721 (m).

Elemental Analysis: calculated: C, 40.55%; H, 4.42%; N, 4.73%.

found: C, 40.27%; H, 4.35%; N, 4.49%.

***trans*-$PtCl_2$[2,2′-($NC_5H_4(CH_2O(CH_2)_4OCH_2)H_4C_5N$)] (*trans*-3a)**

Grubbs′ first generation catalyst (0.0251 g, 0.0305 mmol, 3.97 mol%), *trans*-**2a** (0.4344 g, 0.7697 mmol), and Pd/C (0.0325 g of 10% w/w, 0.0305 mmol Pd, 3.97 mol%) were combined as described above (syntheses of macrocycles). This gave *trans*-**3a** (0.2593 g, 0.4187 mmol, 63%) as a light yellow solid.

^{1}H NMR ($CDCl_3$): δ 9.01 (m, 2H, *o*-HC_{6pyr}), 7.76 (m, 2H, *p*-HC_{4pyr}), 7.54 (m, 2H, *m*-HC_{3pyr}), 7.28 (m, 2H, *m*-HC_{5pyr}), 5.63 (s, 4H, CH_2O), 3.90 (m, 4H, OCH_2CH_2), 2.10 (m, 4H, OCH_2CH_2). $^{13}C\{^1H\}$ NMR ($CDCl_3$): δ 160.4 (*o*-C_{2pyr}), 154.7 (*o*-C_{6pyr}), 138.6 (*p*-C_{4pyr}), 126.7 (*m*-C_{3pyr}), 124.8 (*m*-C_{5pyr}), 72.2 (CH_2O), 69.8 (OCH_2CH_2), 24.6 (CH_2).

m.p. 227-229 ˚C, decomposition.

IR (cm^{-1}, powder film): 2966 (w), 2911 (w), 2851 (w), 2149 (w), 1981 (w), 1607 (m), 1437 (m), 1225 (m), 1109 (s), 930 (m), 789 (s), 772 (s).

Elemental Analysis: calculated: C, 35.70%; H, 3.74%; N, 5.20%.

found: C, 35.39%; H, 3.81%; N, 5.12%.

***trans*-$PtCl_2$[2,2′-($NC_5H_4(CH_2O(CH_2)_6OCH_2)H_4C_5N$)] (*trans*-3b)**

Grubbs′ first generation catalyst (two charges, 0.0132 g and 0.0126 g, 0.0314 mmol, 7.96 mol%), *trans*-**2b** (0.2334 g, 0.3940 mmol), and Pd/C (0.0174 g of 10% w/w, 0.0164 mmol Pd, 4.15 mol%) were combined as described above (syntheses of macrocycles). This gave *trans*-**3b** (0.1761 g, 0.3109 mmol, 79%) as an off white solid.

^{1}H NMR ($CDCl_3$): δ 8.91 (m, 2H, *o*-*H*C_{6pyr}), 7.76 (m, 2H, *p*-*H*C_{4pyr}), 7.63 (m, 2H, *m*-*H*C_{3pyr}), 7.24 (m, 2H, *m*-*H*C_{5pyr}), 5.77 (s, 4H, CH_2O), 3.87 (t, 4H, $^{3}J_{HH}$ = 6.4 Hz, OCH_2CH_2), 1.89 (m, 4H, OCH_2CH_2), 1.68 (m, 4H, OCH_2CH_2CH_2). ^{13}C{^{1}H} NMR ($CDCl_3$): δ 161.7 (*o*-C_{2pyr}), 153.5 (*o*-C_{6pyr}), 138.5 (*p*-C_{4pyr}), 124.1 (*m*-C_{3pyr}), 124.0 (*m*-C_{5pyr}), 71.8 (*C*H_2O), 70.2 (O*C*H_2CH_2), 27.3 (CH_2), 23.9 (CH_2).

m.p. 242-244 ˚C, decomposition.

IR (cm^{-1}, powder film): 3061 (w), 2941 (m), 2859 (m), 1607 (m), 1570 (m), 1477 (m), 1229 (m), 1126 (s), 1101 (s), 787 (s), 768 (s), 719 (s).

Elemental Analysis: calculated: C, 38.17%; H, 4.27%; N, 4.95%.

found: C, 38.57%; H, 4.29%; N, 4.96%.

3-NC_5H_4($CH_2OCH_2CH=CH_2$) (4a)

Allyl alcohol (14.1138 g, 243.006 mmol), sodium (0.9319 g, 40.54 mmol), and 3-(chloromethyl)pyridine hydrochloride (2.2593 g, 13.773 mmol) were combined as described above (ligand synthesis; sodium dissolved and reaction conducted at 80 °C for 12 h). This gave **4a** (1.7175 g, 11.512 mmol, 84%) as a yellow-brown oil.

^{1}H NMR ($CDCl_3$): δ 8.58 (m, 1H, *o*-*H*C_{2pyr}), 8.54 (m, 1H, *o*-*H*C_{6pyr}), 7.69 (m, 1H, *p*-*H*C_{4pyr}), 7.28 (m, 1H, *m*-*H*C_{5pyr}), 6.01-5.88 (ddt, 1H, $^{3}J_{HH}$*trans* = 17.3 Hz, $^{3}J_{HH}$*cis* = 10.4 Hz, $^{3}J_{HH}$ = 5.6 Hz, C*H*=), 5.32 (dt, 1H, $^{3}J_{HH}$ = 17.3 Hz, $^{2}J_{HH}$ = 1.7 Hz =CH_EH$_Z$), 5.23 (dt, 1H, $^{3}J_{HH}$ = 10.4 Hz, $^{2}J_{HH}$ = 1.7 Hz =CH$_E$$H_Z$), 4.53 (s, 2H, C$H_2$O), 4.05 (dt, 2H, $^{3}J_{HH}$ = 5.6 Hz, $^{4}J_{HH}$ = 1.4 Hz, OCH_2CH). ^{13}C{^{1}H} NMR ($CDCl_3$): δ 149.4 and 149.3 (*o*-C_{2pyr} and *o*-C_{6pyr}), 135.6 (*C*H=), 134.5 (*p*-C_{4pyr}), 133.9 (*m*-C_{3pyr}), 123.6 (*m*-C_{5pyr}), 117.8 (=*C*H_2), 71.8 (*C*H_2O), 69.7 (O*C*H_2CH_2).

IR (cm^{-1}, neat oil): 2857 (w), 1724 (w), 1578 (m), 1425 (m), 1082 (s), 1026 (m), 926 (m), 791 (m), 712 (s).

3-$NC_5H_4(CH_2O(CH_2)_2CH=CH_2)$ (4b)

3-Buten-1-ol (23.1913 g, 321.624 mmol), sodium (1.0569 g, 45.973 mmol), and 3-(chloromethyl)pyridine hydrochloride (2.4873 g, 15.163 mmol) were combined as described above (ligand synthesis; sodium dissolved and reaction conducted at 80 °C for 12 h). This gave **4b** (2.2722 g, 13.921 mmol, 92%) as a yellow-brown oil.

^{1}H NMR ($CDCl_3$): δ 8.57 (m, 1H, *o*-*H*C_{2pyr}), 8.53 (m, 1H, *o*-*H*C_{6pyr}), 7.67 (m, 1H, *p*-*H*C_{4pyr}), 7.27 (m, 1H, *m*-*H*C_{5pyr}), 5.90-5.76 (ddt, 1H, $^3J_{HH}$*trans* = 17.0 Hz, $^3J_{HH}$*cis* = 10.2 Hz, $^3J_{HH}$ = 6.8 Hz, C*H*=), 5.14-5.02 (m, 2H, =CH_2), 4.53 (s, 2H, CH_2O), 3.54 (t, 2H, $^3J_{HH}$ = 6.8 Hz, OCH_2CH_2), 2.38 (qt, 2H, $^3J_{HH}$ = 6.6 Hz, $^3J_{HH}$ = 1.4 Hz, OCH_2CH_2). ^{13}C{^{1}H} NMR ($CDCl_3$): δ 149.34 and 149.28 (*o*-C_{2pyr} and *o*-C_{6pyr}), 135.5 (*C*H=), 135.2 (*p*-C_{4pyr}), 134.0 (*m*-C_{3pyr}), 123.6 (*m*-C_{5pyr}), 116.8 (=*C*H_2), 70.6 (*C*H_2O), 70.1 (O*C*H_2CH_2), 34.3 (*C*H_2).

IR (cm^{-1}, neat oil): 2860 (w), 1722 (s), 1591 (m), 1427 (m), 1283 (s), 1096 (s), 1024 (s), 916 (s), 791 (m), 743 (s), 712 (s).

3-$NC_5H_4(CH_2O(CH_2)_3CH=CH_2)$ (4c)

4-Penten-1-ol (27.3842 g, 39.7926 mmol), sodium (1.0307 g, 44.833 mmol), and 2-(chloromethyl)pyridine hydrochloride (2.9548 g, 18.013 mmol) were combined as described above (ligand synthesis; sodium dissolved at 80 °C and reaction conducted at 100 °C for 12 h). This gave **4c** (2.2281 g, 12.571 mmol, 70%) as a yellow oil.

^{1}H NMR ($CDCl_3$): δ 8.57 (m, 1H, *o*-*H*C_{2pyr}), 8.53 (m, 1H, *o*-*H*C_{6pyr}), 7.68 (m, 1H, *p*-*H*C_{4pyr}), 7.28 (m, 1H, *m*-*H*C_{5pyr}), 5.87-5.73 (ddt, 1H, $^3J_{HH}$*trans* = 17.1 Hz, $^3J_{HH}$*cis* = 10.3 Hz, $^3J_{HH}$ = 6.6 Hz, C*H*=), 5.05-4.93 (m, 2H, =CH_2), 4.51 (s, 2H, CH_2O), 3.50 (t, 2H, $^3J_{HH}$ = 6.5 Hz, OCH_2CH_2), 2.14 (m, 2H, CH_2CH=CH_2), 1.71 (m, 2H, OCH_2CH_2). ^{13}C{^{1}H} NMR ($CDCl_3$): δ 149.2 and 149.1 (*o*-C_{2pyr} and *o*-C_{6pyr}), 138.3

(*C*H=), 135.6 (*p*-C_{4pyr}), 134.2 (*m*-C_{3pyr}), 123.6 (*m*-C_{5pyr}), 115.1 (=*C*H_2), 70.5 (*C*H_2O), 70.3 (O*C*H_2CH_2), 30.5 (*C*H_2), 29.0 (*C*H_2).

IR (cm^{-1}, neat oil): 2938 (m), 2860 (m), 1722 (s), 1427 (m), 1281 (s), 1097 (s), 912 (s), 712 (s).

3-$NC_5H_4(CH_2O(CH_2)_4CH=CH_2)$ (4d)

5-Hexen-1-ol (12.9850 g, 129.642 mmol), sodium (0.7838 g, 34.09 mmol), and 3-(chloromethyl)pyridine hydrochloride (1.9432 g, 11.846 mmol) were combined as described above (ligand synthesis; sodium dissolved and reaction conducted at 100 °C for 12 h). This gave **4d** (1.0806 g, 5.6496 mmol, 48%) as a yellow-brown oil.

^{1}H NMR ($CDCl_3$): δ 8.56 (m, 1H, *o*-*H*C_{2pyr}), 8.53 (m, 1H, *o*-*H*C_{6pyr}), 7.67 (m, 1H, *p*-*H*C_{4pyr}), 7.27 (m, 1H, *m*-*H*C_{5pyr}), 5.87-5.72 (ddt, 1H, $^3J_{HH}$*trans* = 17.0 Hz, $^3J_{HH}$*cis* = 10.3 Hz, $^3J_{HH}$ = 6.6 Hz, C*H*=), 5.04-4.91 (m, 2H, =CH_2), 4.50 (s, 2H, CH_2O), 3.49 (t, 2H, $^3J_{HH}$ = 6.5 Hz, OCH_2CH_2), 2.06 (m, 2H, CH_2CH=CH_2), 1.63 (m, 2H, OCH_2CH_2), 1.46 (m, 2H, OCH_2CH_2CH_2). ^{13}C{^{1}H} NMR ($CDCl_3$): δ 152.7 and 152.5 (*o*-C_{2pyr} and *o*-C_{6pyr}), 138.8 (*C*H=), 137.4 (*p*-C_{4pyr}), 136.8 (*m*-C_{3pyr}), 125.1 (*m*-C_{5pyr}), 114.9 (=*C*H_2), 71.2 (*C*H_2O), 69.3 (O*C*H_2CH_2), 33.7 (*C*H_2), 29.2 (*C*H_2), 25.6 (*C*H_2).

IR (cm^{-1}, neat oil): 2934 (m), 2859 (m), 1639 (m), 1429 (m), 1097 (s), 1028 (m), 933 (m), 791 (m), 712 (s).

3-$NC_5H_4(CH_2O(CH_2)_5CH=CH_2)$ (4e)

6-Hepten-1-ol (23.7783 g, 208.239 mmol), sodium (0.6665 g, 28.93 mmol) and 2-(chloromethyl)pyridine hydrochloride (1.9377 g, 11.813 mmol) were combined as described above (ligand synthesis; sodium dissolved and reaction conducted at 100 °C for 12 h). This gave **4e** (1.9577 g, 9.5358 mmol, 81%) as a yellow-brown oil.

^{1}H NMR ($CDCl_3$): δ 8.56 (m, 1H, *o*-*H*C_{2pyr}), 8.52 (m, 1H, *o*-*H*C_{6pyr}), 7.68 (m, 1H, *p*-*H*C_{4pyr}), 7.28 (m, 1H, *m*-*H*C_{5pyr}), 5.86-5.73 (ddt, 1H, $^3J_{HH}$*trans* = 17.1 Hz,

$^{3}J_{HHcis}$ = 10.3 Hz, $^{3}J_{HH}$ = 6.6 Hz, C*H*=), 5.03-4.90 (m, 2H, =CH_2), 4.50 (s, 2H, CH_2O), 3.48 (t, 2H, $^{3}J_{HH}$ = 6.6 Hz, OCH_2CH$_2$), 2.04 (m, 2H, CH_2CH=CH$_2$), 1.62 (m, 2H, OCH$_2$CH_2), 1.44-1.34 (m, 4H, -CH_2-). ^{13}C{^{1}H} NMR ($CDCl_3$): δ 149.2 and 149.0 (*o*-C_{2pyr} and *o*-C_{6pyr}), 139.1 (*C*H=), 135.6 (*p*-C_{4pyr}), 134.3 (*m*-C_{3pyr}), 123.6 (*m*-C_{5pyr}), 114.6 (=*C*H$_2$), 71.0 (*C*H$_2$O), 70.5 (O*C*H$_2$CH$_2$), 33.9 (*C*H$_2$), 29.7 (*C*H$_2$), 28.9 (*C*H$_2$), 25.8 (*C*H$_2$).

IR (cm^{-1}, neat oil): 2932 (m), 2859 (m), 1722 (s), 1420 (m), 1281 (s), 1113 (s), 1024 (m), 910 (m), 743 (s), 702 (s).

3-NC$_5$H$_4$(CH$_2$O(CH$_2$)$_8$CH=CH$_2$) (4h)

9-Decen-1-ol (16.7254 g, 107.030 mmol), sodium (0.3096 g, 13.47 mmol), and 3-(chloromethyl)pyridine hydrochloride (0.8856 g, 5.399 mmol) were combined as described above (ligand synthesis; sodium dissolved at 100 °C and reaction conducted at 125 °C for 16 h). This gave **4h** (1.1231 g, 4.5400 mmol, 84%) as a yellow-brown oil.

^{1}H NMR ($CDCl_3$): δ 8.57 (m, 1H, *o*-*H*C$_{2pyr}$), 8.53 (m, 1H, *o*-*H*C$_{6pyr}$), 7.68 (m, 1H, *p*-*H*C$_{4pyr}$), 7.27 (m, 1H, *m*-*H*C$_{5pyr}$), 5.87-5.73 (ddt, 1H, $^{3}J_{HHtrans}$ = 17.1 Hz, $^{3}J_{HHcis}$ = 10.3 Hz, $^{3}J_{HH}$ = 6.6 Hz, C*H*=), 5.02-4.89 (m, 2H, =CH_2), 4.51 (s, 2H, CH_2O), 3.48 (t, 2H, $^{3}J_{HH}$ = 6.6 Hz, OCH_2CH$_2$), 2.03 (m, 2H, CH_2CH=CH$_2$), 1.61 (m, 2H, OCH$_2$CH_2), 1.45-1.27 (m, 12H, -CH_2-). ^{13}C{^{1}H} NMR ($CDCl_3$): δ 149.4 and 149.2 (*o*-C_{2pyr} and *o*-C_{6pyr}), 139.4 (*C*H=), 135.5 (*p*-C_{4pyr}), 134.2 (*m*-C_{3pyr}), 123.6 (*m*-C_{5pyr}), 114.3 (=*C*H$_2$), 71.1 (*C*H$_2$O), 70.5 (O*C*H$_2$CH$_2$), 34.0 (*C*H$_2$), 29.9 (*C*H$_2$), 29.6 (2 × *C*H$_2$), 29.3 (*C*H$_2$), 29.1 (*C*H$_2$), 26.3 (*C*H$_2$).

IR (cm^{-1}, neat oil): 2926 (s), 2854 (s), 1724 (s), 1281 (s), 1111 (s), 1024 (m), 908 (s), 743 (s), 710 (s).

3-$NC_5H_4(CH_2O(CH_2)_9CH=CH_2)$ (4i)

10-Undecen-1-ol (23.3818 g, 137.308 mmol), sodium (0.4430 g, 19.27 mmol), and 2-(chloromethyl)pyridine hydrochloride (1.4139 g, 8.6195 mmol) were combined as described above (ligand synthesis; sodium dissolved at 100 °C and reaction conducted at 125 °C for 16 h). This gave **4i** (1.7982 g, 6.8791 mmol, 80%) as a yellow-brown oil.

^{1}H NMR ($CDCl_3$): δ 8.57 (m, 1H, *o*-*H*C_{2pyr}), 8.53 (m, 1H, *o*-*H*C_{6pyr}), 7.68 (m, 1H, *p*-*H*C_{4pyr}), 7.28 (m, 1H, *m*-*H*C_{5pyr}), 5.85-5.76 (ddt, 1H, $^3J_{HH}$*trans* = 17.1 Hz, $^3J_{HH}$*cis* = 10.3 Hz, $^3J_{HH}$ = 6.8 Hz, C*H*=), 5.01-4.91 (m, 2H, =CH_2), 4.51 (s, 2H, CH_2O), 3.48 (t, 2H, $^3J_{HH}$ = 6.5 Hz, OCH_2CH_2), 2.03 (m, 2H, CH_2CH=CH_2), 1.61 (m, 2H, OCH_2CH_2), 1.40-1.24 (m, 12H, -CH_2-). ^{13}C{^{1}H} NMR ($CDCl_3$): δ 148.9 and 148.8 (*o*-C_{2pyr} and *o*-C_{6pyr}), 139.2 (*C*H=), 135.5 (*p*-C_{4pyr}), 134.1 (*m*-C_{3pyr}), 123.4 (*m*-C_{5pyr}), 114.1 (=*C*H_2), 70.9 (*C*H_2O), 70.3 (O*C*H_2CH_2), 33.8 (*C*H_2), 29.7 (*C*H_2), 29.4 (2 × *C*H_2), 29.4 (*C*H_2), 29.1 (2 × *C*H_2), 26.1 (*C*H_2).

IR (cm^{-1}, neat oil): 2924 (s), 2853 (s), 1724 (s), 1427 (m), 1281 (s), 1098 (s), 908 (s), 712 (s).

***trans*-$PtCl_2$(3-$NC_5H_4(CH_2OCH_2CH=CH_2))_2$ (*trans*-5a)**

$PtCl_2$ (1.0038 g, 3.7738 mmol) and **4a** (1.2028 g, 8.0620 mmol) were combined as described above (syntheses of metal complexes). This gave *trans*-**5a** (1.8265 g, 3.236 mmol, 86%) as a yellow solid.

^{1}H NMR ($CDCl_3$): δ 8.84 (m, 2H, *o*-*H*C_{2pyr}), 8.80 (m, 2H, *o*-*H*C_{6pyr}), 7.80 (m, 2H, *p*-*H*C_{4pyr}), 7.29 (m, 2H, *m*-*H*C_{5pyr}), 6.00-5.87 (ddt, 2H, $^3J_{HH}$*trans* = 17.0 Hz, $^3J_{HH}$*cis* = 10.4 Hz, $^3J_{HH}$ = 6.8 Hz, C*H*=), 5.32-5.18 (m, 4H, =CH_2), 4.54 (s, 4H, CH_2O), 4.07 (m, 4H, OCH_2CH). ^{13}C{^{1}H} NMR ($CDCl_3$): δ 152.8 and 152.6 (*o*-C_{2pyr} and *o*-C_{6pyr}), 137.6 (*C*H=), 136.6 (*p*-C_{4pyr}), 134.1 (*m*-C_{3pyr}), 125.1 (*m*-C_{5pyr}), 118.3 (=*C*H_2), 72.0 (*C*H_2O), 68.4 (O*C*H_2CH_2).

m.p. 120-121 ˚C.

IR (cm^{-1}, powder film): 2924 (w), 2857 (w), 1609 (w), 1423 (m), 1096 (s), 924 (s), 800 (s), 696 (s).

Elemental Analysis: calculated: C, 38.31%; H, 3.93%; N, 4.96%.

found: C, 38.28%; H, 3.81%; N, 4.96%.

$PtCl_2$(3-$NC_5H_4(CH_2O(CH_2)_2CH=CH_2))_2$ (*cis* and *trans*-5b)

$PtCl_2$ (1.0233 g, 3.8471 mmol) and **4b** (1.3203 g, 8.0891 mmol) were combined as described above (syntheses of metal complexes). This gave *trans*-**5b** (1.1204 g, 1.8912 mmol, 49%) and *cis*-**5b** (0.9764 g, 1.648 mmol, 43%) as yellow solids.

trans-**5b**: ^{1}H NMR ($CDCl_3$): δ 8.83 (m, 2H, *o*-*H*C_{2pyr}), 8.80 (m, 2H, *o*-*H*C_{6pyr}), 7.78 (m, 2H, *p*-*H*C_{4pyr}), 7.29 (m, 2H, *m*-*H*C_{5pyr}), 5.91-5.76 (ddt, 2H, $^3J_{HHtrans}$ = 17.0 Hz, $^3J_{HHcis}$ = 10.4 Hz, $^3J_{HH}$ = 6.8 Hz, C*H*=), 5.16-5.04 (m, 4H, =CH_2), 4.53 (s, 4H, CH_2O), 3.56 (t, 4H, $^3J_{HH}$ = 6.6 Hz, OCH_2CH_2), 2.39 (qt, 4H, $^3J_{HH}$ = 6.6 Hz, $^3J_{HH}$ = 1.4 Hz, CH_2CH=CH_2). ^{13}C{^{1}H} NMR ($CDCl_3$): δ 152.8 and 152.5 (*o*-C_{2pyr} and *o*-C_{6pyr}), 137.5 (*C*H=), 136.7 (*p*-C_{4pyr}), 135.0 (*m*-C_{3pyr}), 125.1 (*m*-C_{5pyr}), 117.0 (=*C*H_2), 70.5 (*C*H_2O), 69.3 (O*C*H_2CH_2), 34.3 (*C*H_2).

m.p. 118-119 ˚C.

IR (cm^{-1}, powder film): 2943 (w), 2870 (m), 1641 (m), 1477 (m), 1436 (s), 1364 (m), 1101 (s), 927 (s), 799 (s).

Elemental Analysis: calculated: C, 40.55%; H, 4.42%; N, 4.73%.

found: C, 40.50%; H, 4.37%; N, 4.71%.

cis-**5b**: ^{1}H NMR ($CDCl_3$): δ 8.85 (m, 4H, *o*-*H*C_{2pyr} and *o*-*H*C_{6pyr}), 7.75 (m, 2H, *p*-*H*C_{4pyr}), 7.27 (m, 2H, *m*-*H*C_{5pyr}), 5.84-5.70 (ddt, 2H, $^3J_{HHtrans}$ = 17.3 Hz, $^3J_{HHcis}$ = 10.3 Hz, $^3J_{HH}$ = 6.6 Hz, C*H*=), 5.12-5.01 (m, 4H, =CH_2), 4.47 (s, 4H, CH_2O), 3.50 (t, 4H, $^3J_{HH}$ = 6.6 Hz, OCH_2CH_2), 2.32 (qt, 4H, $^3J_{HH}$ = 6.6 Hz, $^3J_{HH}$ = 1.4 Hz,

CH_2CH=CH_2). ^{13}C{^{1}H} NMR ($CDCl_3$): δ 152.1 and 151.7 (*o*-C_{2pyr} and *o*-C_{6pyr}), 137.9 (*C*H=), 137.5 (*p*-C_{4pyr}), 134.9 (*m*-C_{3pyr}), 126.2 (*m*-C_{5pyr}), 117.0 (=*C*H_2), 70.6 (*C*H_2O), 69.0 (O*C*H_2CH_2), 34.2 (*C*H_2).

m.p. 54-56 ˚C.

IR (cm^{-1}, powder film): 3068 (w), 2904 (w), 2860 (w), 1608 (m), 1479 (m), 1437 (m), 1098 (s), 912 (s), 702 (s).

***trans*-$PtCl_2$(3-NC_5H_4($CH_2O(CH_2)_3CH=CH_2$))$_2$ (*trans*-5c)**

$PtCl_2$ (1.1893 g, 4.4711 mmol) and **4c** (1.6721 g, 9.4338 mmol) were combined as described above (syntheses of metal complexes). This gave *trans*-**5c** (2.3537 g, 3.793 mmol, 85%) as a yellow solid.

^{1}H NMR ($CDCl_3$): δ 8.84 (m, 2H, *o*-*H*C_{2pyr}), 8.81 (m, 2H, *o*-*H*C_{6pyr}), 7.78 (m, 2H, *p*-*H*C_{4pyr}), 7.29 (m, 2H, *m*-*H*C_{5pyr}), 5.86-5.78 (ddt, 2H, $^3J_{HH}$*trans* = 17.0 Hz, $^3J_{HH}$*cis* = 10.1 Hz, $^3J_{HH}$ = 6.4 Hz, C*H*=), 5.07-4.97 (m, 4H, =CH_2), 4.52 (s, 4H, CH_2O), 3.52 (t, 4H, $^3J_{HH}$ = 6.4 Hz, OCH_2CH_2), 2.16 (m, 4H, CH_2CH=CH_2), 1.74 (m, 4H, OCH_2CH_2). ^{13}C{^{1}H} NMR ($CDCl_3$): δ 152.8 and 152.6 (*o*-C_{2pyr} and *o*-C_{6pyr}), 138.2 (*C*H=), 137.4 (*p*-C_{4pyr}), 136.8 (*m*-C_{3pyr}), 125.1 (*m*-C_{5pyr}), 115.2 (=*C*H_2), 70.7 (*C*H_2O), 69.3 (O*C*H_2CH_2), 30.4 (*C*H_2), 29.0 (*C*H_2).

m.p. 77-79 ˚C.

IR (cm^{-1}, powder film): 2938 (m), 2872 (m), 1643 (m), 1611 (m), 1441 (m), 1366 (m), 1096 (s), 1078 (s), 988 (m), 926 (m), 816 (s), 698 (s), 638 (m).

Elemental Analysis: calculated: C, 42.59%; H, 4.87%; N, 4.51%.

found: C, 43.00%; H, 4.78%; N, 4.10%.

***trans*-$PtCl_2(3\text{-}NC_5H_4(CH_2O(CH_2)_4CH{=}CH_2))_2$ (*trans*-5d)**

$PtCl_2$ (1.4588 g, 5.4844 mmol) and **4d** (2.2421 g, 11.722 mmol) were combined as described above (syntheses of metal complexes). This gave *trans*-**5d** (2.9313 g, 4.5199 mmol, 82%) as a yellow solid.

^{1}H NMR ($CDCl_3$): δ 8.83 (m, 2H, *o*-*H*C_{2pyr}), 8.80 (m, 2H, *o*-*H*C_{6pyr}), 7.78 (m, 2H, *p*-*H*C_{4pyr}), 7.29 (m, 2H, *m*-*H*C_{5pyr}), 5.88-5.74 (ddt, 2H, $^3J_{HH}$*trans* = 17.0 Hz, $^3J_{HH}$*cis* = 10.3 Hz, $^3J_{HH}$ = 6.6 Hz, C*H*=), 5.06-4.93 (m, 4H, =CH_2), 4.51 (s, 4H, CH_2O), 3.50 (t, 4H, $^3J_{HH}$ = 6.4 Hz, OCH_2CH_2), 2.08 (m, 4H, CH_2CH=CH_2), 1.65 (m, 4H, OCH_2CH_2), 1.48 (m, 4H, OCH_2CH_2CH_2). ^{13}C{^{1}H} NMR ($CDCl_3$): δ 152.7 and 152.5 (*o*-C_{2pyr} and *o*-C_{6pyr}), 138.8 (*C*H=), 137.4 (*p*-C_{4pyr}), 136.8 (*m*-C_{3pyr}), 125.1 (*m*-C_{5pyr}), 114.9 (=*C*H_2), 71.2 (*C*H_2O), 69.3 (O*C*H_2CH_2), 33.7 (*C*H_2), 29.2 (*C*H_2), 25.6 (*C*H_2).

m.p. 85-87 ˚C.

IR (cm^{-1}, powder film): 2934 (m), 2872 (m), 1641 (w), 1611 (w), 1483 (w), 1439 (m), 1369 (m), 1084 (s), 995 (m), 920 (s), 808 (s), 698 (s), 650 (m).

Elemental Analysis: calculated: C, 44.45%; H, 5.28%; N, 4.32%.

found: C, 44.71%; H, 4.97%; N, 4.24%.

***trans*-$PtCl_2(3\text{-}NC_5H_4(CH_2O(CH_2)_5CH{=}CH_2))_2$ (*trans*-5e)**

$PtCl_2$ (0.9657 g, 3.630 mmol) and **4e** (1.5794 g, 7.6913 mmol) were combined as described above (syntheses of metal complexes). This gave *trans*-**5e** (2.2861 g, 3.3789 mmol, 93%) as a yellow solid.

^{1}H NMR ($CDCl_3$): δ 8.83 (m, 2H, *o*-*H*C_{2pyr}), 8.80 (m, 2H, *o*-*H*C_{6pyr}), 7.78 (m, 2H, *p*-*H*C_{4pyr}), 7.28 (m, 2H, *m*-*H*C_{5pyr}), 5.85-5.77 (ddt, 2H, $^3J_{HH}$*trans* = 17.0 Hz, $^3J_{HH}$*cis* = 10.1 Hz, $^3J_{HH}$ = 6.9 Hz, C*H*=), 5.02-4.92 (m, 4H, =CH_2), 4.51 (s, 4H, CH_2O), 3.49 (t, 4H, $^3J_{HH}$ = 6.4 Hz, OCH_2CH_2), 2.06 (m, 4H, CH_2CH=CH_2), 1.63 (m, 4H, OCH_2CH_2), 1.44-1.36 (m, 8H, -CH_2-). ^{13}C{^{1}H} NMR ($CDCl_3$): δ 152.7 and 152.5 (*o*-

C_{2pyr} and *o*-C_{6pyr}), 139.1 (*C*H=), 137.4 (*p*-C_{4pyr}), 136.9 (*m*-C_{3pyr}), 125.0 (*m*-C_{5pyr}), 114.6 (=*C*H_2), 71.4 (*C*H_2O), 69.3 (O*C*H_2CH_2), 33.9 (*C*H_2), 29.7 (*C*H_2), 28.9 (*C*H_2), 25.8 (*C*H_2).

m.p. 86-88 ˚C.

IR (cm^{-1}, powder film): 2931 (m), 2872 (m), 2851 (m), 1643 (w), 1610 (w), 1440 (m), 1089 (s), 986 (m), 924 (s), 816 (s), 698 (s), 648 (m).

Elemental Analysis: calculated: C, 46.16%; H, 4.91%; N, 4.14%.

found: C, 46.21%; H, 4.91%; N, 4.11%.

$PtCl_2$(3-NC_5H_4($CH_2O(CH_2)_8CH=CH_2$))$_2$ (cis and *trans*-5h)

$PtCl_2$ (0.5188 g, 1.950 mmol) and **4h** (1.0658 g, 4.3084 mmol) were combined as described above (syntheses of metal complexes). This gave *trans*-**5h** (0.6785 g, 0.8919 mmol, 46%) and *cis*-**5h** (0.6558 g, 0.8621 mmol, 44%) as yellow solids.

trans-**5h**: ^{1}H NMR ($CDCl_3$): δ 8.83 (m, 2H, *o*-*H*C_{2pyr}), 8.80 (m, 2H, *o*-*H*C_{6pyr}), 7.79 (m, 2H, *p*-*H*C_{4pyr}), 7.29 (m, 2H, *m*-*H*C_{5pyr}), 5.88-5.74 (ddt, 2H, $^3J_{HH}$*trans* = 17.0 Hz, $^3J_{HH}$*cis* = 10.4 Hz, $^3J_{HH}$ = 6.6 Hz, C*H*=), 5.03-4.89 (m, 4H, =CH_2), 4.51 (s, 4H, CH_2O), 3.49 (t, 4H, $^3J_{HH}$ = 6.6 Hz, OCH_2CH_2), 2.04 (m, 4H, CH_2CH=CH_2), 1.62 (m, 4H, OCH_2CH_2), 1.44-1.25 (m, 24H, -CH_2-). ^{13}C{^{1}H} NMR ($CDCl_3$): δ 152.7 and 152.5 (*o*-C_{2pyr} and *o*-C_{6pyr}), 139.4 (*C*H=), 137.5 (*p*-C_{4pyr}), 136.9 (*m*-C_{3pyr}), 125.1 (*m*-C_{5pyr}), 114.3 (=*C*H_2), 71.5 (*C*H_2O), 69.3 (O*C*H_2CH_2), 34.0 (*C*H_2), 29.8 (*C*H_2), 29.6 (2 × *C*H_2), 29.3 (*C*H_2), 29.1 (*C*H_2), 26.3 (*C*H_2).

m.p. 101-102 ˚C.

IR (cm^{-1}, powder film): 2918 (m), 2849 (m), 2357 (w), 1641 (w), 1464 (w), 1439 (w), 1369 (m), 1258 (w), 1227 (w), 1093 (s), 926 (s), 810 (s), 698 (s), 644 (m).

Elemental Analysis: calculated: C, 50.52%; H, 6.62%; N, 3.68%.

found: C, 50.64%; H, 5.78%; N, 3.53%.

cis-**5h**: ^{1}H NMR ($CDCl_3$): δ 8.89 (m, 2H, *o*-*H*C_{2pyr}), 8.86 (m, 2H, *o*-*H*C_{6pyr}), 7.73 (m, 2H, *p*-*H*C_{4pyr}), 7.26 (m, 2H, *m*-*H*C_{5pyr}), 5.85-5.71 (ddt, 2H, $^{3}J_{HHtrans}$ = 17.0 Hz, $^{3}J_{HHcis}$ = 10.2 Hz, $^{3}J_{HH}$ = 6.6 Hz, C*H*=), 5.00-4.87 (m, 4H, =CH_2), 4.42 (s, 4H, CH_2O), 3.41 (t, 4H, $^{3}J_{HH}$ = 6.6 Hz, OCH_2CH_2), 2.06-1.97 (m, 4H, CH_2CH=CH_2), 1.59-1.48 (m, 4H, OCH$_2$CH_2), 1.40-1.22 (m, 24H, -CH_2-). ^{13}C{^{1}H} NMR ($CDCl_3$): δ 152.1 and 151.7 (*o*-C_{2pyr} and *o*-C_{6pyr}), 139.3 (*C*H=), 138.0 (*p*-C_{4pyr}), 137.4 (*m*-C_{3pyr}), 126.1 (*m*-C_{5pyr}), 114.3 (=*C*H$_2$), 71.5 (*C*H$_2$O), 68.9 (O*C*H$_2$CH$_2$), 33.9 (*C*H$_2$), 29.7 (*C*H$_2$), 29.5 (2 × *C*H$_2$), 29.2 (*C*H$_2$), 29.0 (*C*H$_2$), 26.2 (*C*H$_2$).

***trans*-$PtCl_2$(3-NC_5H_4($CH_2O(CH_2)_9CH=CH_2$))$_2$ (*trans*-5i)**

$PtCl_2$ (0.7101 g, 2.670 mmol) and **4i** (1.4690 g, 5.6196 mmol) were combined as described above (syntheses of metal complexes). This gave *trans*-**5i** (1.8760 g, 2.3783 mmol, 89%) as a yellow solid.

^{1}H NMR ($CDCl_3$): δ 8.83 (m, 2H, *o*-*H*C_{2pyr}), 8.80 (m, 2H, *o*-*H*C_{6pyr}), 7.79 (m, 2H, *p*-*H*C_{4pyr}), 7.29 (m, 2H, *m*-*H*C_{5pyr}), 5.85-5.77 (ddt, 2H, $^{3}J_{HHtrans}$ = 17.0 Hz, $^{3}J_{HHcis}$ = 10.1 Hz, $^{3}J_{HH}$ = 6.9 Hz, C*H*=), 5.01-4.91 (m, 4H, =CH_2), 4.51 (s, 4H, CH_2O), 3.49 (t, 4H, $^{3}J_{HH}$ = 6.4 Hz, OCH_2CH_2), 2.03 (m, 4H, CH_2CH=CH_2), 1.62 (m, 4H, OCH$_2$CH_2), 1.40-1.26 (m, 24H, -CH_2-). ^{13}C{^{1}H} NMR ($CDCl_3$): δ 152.7 and 152.5 (*o*-C_{2pyr} and *o*-C_{6pyr}), 139.5 (*C*H=), 137.4 (*p*-C_{4pyr}), 136.9 (*m*-C_{3pyr}), 125.1 (*m*-C_{5pyr}), 114.3 (=*C*H$_2$), 71.5 (*C*H$_2$O), 69.3 (O*C*H$_2$CH$_2$), 34.0 (*C*H$_2$), 29.8 (*C*H$_2$), 29.7 (*C*H$_2$), 29.6 (2 × *C*H$_2$), 29.3 (*C*H$_2$), 29.1 (*C*H$_2$), 26.3 (*C*H$_2$).

m.p. 102-103 ˚C.

IR (cm^{-1}, powder film): 2920 (s), 2847 (s), 2324 (w), 1641 (w), 1611 (w), 1462 (m), 1366 (m), 1096 (s), 920 (s), 810 (s), 700 (s).

Elemental Analysis: calculated: C, 51.77%; H, 6.90%; N, 3.55%.

found: C, 51.71%; H, 6.00%; N, 3.40%.

***trans*-$PtCl_2[3,3'-(NC_5H_4(CH_2O(CH_2)_{10}OCH_2)H_4C_5N)]$ (*trans*-6d)**

Grubbs′ first generation catalyst (0.0254 g, 0.0306 mmol, 3.85 mol%), *trans*-**5d** (0.5158 g, 0.7953 mmol), and Pd/C (0.0423 g of 10% w/w, 0.0398 mmol Pd, 5.00 mol%) were combined as described above (syntheses of macrocycles). This gave *trans*-**6d** (0.4615 g, 0.7414 mmol, 93%) as a light yellow solid.

^{1}H NMR ($CDCl_3$): δ 9.05 (m, 2H, *o*-*H*C_{2pyr}), 8.82 (m, 2H, *o*-*H*C_{6pyr}), 7.54 (m, 2H, *p*-*H*C_{4pyr}), 7.23 (m, 2H, *m*-*H*C_{5pyr}), 4.53 (s, 4H, C*H*$_2$O), 3.54 (t, 4H, $^3J_{HH}$ = 5.7 Hz, OC*H*$_2$CH$_2$), 1.64 (m, 4H, OCH$_2$C*H*$_2$), 1.56 (m, 4H, O(CH$_2$)$_2$C*H*$_2$), 1.45-1.35 (m, 8H, -C*H*$_2$-). ^{13}C{^{1}H} NMR ($CDCl_3$): δ 153.1 and 152.5 (*o*-*C*$_{2pyr}$ and *o*-*C*$_{6pyr}$), 136.8 (*p*-*C*$_{4pyr}$), 136.5 (*m*-*C*$_{3pyr}$), 124.5 (*m*-*C*$_{5pyr}$), 71.3 (*C*H$_2$O), 69.6 (OC*H*$_2$CH$_2$), 30.1 (*C*H$_2$), 29.8 (*C*H$_2$), 29.4 (*C*H$_2$), 26.5 (*C*H$_2$).

m.p. 204-208 ˚C.

IR (cm^{-1}, powder film): 2922 (m), 2853 (m), 1609 (w), 1439 (m), 1358 (m), 1315 (m), 1103 (s), 802 (s), 698 (s).

Elemental Analysis: calculated: C, 42.45%; H, 5.18%; N, 4.50%.

found: C, 42.52%; H, 4.78%; N, 4.45%.

***trans*-$PtCl_2[3,3'-(NC_5H_4(CH_2O(CH_2)_{18}OCH_2)H_4C_5N)]$ (*trans*-6h)**

Grubbs′ first generation catalyst (0.0237 g, 0.0288 mmol, 4.97 mmol%), *trans*-**5h** (0.4409 g, 0.5796 mmol), and Pd/C (0.0316 g of 10% w/w, 0.0297 mmol Pd, 5.12 mol%) were combined as described above (syntheses of macrocycles). This gave *trans*-**6h** (0.3398 g, 0.4625 mmol, 80%) as a yellow solid.

^{1}H NMR ($CDCl_3$): δ 8.93 (m, 2H, *o*-*H*C_{2pyr}), 8.82 (m, 2H, *o*-*H*C_{6pyr}), 7.71 (m, 2H, *p*-*H*C_{4pyr}), 7.28 (m, 2H, *m*-*H*C_{5pyr}), 4.51 (s, 4H, C*H*$_2$O), 3.50 (t, 4H, $^3J_{HH}$ = 6.7 Hz,

OCH_2CH$_2$), 1.63 (m, 4H, OCH$_2$CH_2), 1.41-1.24 (m, 28H, -CH_2-). ^{13}C{^{1}H} NMR (CDCl$_3$): δ 153.1 and 152.8 (*o*-C_{2pyr} and *o*-C_{6pyr}), 137.5 (*p*-C_{4pyr}), 136.8 (*m*-C_{3pyr}), 124.9 (*m*-C_{5pyr}), 71.4 (*C*H$_2$O), 69.5 (O*C*H$_2$CH$_2$), 29.7 (*C*H$_2$), 29.4 (5 × *C*H$_2$), 29.3 (*C*H$_2$), 26.1 (*C*H$_2$).

m.p. 131-134 ˚C.

IR (cm^{-1}, powder film): 2924 (s), 2851 (s), 1611 (w), 1435 (m), 1364 (m), 1103 (s), 800 (s), 692 (s).

Elemental Analysis: calculated: C, 49.04%; H, 6.59%; N, 3.81%.

found: C, 49.16%; H, 5.82%; N, 3.75%.

***trans*-PtCl$_2$[3,3′-(NC$_5$H$_4$(CH$_2$O(CH$_2$)$_{20}$OCH$_2$)H$_4$C$_5$N)] (*trans*-6i)**

Grubbs′ first generation catalyst (two charges, 0.0219 g and 0.0196 g, 0.0505 mmol, 7.55 mol%), *trans*-**5i** (0.5273 g. 0.6685 mmol), and Pd/C (0.0363 g of 10% w/w, 0.0341 mmol Pd, 5.10 mol%) were combined as described above (syntheses of macrocycles). This gave *trans*-**6i** (0.4581 g, 0.6006 mmol, 90%) as an off white solid.

^{1}H NMR (CDCl$_3$): δ 8.91 (m, 2H, *o*-*H*C$_{2pyr}$), 8.81 (m, 2H, *o*-*H*C$_{6pyr}$), 7.72 (m, 2H, *p*-*H*C$_{4pyr}$), 7.28 (m, 2H, *m*-*H*C$_{5pyr}$), 4.52 (s, 4H, CH_2O), 3.49 (t, 4H, $^3J_{HH}$ = 6.4 Hz, OCH_2CH$_2$), 1.63 (m, 4H, OCH$_2$CH_2), 1.40-1.22 (m, 32H, -CH_2-). ^{13}C{^{1}H} NMR (CDCl$_3$): δ 153.0 and 152.8 (*o*-C_{2pyr} and *o*-C_{6pyr}), 137.5 (*p*-C_{4pyr}), 136.8 (*m*-C_{3pyr}), 124.9 (*m*-C_{5pyr}), 71.3 (*C*H$_2$O), 69.4 (O*C*H$_2$CH$_2$), 29.7 (*C*H$_2$), 29.5 (5 × *C*H$_2$), 29.4 (*C*H$_2$), 29.3 (*C*H$_2$), 26.1 (*C*H$_2$).

m.p. 134-136 ˚C.

IR (cm^{-1}, powder film): 2922 (s), 2851 (s), 2341 (w), 2160 (w), 2039 (w), 1981 (w), 1476 (w), 1458 (w), 1435 (m), 1103 (s), 800 (s), 692 (s).

Elemental Analysis: calculated: C, 50.39%; H, 6.87%; N, 3.67%.

found: C, 50.40%; H, 6.75%; N, 3.55%.

***trans*-PtCl(CH$_3$)(3-NC$_5$H$_4$(CH$_2$O(CH$_2$)$_2$CH=CH$_2$))$_2$ (*trans*-7b)**

Methylmagnesium bromide (0.86 mL of a 2.94 M solution in ether, 2.5 mmol), and *trans*-**5b** (0.6121 g, 1.033 mmol) were combined as described above (methylations). This gave *trans*-**7b** (0.5549 g, 0.9701 mmol, 94%) as a colorless solid.

^{1}H NMR ($CDCl_3$): δ 8.89 (m, 2H, *o*-*H*C$_{2pyr}$), 8.85 (m, 2H, *o*-*H*C$_{6pyr}$), 7.74 (m, 2H, *p*-*H*C$_{4pyr}$), 7.23 (m, 2H, *m*-*H*C$_{5pyr}$), 5.90-5.76 (ddt, 2H, $^3J_{HH}$*trans* = 17.0 Hz, $^3J_{HH}$*cis* = 10.2 Hz, $^3J_{HH}$ = 6.6 Hz, C*H*=), 5.15-5.03 (m, 4H, =C*H*$_2$), 4.52 (s, 4H, C*H*$_2$O), 3.56 (t, 4H, $^3J_{HH}$ = 6.6 Hz, OC*H*$_2$CH$_2$), 2.39 (qt, 4H, $^3J_{HH}$ = 6.6 Hz, C*H*$_2$CH=CH$_2$), 0.87 (s, 3H, PtC*H*$_3$). ^{13}C{^{1}H} NMR ($CDCl_3$): δ 153.1 and 152.9 (*o*-*C*$_{2pyr}$ and *o*-*C*$_{6pyr}$), 136.5 (*C*H=), 136.1 (*p*-*C*$_{4pyr}$), 135.0 (*m*-*C*$_{3pyr}$), 125.2 (*m*-*C*$_{5pyr}$), 117.0 (=*C*H$_2$), 70.5 (*C*H$_2$O), 69.4 (O*C*H$_2$CH$_2$), 34.3 (*C*H$_2$), −6.6 (Pt*C*H$_3$).

***trans*-PtCl(CH$_3$)(3-NC$_5$H$_4$(CH$_2$O(CH$_2$)$_8$CH=CH$_2$))$_2$ (*trans*-7h)**

Methylmagnesium bromide (1.50 mL of a 2.94 M solution in ether, 4.41 mmol), and *trans*-**5h** (0.9494 g, 1.248 mmol) were combined as described above (methylations). This gave *trans*-**7h** (0.6175 g, 0.8341 mmol, 67%) as a colorless waxy solid.

^{1}H NMR ($CDCl_3$): δ 8.89 (m, 2H, *o*-*H*C$_{2pyr}$), 8.86 (m, 2H, *o*-*H*C$_{6pyr}$), 7.75 (m, 2H, *p*-*H*C$_{4pyr}$), 7.24 (m, 2H, *m*-*H*C$_{5pyr}$), 5.87-5.74 (ddt, 2H, $^3J_{HH}$*trans* = 17.0 Hz, $^3J_{HH}$*cis* = 10.4 Hz, $^3J_{HH}$ = 6.6 Hz, C*H*=), 4.94 (m, 4H, =C*H*$_2$), 4.50 (s, 4H, C*H*$_2$O), 3.49 (t, 4H, $^3J_{HH}$ = 6.6 Hz, OC*H*$_2$CH$_2$), 2.03 (m, 4H, C*H*$_2$CH=CH$_2$), 1.62 (m, 4H, OCH$_2$C*H*$_2$), 1.42-1.26 (m, 20H, -C*H*$_2$-), 0.88 (s, 3H, PtC*H*$_3$). ^{13}C{^{1}H} NMR ($CDCl_3$): δ 153.0 and 152.9 (*o*-*C*$_{2pyr}$ and *o*-*C*$_{6pyr}$), 139.4 (*C*H=), 136.7 (*p*-*C*$_{4pyr}$), 136.1 (*m*-*C*$_{3pyr}$), 125.1 (*m*-*C*$_{5pyr}$), 114.3 (=*C*H$_2$), 71.5 (*C*H$_2$O), 69.4 (O*C*H$_2$CH$_2$), 34.0 (*C*H$_2$), 29.8 (*C*H$_2$), 29.6 (2 × *C*H$_2$), 29.3 (*C*H$_2$), 29.1 (*C*H$_2$), 26.3 (*C*H$_2$), −6.6 (Pt*C*H$_3$).

***trans*-PtClMe[3,3′-($NC_5H_4(CH_2O(CH_2)_{10}OCH_2)H_4C_5N$)] (*trans*-8d)**

Methylmagnesium bromide (0.33 mL of a 2.94 M solution in ether, 0.97 mmol) and *trans*-**6d** (0.2038 g, 0.3274 mmol) were combined as described above (methylations). This gave *trans*-**8d** (0.1273 g, 0.2114 mmol, 65%) as a colorless solid.

^{1}H NMR ($CDCl_3$): δ 9.06 (m, 2H, *o*-*H*C_{2pyr}), 8.94 (m, 2H, *o*-*H*C_{6pyr}), 7.51 (m, 2H, *p*-*H*C_{4pyr}), 7.19 (m, 2H, *m*-*H*C_{5pyr}), 4.52 (s, 4H, C*H*$_2$O), 3.55 (t, 4H, $^3J_{HH}$ = 5.5 Hz, OC*H*$_2$CH$_2$), 1.64 (m, 4H, OCH$_2$C*H*$_2$), 1.54 (m, 4H, -C*H*$_2$-), 1.39 (m, 8H, -C*H*$_2$-), 0.93 (s, 3H, PtC*H*$_3$). ^{13}C{^{1}H} NMR ($CDCl_3$): δ 153.6 and 152.7 (*o*-*C*$_{2pyr}$ and *o*-*C*$_{6pyr}$), 136.7 (*p*-*C*$_{4pyr}$), 135.2 (*m*-*C*$_{3pyr}$), 124.5 (*m*-*C*$_{5pyr}$), 71.2 (*C*H$_2$O), 69.8 (O*C*H$_2$CH$_2$), 30.2 (*C*H$_2$), 29.9 (*C*H$_2$), 29.6 (*C*H$_2$), 26.7 (*C*H$_2$), −6.4 (Pt*C*H$_3$).

***trans*-PtClMe[3,3′-($NC_5H_4(CH_2O(CH_2)_{18}OCH_2)H_4C_5N$)] (*trans*-8h)**

Methylmagnesium bromide (0.28 mL of a 2.94 M solution in ether, 0.82 mmol) and *trans*-**6h** (0.2034 g, 0.2768 mmol) were combined as described above (methylations). This gave *trans*-**8h** (0.0815 g, 0.114 mmol, 41%) as an off white solid.

^{1}H NMR ($CDCl_3$): δ 8.97 (m, 2H, *o*-*H*C_{2pyr}), 8.91 (m, 2H, *o*-*H*C_{6pyr}), 7.68 (m, 2H, *p*-*H*C_{4pyr}), 7.22 (m, 2H, *m*-*H*C_{5pyr}), 4.50 (s, 4H, C*H*$_2$O), 3.50 (t, 4H, $^3J_{HH}$ = 6.4 Hz, OC*H*$_2$CH$_2$), 1.63 (m, 4H, OCH$_2$C*H*$_2$), 1.40-1.22 (m, 28H, -C*H*$_2$-), 0.91 (s, 3H, PtC*H*$_3$). ^{13}C{^{1}H} NMR ($CDCl_3$): δ 153.3 and 153.2 (*o*-*C*$_{2pyr}$ and *o*-*C*$_{6pyr}$), 136.6 (*p*-*C*$_{4pyr}$), 136.2 (*m*-*C*$_{3pyr}$), 125.0 (*m*-*C*$_{5pyr}$), 71.3 (*C*H$_2$O), 69.7 (O*C*H$_2$CH$_2$), 29.6 (*C*H$_2$), 29.45 (*C*H$_2$), 29.44 (*C*H$_2$), 29.41 (*C*H$_2$), 29.38 (*C*H$_2$), 29.37 (*C*H$_2$), 29.25 (*C*H$_2$), 26.1 (*C*H$_2$), −6.5 (Pt*C*H$_3$).

3,5-Diphenylpyridine (9)[29]

METHOD A: A scintillation vial was charged with **XVIII** (0.0060 g, 0.00530 mmol), THF (5 mL), and 3,5-dichloropyridine (0.1486 g, 1.004 mmol). Then phenylmagnesium bromide (2.00 mL of a 1.0 M solution in THF, 2.0 mmol) was added with stirring. After 24 h, the mixture was cooled to 0 °C, and methanol (1.0 mL) was added. The volatiles were removed by oil pump vacuum. Water (20 mL) was added to the residue and the mixture was extracted with dichloromethane (3 × 20 mL). The dichloromethane layers were combined and dried ($MgSO_4$). The solvent was removed by oil pump vacuum The residue was then chromatographed on a silica column (16 × 2.5 cm) eluted with 1:4 v/v ethyl acetate/hexanes. Once the first fraction eluted, the eluent was ramped to 100% ethyl acetate to elute the second, product containing, fraction. Solvent removal from the product containing fraction by oil pump vacuum gave **9** (0.2092 g, 0.9045 mmol, 90.1%) as a colorless solid.

METHOD B: A scintillation vial was charged with **XIX** (0.0056 g, 0.010 mmol), THF (5 mL), and 3,5-dichloropyridine (0.1484 g, 1.003 mmol). Then phenylmagnesium bromide (2.00 mL of a 1.0 M solution in THF, 2.0 mmol) was added with stirring. After 24 h, the mixture was cooled to 0 °C, and methanol (1.0 mL) was added. The volatiles were removed by oil pump vacuum. Water (20 mL) was added to the residue and the mixture was extracted with dichloromethane (3 × 20 mL). The dichloromethane layers were combined and dried ($MgSO_4$). The solvent was removed by oil pump vacuum The residue was then chromatographed on a silica column (16 × 2.5 cm) eluted with 1:4 v/v ethyl acetate/hexanes. Once the first fraction eluted, the eluent was ramped to 100% ethyl acetate to elute the second, product containing, fraction. Solvent removal from the product containing fraction by oil pump vacuum gave **9** (0.2121 g, 0.9170 mmol, 91.4%) as a colorless solid.

^{1}H NMR ($CDCl_3$): δ 8.83 (d, 2H, $^4J_{HH}$ = 2.2 Hz, *o*-H_{pyr}), 8.05 (t, 1H, $^4J_{HH}$ = 2.2 Hz, *p*-H_{pyr}), 7.65 (m, 4H, *m*-H_{Ph}), 7.51 (m, 4H, *o*-H_{Ph}), 7.45 (m, 2H, *p*-H_{Ph}). These data agreed with those previously reported.[34]

3,5-bis(4-methoxyphenyl)pyridine (10)[31a]

A 100 mL three neck round bottom flask was charged with magnesium (0.5821 g, 23.95 mmol) and fitted with a septum, a stopper, and a condenser capped with a 180˚ glass needle valve. The flask was then evacuated and back filled with nitrogen. THF (30 mL) was added *via* cannula. Then 1,2-dibromoethane (0.30 mL) was added with stirring. After 10 min, *p*-bromoanisole (2.50 mL, 20.0 mmol) was added by syringe. A Schlenk flask was charged with 3,5-dichloropyridine (1.3697 g, 9.2552 mmol), **XIX** (0.0503 g, 0.0928 mmol, 1 mol%), and THF (20 mL), and cooled to 0 °C. The Grignard mixture from the round bottom flask was then added dropwise with stirring over 10 min. The cooling bath was removed. After 15 h, the sample was refluxed (oil bath). After 2 h, the mixture was cooled (0 °C), and methanol (10 mL) was added. The volatiles were removed by oil pump vacuum. Water (200 mL) was added, and was extracted with dichloromethane (3 × 200 mL). The dichloromethane layers were combined, washed with water (150 mL) and brine (150 mL), and dried ($MgSO_4$). The solvent was removed by oil pump vacuum. The residue was then recrystallized from toluene to afford **10** (1.8531 g, 6.3606 mmol, 73%) as colorless plates.

m.p. 228-231 ˚C. Lit: 233-235 ˚C.[34]

^{1}H NMR ($CDCl_3$): δ 8.75 (bs, 2H, *o*-H_{pyr}), 7.97 (s, 1H, *p*-H_{pyr}), 7.58 (d, 4H, $^3J_{HH}$ = 8.6 Hz, MeOCC*H*), 7.04 (d, 4H, $^3J_{HH}$ = 8.6 Hz, MeOCCHC*H*), 3.88 (s, 6H, CH_3). These data agreed with those previously reported.[34]

3,5-bis(4-hydroxyphenyl)pyridine (11)[31b]

A round bottom flask was charged with **10** (1.0944 g, 3.7564 mmol), dichloromethane (25 mL) and BBr_3 (16.0 mL of a 1.0 M solution in dichloromethane, 16.0 mmol). The mixture stirred for 14 h, and methanol (10 mL) was added. The volatiles were removed by oil pump vacuum and the residue chromatographed on a silica column (37 × 4 cm) eluted with 1:9 v/v petroleum ether/ethyl acetate. The solvent was removed from the faint yellow band by rotary evaporation to give **11** (0.6539 g, 2.484 mmol, 66%) as an off white solid.

^{1}H NMR (DMSO-d_6): δ 10.06 (br s, 2H, PhO*H*), 9.37 (bs, 2H, *o*-H_{pyr}), 8.90 (t, 1H, $^4J_{HH}$ = 2.0 Hz, *p*-H_{pyr}), 7.77 (m, 4H, HOCC*H*), 6.99 (m, 4H, HOCCHC*H*). These data agreed with those previously reported.[31b]

3,5-bis(4-(6-heptenoxy)-phenyl)pyridine (12)

A round bottom flask was charged with **11** (0.5179 g, 1.967 mmol), Cs_2CO_3 (1.5166 g, 4.6549 mmol), and DMF (50 mL). The flask was fitted with a septum connected by a needle to an oil bubbler and purged with nitrogen (10 min). Then 7-bromo-1-heptene was added by syringe with stirring. The mixture was heated to 100 ˚C for 1 h. The solvent was removed by oil pump vacuum. Water (100 mL) and dichloromethane (100 mL) were then added and the phases separated. The aqueous phase was extracted with dichloromethane (2 × 100 mL). The dichloromethane layers were combined and dried ($MgSO_4$). The solvent was then removed by oil pump vacuum. The residue was chromatographed on a silica column (37 × 4 cm) eluted with 50:50 v/v ethyl acetate/dichloromethane. The solvent was removed from the product containing fraction by rotary evaporation to give **12** (0.2902 g, 0.6369 mmol, 32%) as a colorless solid.

^{1}H NMR ($CDCl_3$): δ 8.73 (bs, 2H, *o*-H_{pyr}), 7.97 (t, 1H, $^4J_{HH}$ = 2.3 Hz, *p*-H_{pyr}), 7.56 and 7.01 (2 m, 2 × 4H, pyr-CC*H* and pyr-CCHC*H*), 5.87-5.79 (ddt, 2H, $^3J_{HH}$*trans* = 17.3 Hz, $^3J_{HH}$*cis* = 10.3 Hz, $^3J_{HH}$ = 6.4 Hz, C*H*=), 5.05-4.94 (m, 4H, =CH_2), 4.02 (t, 4H, $^3J_{HH}$ = 6.7 Hz, OCH_2), 2.10 (m, 4H, CH_2CH=CH_2), 1.83 (m, 4H, OCH_2CH_2), 1.52-1.47 (m, 8H, -CH_2-). ^{13}C{^{1}H} NMR ($CDCl_3$): δ 159.6 (*C*OCH_2), 145.8 (*o*-C_{pyr}), 139.0 (=*C*H_2), 136.6 (*m*-C_{pyr}), 132.3 (*p*-C_{pyr}), 130.1 (Pyr-*C*$(CH)_2$), 128.5 (Pyr-C(*C*H)$_2$), 115.4 ((*C*H)$_2$CO), 114.7 (*C*H=), 68.3 ($C_6H_4OCH_2$), 33.9 (*C*H_2), 29.3 (*C*H_2), 28.8 (*C*H_2), 25.8 (*C*H_2).

m.p. 151-154 ˚C.

IR (cm^{-1}, powder film): 2936 (m), 2864 (w), 1715 (w), 1605 (m), 1510 (m), 1287 (m), 1246 (s), 1180 (m), 910 (m), 824 (s), 716 (m).

Elemental Analysis: calculated: C, 81.72%; H, 8.19%; N, 3.07%.

found: C, 75.75%; H, 7.50%; N, 2.96%.

***trans*-$PtCl_2$-bis(3,5-bis(4-(6-heptenoxy)-phenyl)pyridine) (*trans*-13)**

$PtCl_2$ (0.0162 g, 0.0609 mmol) and **12** (0.0570 g, 0.125 mmol) were combined as described above (syntheses of metal complexes). This gave *trans*-**13** (0.0687 g, 0.0584 mmol, 96%) as a light yellow solid.

^{1}H NMR ($CDCl_3$): δ 9.01 (d, 4H, $^4J_{HH}$ = 1.8 Hz, *o*-H_{pyr}), 8.00 (t, 2H, $^4J_{HH}$ = 1.8 Hz, *p*-H_{pyr}), 7.57 and 7.01 (2 m, 2 × 8H, pyr-CC*H* and C_{pyr}CCHC*H*), 5.88-5.79 (ddt, 4H, $^3J_{HH}$*trans* = 17.0 Hz, $^3J_{HH}$*cis* = 10.1 Hz, $^3J_{HH}$ = 6.4 Hz, C*H*=), 5.06-4.94 (m, 8H, =CH_2), 4.02 (t, 8H, $^3J_{HH}$ = 6.4 Hz, OCH_2), 2.11 (m, 8H, CH_2CH=CH_2), 1.83 (m, 8H, OCH_2CH_2), 1.50 (m, 16H, -CH_2-). ^{13}C{^{1}H} NMR ($CDCl_3$): δ 160.2 (*C*OCH_2), 149.6 (*o*-C_{pyr}), 139.0 (=*C*H_2), 138.4 (*m*-C_{pyr}), 133.9 (*p*-C_{pyr}), 128.7 (Pyr-*C*$(CH)_2$), 128.0 (Pyr-C(*C*H)$_2$), 115.5 ((*C*H)$_2$CO), 114.7 (*C*H=), 68.3 ($C_6H_4OCH_2$), 33.9 (*C*H_2), 29.3 (*C*H_2), 28.8 (*C*H_2), 25.7 (*C*H_2).

m.p. 190-192 ˚C.

IR (cm^{-1}, powder film): 3074 (w), 2930 (m), 2857 (m), 1607 (s), 1512 (s), 1449 (s), 1287 (s), 1240 (s), 1180 (s), 995 (m), 908 (s), 823 (s), 696 (m).

Elemental Analysis: calculated: C, 63.25%; H, 6.34%; N, 2.38%.

found: C, 62.59%; H, 6.31%; N, 2.30%.

***trans*-$PtCl_2$[3,5,3′,5′-(NC_5H_3(*p*-$C_6H_4O(CH_2)_{12}O$-*p*-$C_6H_4)_2H_3C_5N$)] (*trans*-14)**

Grubbs′ first generation catalyst (0.0287 g, 0.0349 mmol, 15.0 mol%), *trans*-**13** (0.2737 g. 0.2325 mmol), and Pd/C (three charges 0.0203 g, 0.0217 g, and 0.0217 g of 10% w/w, 0.0599 mmol Pd, 25.7 mol%) were combined as described above (syntheses of macrocycles). This gave *trans*-**14** (0.1036 g, 0.09207 mmol, 40%) as a yellow solid.

^{1}H NMR ($CDCl_3$): δ 8.83 (d, 4H, $^4J_{HH}$ = 2.0 Hz, *o*-H_{pyr}), 7.96 (t, 2H, $^4J_{HH}$ = 2.0 Hz, *p*-H_{pyr}), 7.48 and 6.97 (2 m, 2 × 8H, pyr-CC*H* and C_{pyr}CCHC*H*), 4.05 (t, 8H, $^3J_{HH}$ = 6.9 Hz, OCH_2), 1.86-1.76 (m, 8H, OCH_2CH_2), 1.54-1.44 (m, 8H, -CH_2-), 1.44-1.28 (m, 24H, -CH_2-). $^{13}C\{^1H\}$ NMR ($CDCl_3$): δ 160.1 (*C*OCH_2), 149.2 (*o*-C_{pyr}), 137.7 (*m*-C_{pyr}), 133.1 (*p*-C_{pyr}), 128.7 (Pyr-*C*$(CH)_2$), 127.5 (Pyr-C(*C*$H)_2$), 115.4 ((*C*$H)_2CO$), 68.2 ($C_6H_4OCH_2$), 29.2 (*C*H_2), 29.1 (*C*H_2), 29.0 (2 × *C*H_2), 25.8 (*C*H_2).

m.p. 198-204 ˚C, decomposition.

IR (cm^{-1}, powder film): 2924 (s), 2853 (m), 2359 (w), 1607 (s), 1512 (s), 1449 (s), 1287 (s), 1240 (s), 1180 (s), 1028 (m), 824 (s), 698 (m).

Elemental Analysis: calculated: C, 61.91%; H, 6.27%; N, 2.49%.

found: C, 60.58%; H, 6.07%; N, 2.42%.

Crystallography

Single crystal X-ray diffraction studies were performed on complexes *trans*-**3b**, *trans*-**6d**, and *trans*-**6h**. Summaries of crystal and refinement data are presented below.

Single crystals of *trans*-**3b** suitable for X-ray diffraction were grown from a saturated CH_2Cl_2 solution layered with ethyl acetate at room temperature. After one day, the yellow plates were taken directly to an APEXII BRUKER X-ray diffractometer for data collection as outlined in Table 2.3. Cell parameters were obtained from 36 frames using a 5° scan and refined with 17016 reflections. A suitable cell was found and refined by nonlinear least squares and Bravais lattice procedures. No super-cell or erroneous reflections were observed. Integrated intensity information for each reflection was obtained by reduction of the data frames with the program APEX2.[35] Lorentz, polarization, and absorption corrections[36] were applied. The space group, P1, was determined from systematic reflection conditions and statistical tests. The structure was solved by direct methods using SHELXTL (SHELXS).[37] All non-hydrogen atoms were refined with anisotropic thermal parameters. The hydrogen atoms were placed in idealized positions. The parameters were refined by weighted least squares refinement on F^2 to convergence.[37] Two independent molecules were found in the unit cell.

Table 2.3. Summary of crystal and refinement data for *trans*-**3b**.

Empirical formula	$C_{18}H_{24}Cl_2N_2O_2Pt$
Formula weight	566.38
Temperature	120(2) K
Wavelength	0.71073 Å
Crystal system	Triclinic
Space group	P1
Unit cell dimensions	a = 8.411(2) Å
	b = 8.542(2) Å
	c = 15.116(4) Å
	α = 80.430(3)°
	β = 77.450(3)°
	γ = 65.099(2)°
Volume	957.5(4) $Å^3$
Z	2
Density (calculated)	1.965 Mg/m^3
Absorption coefficient	7.621 mm^{-1}
F (000)	548
Crystal size	0.17 × 0.16 × 0.06 mm^3
Theta range for data collection	2.64 to 29.34°
Index range (h, k, l)	−11, 11; −11, 11; −20, 20
Reflections collected	17016
Independent reflections	9327 [R(int) = 0.0340]
Completeness to theta = 29.34°	92.2%
Absorption correction	Semi-empirical from equivalents
Max. and min. transmission	0.6494 and 0.3490
Refinement method	Full-matrix least-squares on F^2
Data / restraints / parameters	9327 / 3 / 451
Goodness-of-fit on F^2	1.028
Final R indices [I>2sigma(I)]	R1 = 0.0231, wR2 = 0.0595
R indices (all data)	R1 = 0.0249, wR2 = 0.0605
Largest diff. peak and hole	1.169 and −1.065 $eÅ^{-3}$

Single crystals of *trans*-**6d** suitable for X-ray diffraction were grown from a saturated CH_2Cl_2 solution layered with ethyl acetate at room temperature. After one day, the yellow plates were taken directly to an APEXII BRUKER X-ray diffractometer for data collection as outlined in Table 2.4. Cell parameters were obtained from 36 frames using a 5° scan and refined with 24911 reflections. A suitable cell was found and refined by nonlinear least squares and Bravais lattice procedures. No super-cell or erroneous reflections were observed. Integrated intensity information for each reflection was obtained by reduction of the data frames with the program APEX2.[35] Lorentz, polarization, and absorption corrections[36] were applied. The space group, C2/m, was determined from systematic reflection conditions and statistical tests. The structure was solved by direct methods using SHELXTL (SHELXS).[37] All non-hydrogen atoms were refined with anisotropic thermal parameters. The hydrogen atoms bound to carbon were placed in idealized positions. The parameters were refined by weighted least squares refinement on F^2 to convergence.[37] Two independent molecules were found in the unit cell. In one molecule, atom C8 was disordered over two positions and refined to a 59:41 occupancy and atom C9 was disordered over two positions and refined to a 62:38 occupancy.

Table 2.4. Summary of crystal and refinement data for *trans*-**6d**.

Empirical formula	$C_{22}H_{32}Cl_2N_2O_2Pt$
Formula weight	622.49
Temperature	120(2) K
Wavelength	0.71073 Å
Crystal system	Monoclinic
Space group	C2/m
Unit cell dimensions	a = 21.0609(6) Å
	b = 13.9765(5) Å
	c = 19.8213(9) Å
	α = 90°
	β = 121.090(2)°
	γ = 90°
Volume	4996.5(3) $Å^3$
Z	1
Density (calculated)	0.207 Mg/m^3
Absorption coefficient	0.731 mm^{-1}
F (000)	306
Crystal size	0.59 × 0.18 × 0.07 mm^3
Theta range for data collection	2.29 to 28.40°
Index range (h, k, l)	−28, 28; −15, 18; −26, 26
Reflections collected	24911
Independent reflections	6374 [R(int) = 0.0451]
Completeness to theta = 28.40°	97.7%
Absorption correction	Semi-empirical from equivalents
Max. and min. transmission	0.9506 and 0.6722
Refinement method	Full-matrix least-squares on F^2
Data / restraints / parameters	6374 / 0 / 291
Goodness-of-fit on F^2	1.028
Final R indices [I>2sigma(I)]	R1 = 0.0484, wR2 = 0.1312
R indices (all data)	R1 = 0.0732, wR2 = 0.1514
Largest diff. peak and hole	3.719 and −1.646 $eÅ^{-3}$

Single crystals of *trans*-**6h**·CH_2Cl_2 suitable for X-ray diffraction were grown from a saturated CH_2Cl_2 solution layered with ethyl acetate at room temperature. After one day, the yellow plates were taken directly to an APEXII BRUKER X-ray diffractometer for data collection as outlined in Table 2.5. Cell parameters were obtained from 36 frames using a 5° scan and refined with 14813 reflections. A suitable cell was found and refined by nonlinear least squares and Bravais lattice procedures. No super-cell or erroneous reflections were observed. Integrated intensity information for each reflection was obtained by reduction of the data frames with the program APEX2.[35] Lorentz, polarization, and absorption corrections[36] were applied. The space group, P−1, was determined from systematic reflection conditions and statistical tests. The structure was solved by direct methods using SHELXTL (SHELXS).[37] All non-hydrogen atoms were refined with anisotropic thermal parameters. The hydrogen atoms bound to carbon were placed in idealized positions. The parameters were refined by weighted least squares refinement on F^2 to convergence.[37]

Table 2.5. Summary of crystal and refinement data for *trans*-**6h**·CH_2Cl_2.

Empirical formula	$C_{31}H_{50}Cl_4N_2O_2Pt$
Formula weight	819.62
Temperature	120(2) K
Wavelength	0.71073 Å
Crystal system	Triclinic
Space group	P−1
Unit cell dimensions	a = 8.947(3) Å
	b = 9.019(3) Å
	c = 24.758(8) Å
	α = 89.84(2)°
	β = 87.10(2)°
	γ = 60.631(18)°
Volume	1738.3(10) $Å^3$
Z	2
Density (calculated)	1.566 Mg/m^3
Absorption coefficient	4.373 mm^{-1}
F (000)	824
Crystal size	0.22 × 0.11 × 0.10 mm^3
Theta range for data collection	2.59 to 28.59°
Index range (h, k, l)	−11, 11; −11, 11; −33, 32
Reflections collected	14813
Independent reflections	7822 [R(int) = 0.0578]
Completeness to theta = 28.59°	88.3%
Absorption correction	Semi-empirical from equivalents
Max. and min. transmission	0.6689 and 0.4463
Refinement method	Full-matrix least-squares on F^2
Data / restraints / parameters	7822 / 0 / 362
Goodness-of-fit on F^2	1.059
Final R indices [I>2sigma(I)]	R1 = 0.0687, wR2 = 0.1722
R indices (all data)	R1 = 0.1246, wR2 = 0.2116
Largest diff. peak and hole	3.102 and −3.511 $eÅ^{-3}$

CHAPTER III

ORGANOMETALLIC II-ADDUCTS OF POLYACETYLENE FROM RING-OPENING METATHESIS POLYMERIZATION

INTRODUCTION

Although the first synthesis of polyacetylene (PA) was reported in 1958 by Natta and coworkers,[38] it was not until 1977 when Shirakawa and coworkers discovered an increase in conductance of ten orders of magnitude upon iodine doping (Scheme 3.1).[39] This discovery has led to a breadth of research on π-conjugated conducting polymers with potential applications in electronics, nonlinear optics, and solar energy conversion systems.[40]

Scheme 3.1. Doping of PA with I_2.

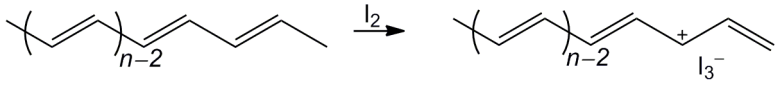

While iodine-doped PA holds the highest conductivity value for an organic polymer reported to date (>10^5 S/cm),[41] it is also one of the most difficult π-conjugated polymers to handle. Typical syntheses of PA form air sensitive intractable films that are consequentially difficult to use in fabrication processes. Therefore, it would be advantageous to develop a soluble, solution processable, form of PA. A few methods have been developed to solubilize PA (*vide infra*).

The first soluble PA synthesis involved polymerization of substituted acetylenes.[42] In this method, trimethylsilylacetylene was polymerized with tungsten(VI) chloride and tetrabutyltin (Scheme 3.2). Although this substituted PA facilitates

solubility, the side groups cause a twist that inhibits conjugation. This type of PA has been referred to as non-conjugated PA.

Scheme 3.2. Polymerization of trimethylsilylacetylene.

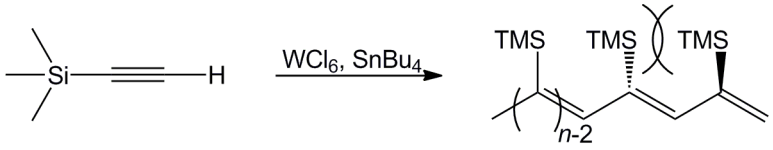

Later, the groups of Feast and Schrock used ROMP of substituted cyclobutenes followed by retro-Diels-Alder reactions to extrude an arene (Scheme 3.3).[43,44] This method forms a soluble polymer to act as a precursor to PA. After solution processing, heating causes the retro-Diels-Alder reaction that extrudes an arene leaving a PA film behind.

Scheme 3.3. Feast and Schrock syntheses of PA.

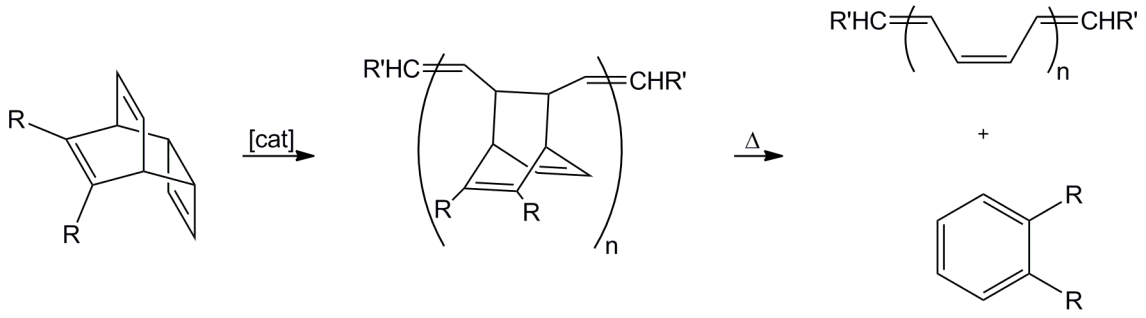

Feast	Schrock
[cat] = WCl_6/Me_4Sn	[cat] = $Mo(CH^tBu)(NC_6H_3\text{-}2,6\text{-}^iPr_2)(O^tBu)_2$
R' = H	R = R' = ^{t}Bu
R = CF_3, CO_2Me, or H	

The Schrock synthesis of PA is of particular interest and utility since it used a well defined olefin metathesis catalyst. Schrock was also able to chromatograph the

polymerization product to separate different chain lengths. Table 3.1 shows the UV-Vis results from Schrock. Since increasing chain length extends conjugation, a red-shift is observed in the UV-Vis spectra. These data are important in establishing the effective conjugation length in PA. The effective conjugation length of other polyenes can be estimated by comparison of their UV-Vis spectra with those in Table 3.1.

Table 3.1. Schrock′s UV-Vis analysis of effective conjugation length in PA.

-ene[a]	**Pentane λ_{max} (nm)**	**Dichloromethane λ_{max} (nm)**
5	344, 326, 312	350, 334, 318
7	394, 372, 354	404, 380, 362
9	432, 406, 384	444, 418, 396
11	466, 438, 414	480, 450, 428
13	490, 460, 434	508, 476, 452
15	508, 478, 454	528, 496, 472

[a] Polyene product in Scheme 3.3.

Additionally, Grubbs and coworkers have utilized ROMP of cyclooctatetraene (COT), employing a variety of substituents (R), with the well defined Schrock tungsten catalyst (**V**; Figure 1.1) to produce PA with one side group per eight carbon atoms (Scheme 3.4).[45] Contrary to the poly-(trimethylsilylacetylene) analogue, this spacing of side groups facilitates solubility while maintaining conductivity. However, in the case of bulky side groups, such as *t*-butyl, steric 1,3-interactions with the nearby hydrogen atoms are significant enough to twist the polymer chain and hinder conductance. The side chains of Grubbs′ PA also cause the polymer to be amorphous resulting in poor

interchain electron transfer. The variety of substituent R groups in Grubbs′ PA together with conductivity values is shown in Table 3.2.

Scheme 3.4. Grubbs′ ROMP of substituted COTs.

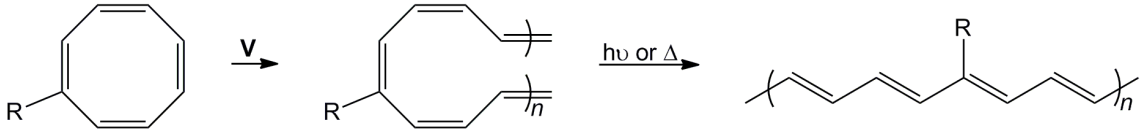

Table 3.2. Conductivity and absorption data from Grubbs′ PA.

R	Conductivity (S/cm)	THF λ_{max} (nm)
methyl	15-44	-
n-butyl	0.25-0.7	614
n-octyl	15-50	632
n-octadecyl	0.6-3.65	630
phenyl	0.3-0.6	620
t-butyl	$<10^{-8}$	432
s-butyl	0.03	556
TMS	0.2	512
neopentyl	15-21	634

Table 3.2 also shows UV-Vis absorption data from Grubbs′ PA. In agreement with trends in effective conjugation length established by Schrock (Table 3.1), lower energy absorptions correlate with higher conductivities. Conductivity is highest when R = *n*-octyl. Accordingly, the λ_{max} value suggests a long effective conjugation length of > 15-ene.

The aim of this work was to investigate a new approach to PA, specifically, using organometallic complexes with conjugated cyclic ligands to potentially serve as PA precursors (Scheme 3.5). Similar to the ROMP synthesis of PA by Grubbs and coworkers, ROMP of a non-coordinated carbon-carbon double bond would form PA. This strategy aims to use organometallic π-adducts, instead of alkyl side chains, to solubilize the PA backbone. Additionally, crystalline aromatic ligands have the potential to better facilitate interchain electron transfer through π-π stacking in the solid state.

Scheme 3.5. General ROMP reactions employing conjugated cyclic ligands with η^2 coordination (top) and η^4 coordination (bottom).

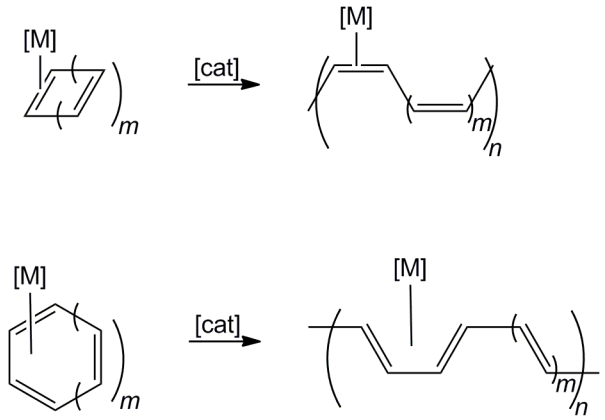

From the generalized structures in Scheme 3.5, it is obvious that a large variety of potential organometallic monomers exist. With respect to η^2 coordination, *m* is likely to be 1 (cyclobutadiene), 2 (benzene), or 3 (COT). With respect to η^4 coordination, *m* is likely to be 1 (benzene) or 2 (COT). In either example, when *m* = 1, the resulting product would be a regioregular polymer with alternating metal adduct and vinylene linkages.

This chapter focuses on a series of potential organometallic monomers for ROMP to form metal adducts of PA (Figure 3.1). The conjugated cyclic ligands investigated include benzene and COT.

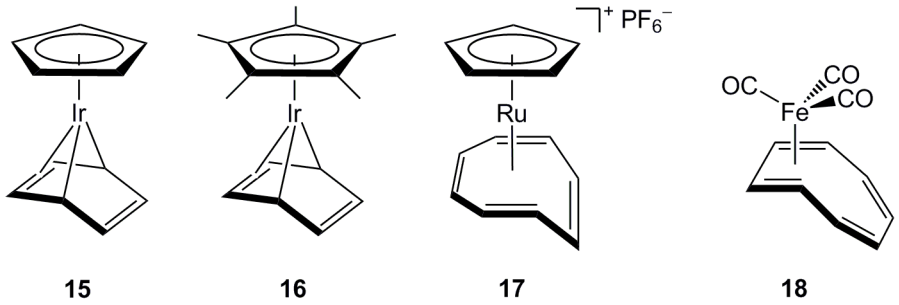

15 **16** **17** **18**

Figure 3.1. Potential organometallic monomers for ROMP.

While metal-arene complexes were first synthesized in 1919,[46] η^4 hapticity is rare.[46] Two limiting resonance structures can be formulated as shown in Scheme 3.6. Bianchini and coworkers have shown a loss in planarity of η^4-benzene in a cationic iridium complex, such that the geometry approaches that of norbornadiene.[47] A 1994 report from Qiao and coworkers partially inspired this chapter. They were able to synthesize (η^4-benzene)IrCp (**15**) (Cp = cyclopentadienyl).[48] In this complex, one carbon-carbon double bond of benzene is not coordinated to the iridium center and has been shown to be reactive.

Scheme 3.6. Resonance structures of (η^4-benzene)IrCp.

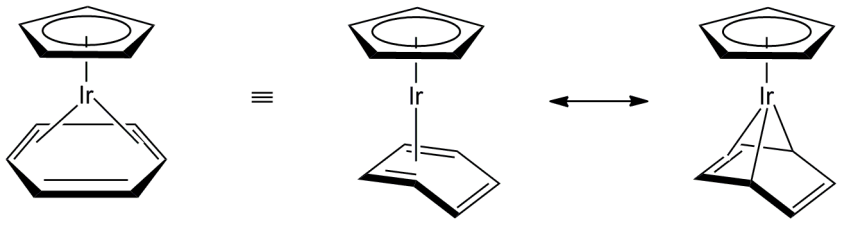

15

RESULTS

The synthesis of **15** is shown in Scheme 3.7. Although, as noted above, this sequence has been reported in the literature, only German language descriptions are available. Hence, full details are given here. In the first step, $IrCl_3 \cdot nH_2O$ and 1,3-cyclohexadiene are reacted to form **19** in 83% yield. A subsequent reaction with CpTl then afforded **20** in 83% yield. Hydride abstraction with 2 equivalents of triphenylcarbenium tetrafluoroborate then generates **21** in 97% yield. Finally, reduction with cobaltocene affords **15** in 98% yield.

Scheme 3.7. Synthesis of η^4-benzene complex **15**.

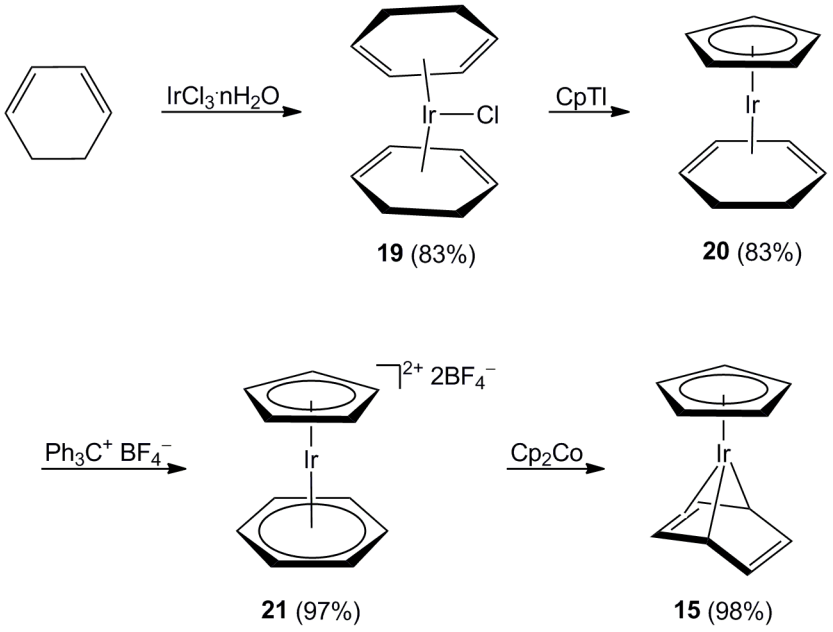

Complex **15** exists as a discrete isomer and is not fluxional on the NMR time scale. Both the ^1H and ^{13}C NMR spectra show three signals for the benzene ligand and one signal for the Cp ligand. A VT-NMR study was performed and no decoalescence was observed up to 80 ˚C in toluene-d_8.

The synthesis of the 1,2,3,4,5-pentamethylcyclopentadienyl (Cp*) analog of **16** is shown in Scheme 3.8.[49,50] Although **23** is a literature compound, the complete synthesis of **16** is described for perspective. In the first step, $IrCl_3 \cdot nH_2O$ and Cp*H were reacted to form the dimer **22** in 75% yield. Using standard iridium arene chemistry, halide abstraction from **22** followed by benzene coordination afforded **23** in 60% yield. Finally, following the synthetic methodology used for **15**, a reduction with cobaltocene afforded (η^4-benzene)IrCp* (**16**) in 99% yield.

Scheme 3.8. Synthesis of η^4-benzene complex **16**.

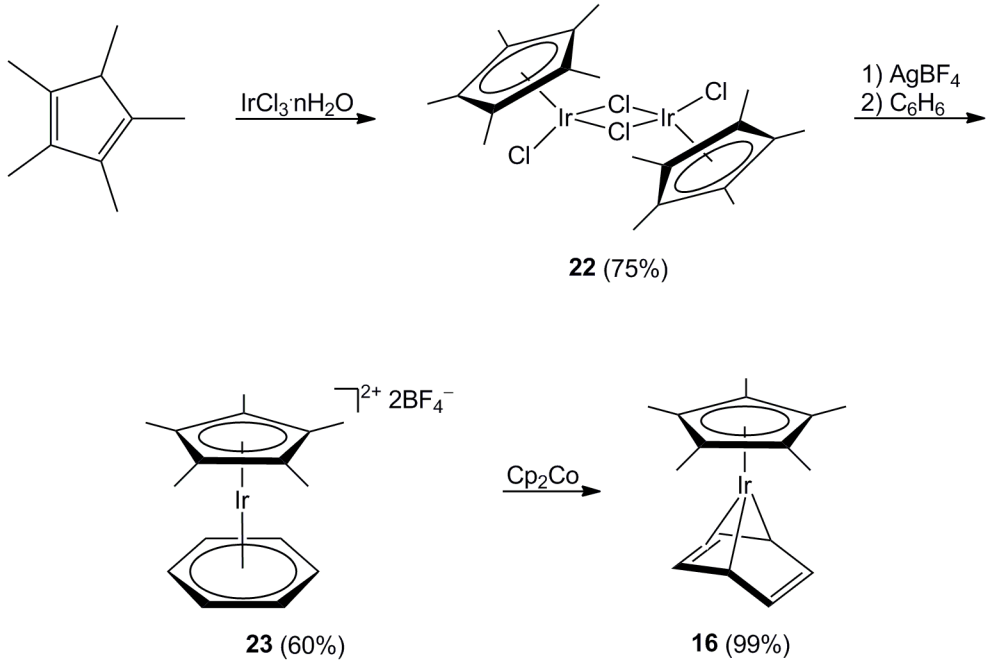

Complex **16** exists as a discrete isomer and is not fluxional on the NMR time scale. The ^1H NMR spectrum shows three signals for the benzene ligand and one signal for the Cp* ligand. The ^{13}C NMR spectrum shows three signals for the benzene ligand and two signals for the Cp* ligand. All NMR signals are upfield of those of **15**.

Single crystals of **16** suitable for X-ray diffraction studies were grown by slow evaporation of a saturated pentane solution. Two independent molecules were found in the unit cell. The X-ray crystal structure of one is depicted in Figure 3.2, and key metrical parameters are given in Table 3.3. As shown in Table 3.3, the C5-C6 bond lengths are 1.311(9) Å for both molecules in the unit cell. This bond length is considerably shorter than any other bond in the benzene ligand, consistent with a loss in conjugation. Additionally, the largest bond angles in the benzene ligand are the C3-C4-C5 and the C5-C6-C1 angles involved with the non-coordinated carbon-carbon double bond. Additional views of the X-ray crystal structure and packing diagrams are depicted in Figures 3.3 and 3.4. A summary of crystal and refinement data is given in the experimental section. This structure clearly illustrates the norbornadiene-like geometry of an η^4-benzene complex. As shown in Figure 3.5, least squares planes can be used to show the out of plane bending of the free double bond. In **16**, the non-coordinated carbon-carbon double bond is bent out of the benzene plane in both independent molecules by 43.5˚.

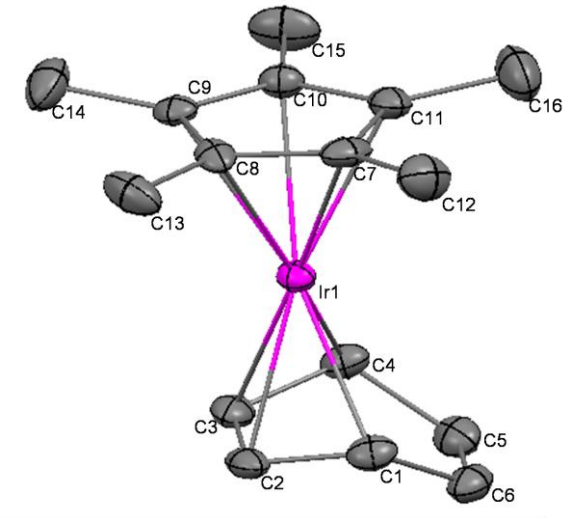

Figure 3.2. Thermal ellipsoid plot (50% probability) of **16**.

Table 3.3. Key bond lengths (Å) and angles (°) in **16**.

	16(1)[a]	**16(2)**[a]
bond lengths		
Ir-C1	2.154(6)	2.137(6)
Ir-C2	2.119(6)	2.119(6)
Ir-C3	2.104(6)	2.125(6)
Ir-C4	2.153(6)	2.157(6)
Ir-C7	2.201(6)	2.192(6)
Ir-C8	2.259(5)	2.274(6)
Ir-C9	2.275(6)	2.285(5)
Ir-C10	2.189(6)	2.202(6)
Ir-C11	2.192(6)	2.185(6)
Ir-Cp	1.857	1.866
C1-C2	1.453(9)	1.466(9)
C2-C3	1.416(9)	1.400(9)
C3-C4	1.449(9)	1.481(9)
C4-C5	1.485(8)	1.477(9)
C5-C6	1.311(9)	1.311(9)
C6-C1	1.484(8)	1.502(8)
bond angles		
C1-C2-C3	112.4(6)	113.0(6)
C2-C3-C4	113.6(6)	112.9(5)
C3-C4-C5	116.8(6)	117.1(6)
C4-C5-C6	113.9(6)	113.7(6)
C5-C6-C1	115.1(6)	115.5(6)
C6-C1-C2	116.4(5)	115.8(5)
C7-C8-C9	108.6(6)	108.9(6)
C8-C9-C10	107.4(5)	108.8(5)
C9-C10-C11	110.0(5)	107.8(5)
C10-C11-C7	105.6(5)	106.6(5)
C11-C7-C8	108.3(6)	107.8(6)

[a] Values for the two independent molecules of **16** in the unit cell.

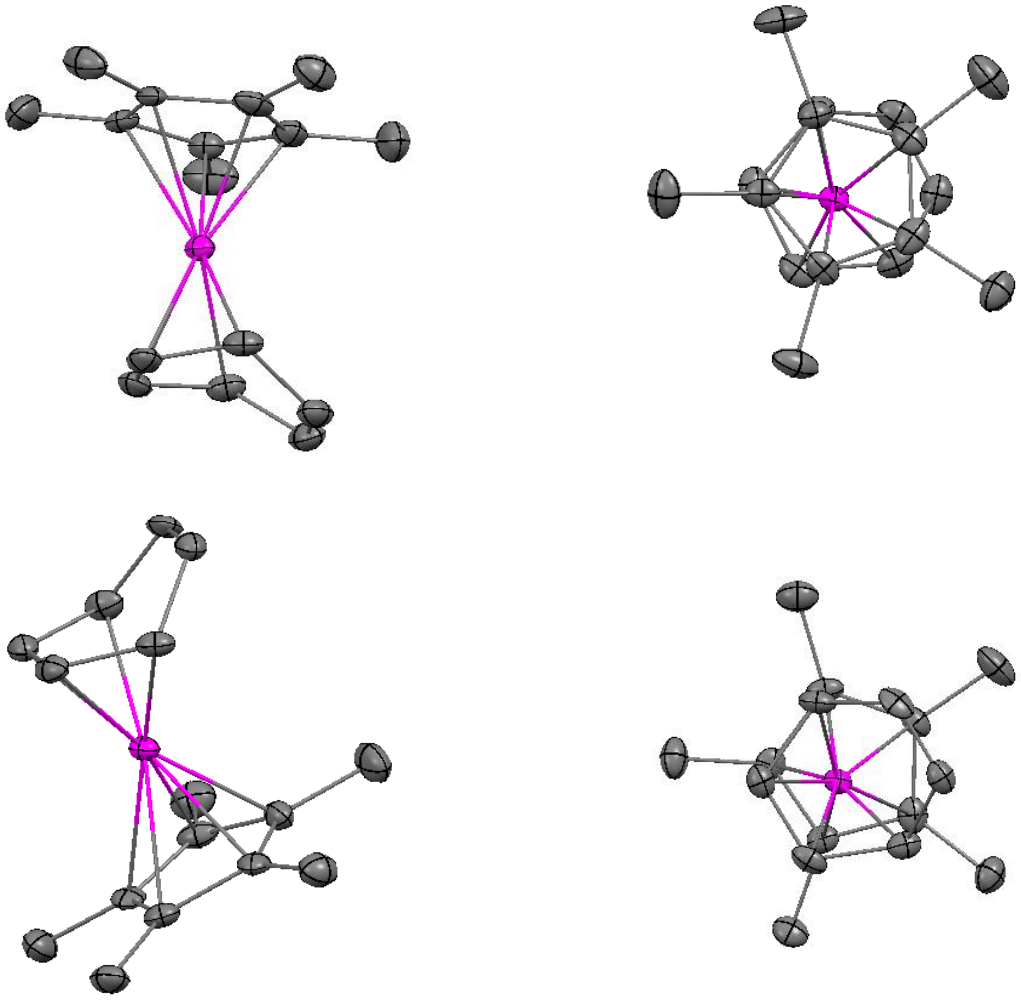

Figure 3.3. Thermal ellipsoid plots (50% probability) of the two independent molecules of **16**: side view (left) and view along the N-Pt-N axis (right).

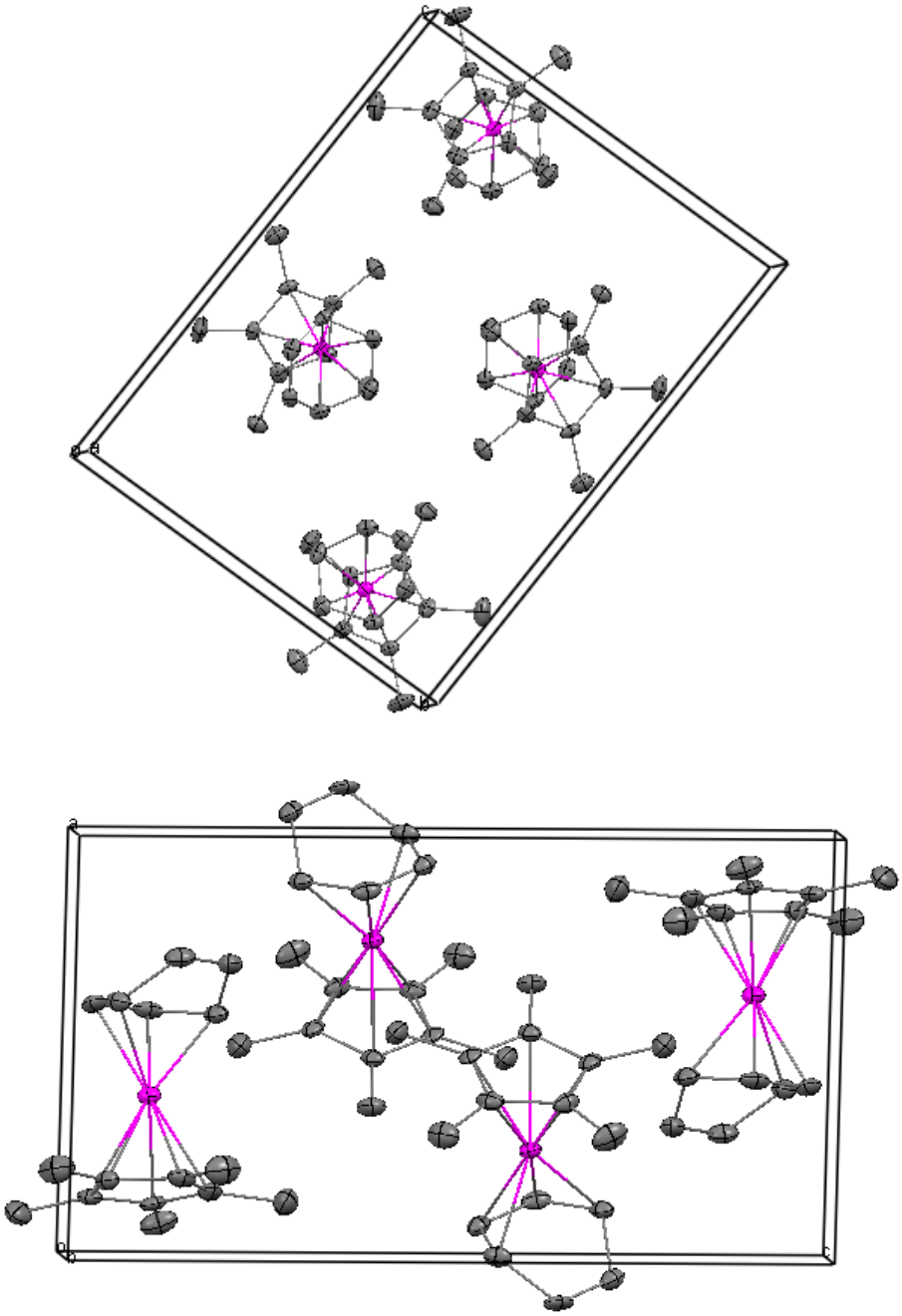

Figure 3.4. Thermal ellipsoid plots (50% probability) of the crystal packing in **16**: view down the a axis (top) and view down the b axis (bottom).

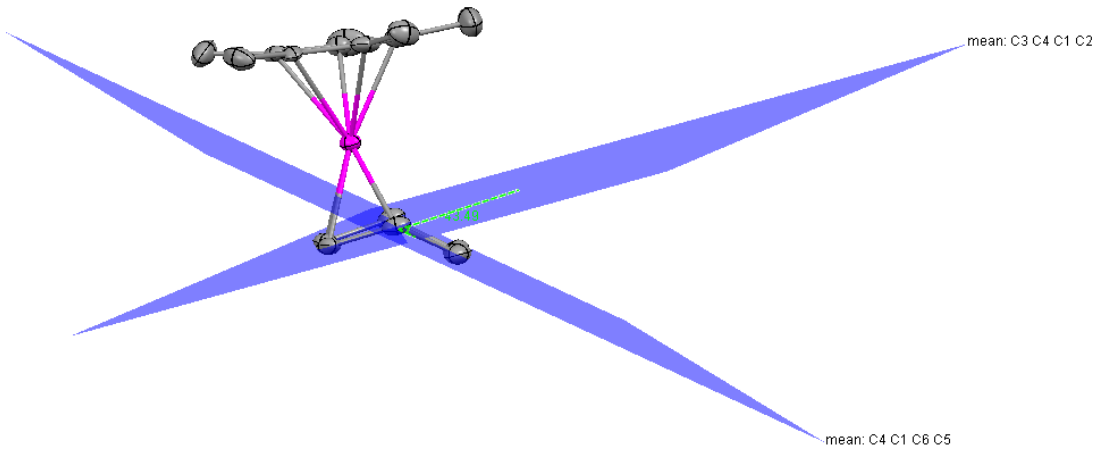

Figure 3.5. Least squares planes associated with the η^4 ligand in **16**.

For a comparative analysis, the out of plane bending in **16** is contrasted with those of norbornene and norbornadiene in Table 3.4.[51,52] Additionally, η^4-benzene complexes from Bianchini and coworkers ([(triphos)(η^4-benzene)Ir][BPh_4]·THF (triphos = $CH_3C(CH_2PPh_2)_3$) and from Huttner and Lange ((η^4-C_6Me_6)(η^6-C_6Me_6)Ru) are evaluated.[47,53] Although the out of plane bend in **16** is not as severe as in norbornene or norbornadiene, it is still significantly out of the benzene plane and suggestive of ring strain. As shown in Table 3.4, non-coordinated carbon-carbon double bond distances are all similar and on the order of an isolated double bond.

Table 3.4. Out of plane bending[a] within unsaturated six membered rings and non-coordinated C=C length.

Molecule	Out of plane bend (˚)	C=C (Å)
16	43.5	1.311(9)
[(triphos)(η^4-benzene)Ir][BPh_4]·THF[42]	45.3	1.36(3)
(η^4-C_6Me_6)(η^6-C_6Me_6)Ru^{47+}	42.7	1.3265(9)
norbornene[46]	68.5	-
norbornadiene[47]	65.5	-

[a] Angle defined by the least squares planes of the coordinated CH-CH=CH-CH segment and partially coordinated CH-CH=CH-CH segment.

Complex **17** is a known compound, and the synthesis is shown in Scheme 3.9.[54-56] Using standard ruthenium arene chemistry, $RuCl_3 \cdot 3H_2O$ and 1,3-cyclohexadiene were reacted to form the dimer **24** in 90% yield. Subsequent reaction with CpTl afforded **25** in 77% yield. Anion exchange was then achieved with [NH_4][PF_6] to afford **26** in 76% yield. Finally, **17** was obtained in 85% yield by photolysis in acetonitrile followed by the addition of COT.

Scheme 3.9. Synthesis of η^6-COT complex **17**.

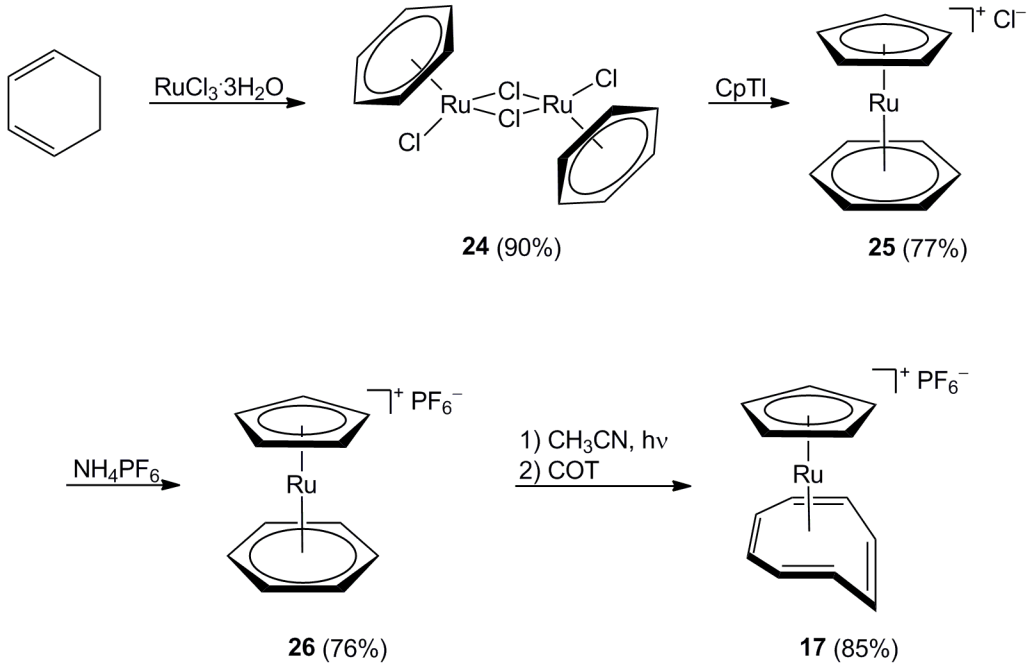

Complex **17** exists as a discrete isomer and is not fluxional on the NMR time scale. Both the ^{1}H and ^{13}C NMR spectra show four signals for the COT ligand and one signal for the Cp ligand.

Conveniently, the iron tricarbonyl monomer **18** (Figure 3.1) is commercially available from Strem. Complex **18** exists as a fluxional molecule in solution on the NMR time scale. The ^{1}H NMR shows one signal for the COT ligand. The ^{13}C NMR shows one signal for the COT ligand and one signal for the carbonyl ligands.

Monomers **15**-**18** (Figure 3.1) were then evaluated in ROMP using catalysts **I**-**V**. However, only monomer **15** was found to undergo polymerization (Scheme 3.10). Suitable reaction conditions for ROMP of **16**-**18** could not be found.

Scheme 3.10. Formation of **poly-15** *via* ROMP.

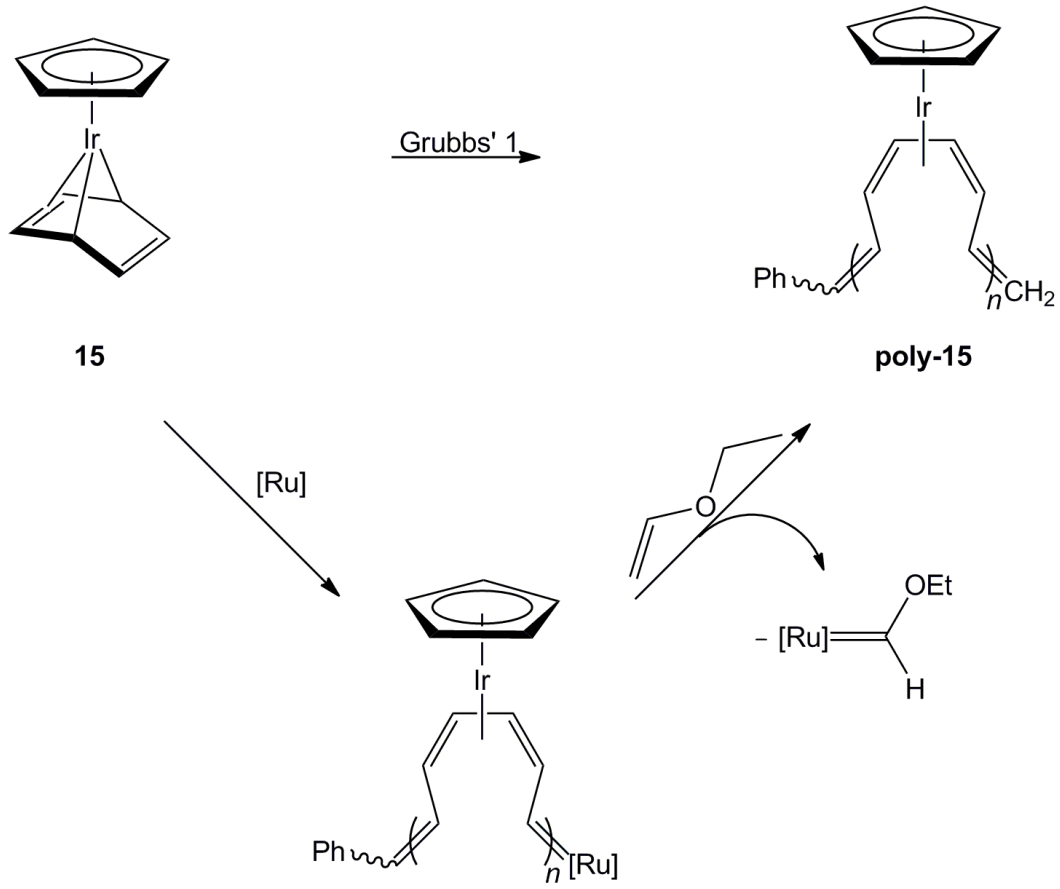

Initially, ROMP of **15** to form **poly-15** was attempted with 10 mol% of Grubbs′ first generation catalyst (**I**) in CD_2Cl_2. Formation of **poly-15** was readily monitored by ^1H or ^{13}C NMR in CD_2Cl_2 (Figure 3.6). In the cyclopentadienyl region of the ^1H NMR spectrum, disappearance of the starting material signal at 5.14 ppm was correlated with appearance of the product signal at 5.22 ppm. The reaction was slow, taking six days to reach *ca.* 90% conversion with **I** (20 mol%). However, heating to 40 ˚C in a sealed tube under the same catalyst loading afforded >93% conversion after two days. Ethyl vinyl ether was then added. In accord with much precedent,[57] this capped the polymer with a vinyl end group as shown in Scheme 3.10 and by the ^1H NMR spectrum in Figure 3.7. Generally, integration of the vinyl protons from the end group compared to the cyclopentadienyl protons shows the degree of polymerization (DP) to be 8-10 (Figure 3.7-inset). However, a DP of as high as 20 has been observed. Grubbs′ second generation catalyst, **II**, and Schrock′s catalyst, **IV**, also effected ROMP of **15**, albeit at a diminished rate.

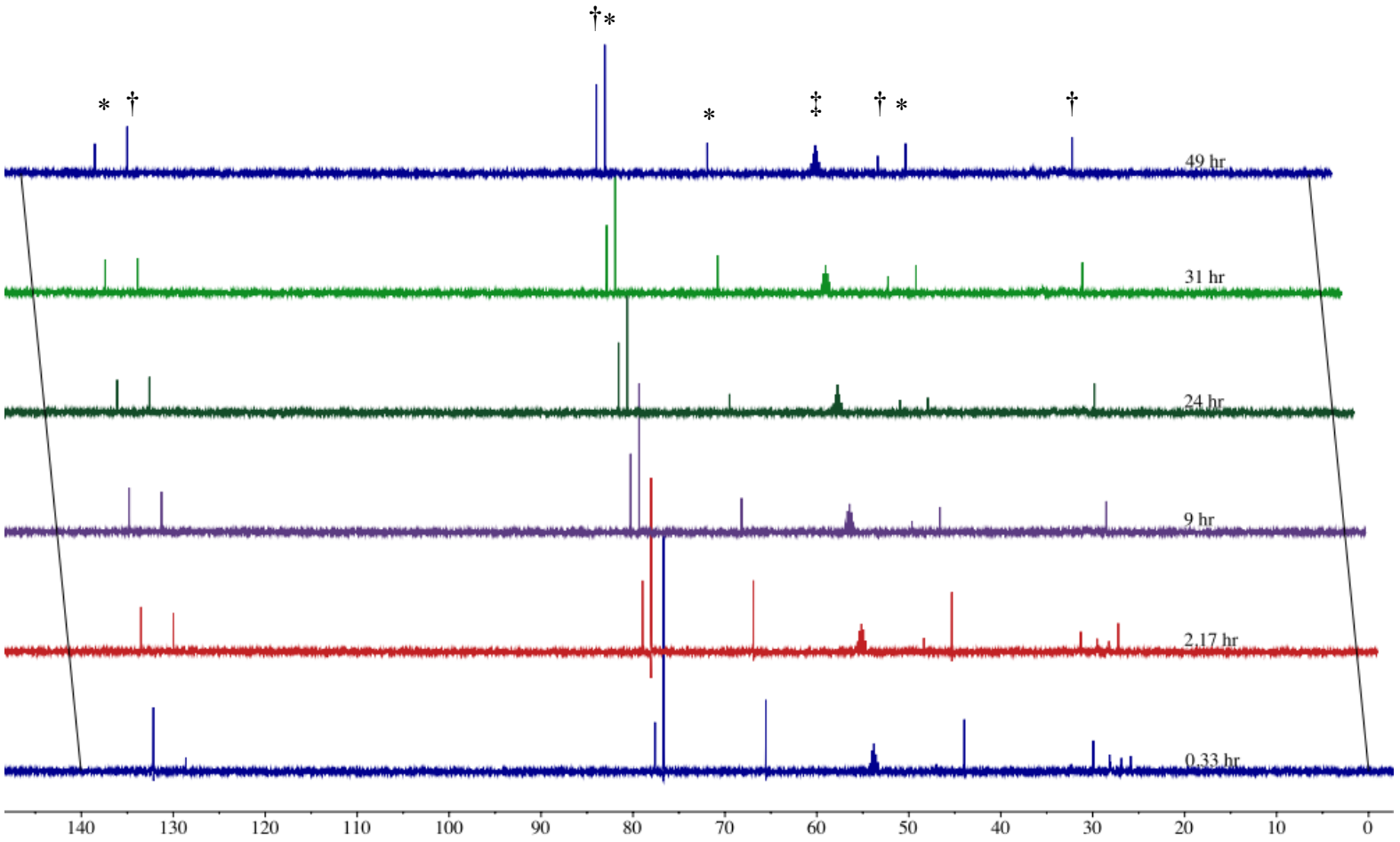

Figure 3.6. ROMP of **15** monitored by ^{13}C NMR in CD_2Cl_2 (* = starting material, † = product, and ‡ = solvent).

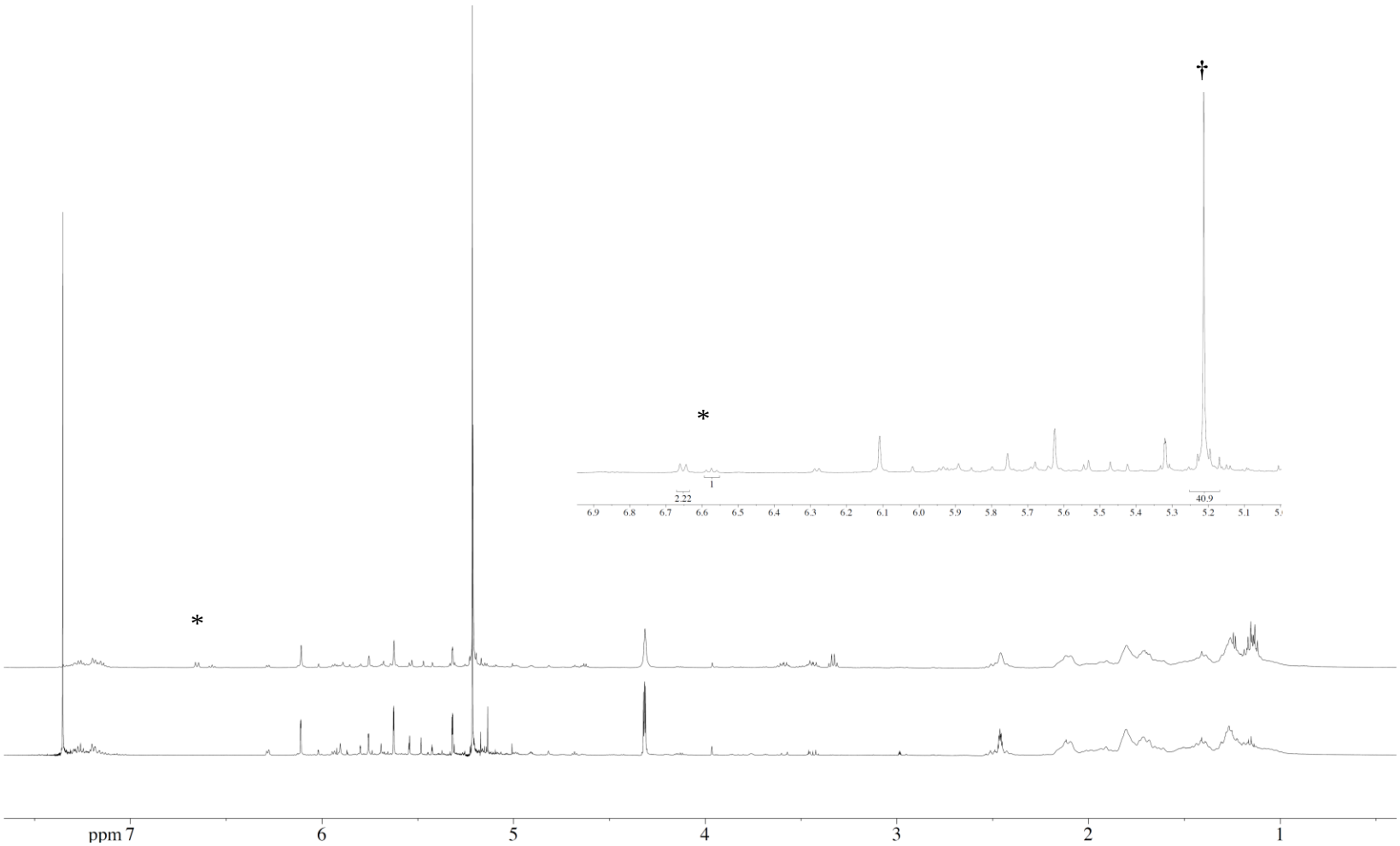

Figure 3.7. ^{1}H NMR spectra of **poly-15** (CD_2Cl_2) before (bottom) and after (top) quenching with ethyl vinyl ether; expanded view of end group vs. Cp region (inset, * = terminal vinyl group, † = Cp signal).

The electronic nature of **poly-15** was then investigated. The UV-Vis spectrum of **poly-15** shows a shoulder on the d-d transition peak near 360 nm (Figure 3.8). By comparison with Schrock′s results (Table 3.1), this suggests an effective conjugation length equivalent to 6-7 uncoordinated double bonds.

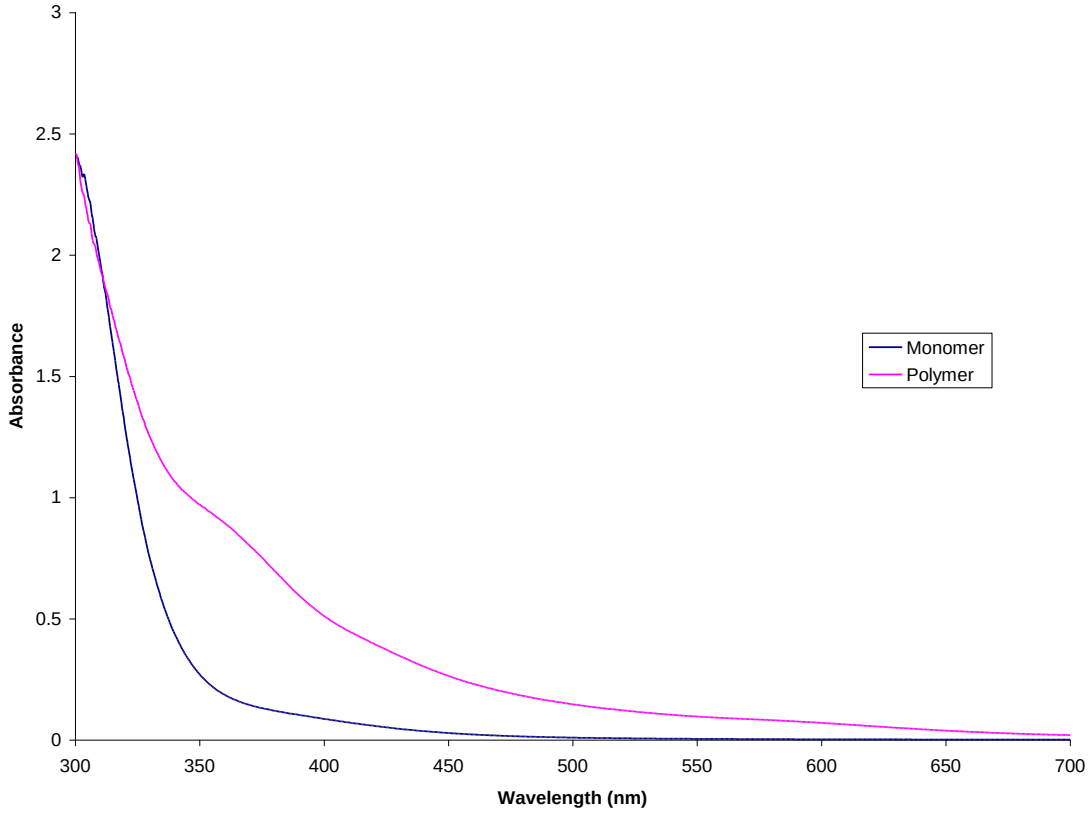

Figure 3.8. UV-Vis spectrum of **15** (0.662 mM or 0.222 g/L in CH_2Cl_2) and **poly-15** (0.205 g/L in CH_2Cl_2).

Interdigitated electrode arrays (Figure 3.9) have often been used to evaluate conductivity.[58,59] This simple process uses a conducting polymer to complete a circuit between two electrodes. If a polymer is capable of conducting electricity, a polymer film

can be cast across the area of the electrodes to complete the circuit. A potential was then applied and the current through the polymer film was measured.

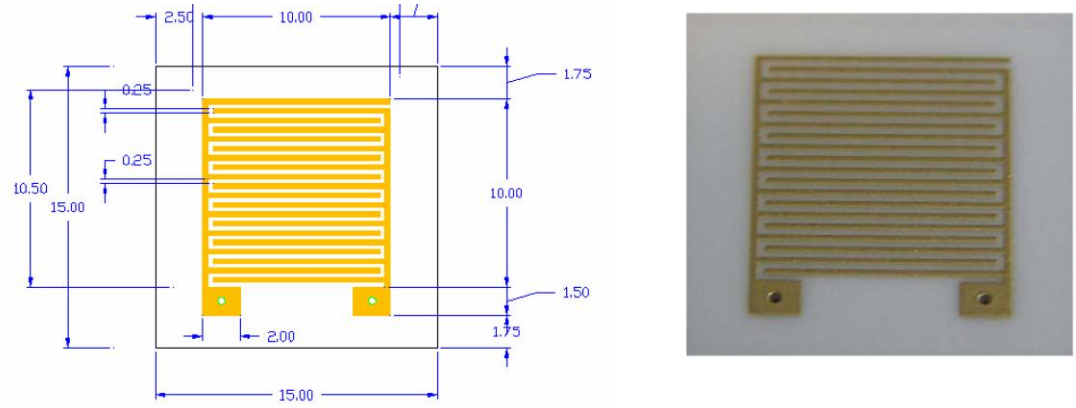

Figure 3.9. Interdigitated electrode schematic drawing (left) and photo (right).

It was found that CH_2Cl_2 solutions of **poly-15** readily gave films upon evaporation. Iodine doping of a drop-cast film of **poly-15** affords a lustrous brown film (Figure 3.10). A potential was then applied across the film using the potentiostat from a cyclic voltammetry instrument. Upon applying the potential, current was measured as shown in Figure 3.11. Although **poly-15** is air sensitive and blackens upon prolonged exposure, some conductivity was retained after exposure to air. After exposing the film coated electrode to air for 1 day, conductance was reduced to *ca.* 15%. After 45 days, conductance was reduced to *ca.* 5% of the pristine sample. While this method is a convenient way to test for conductivity, it does not allow for the determination of specific values.

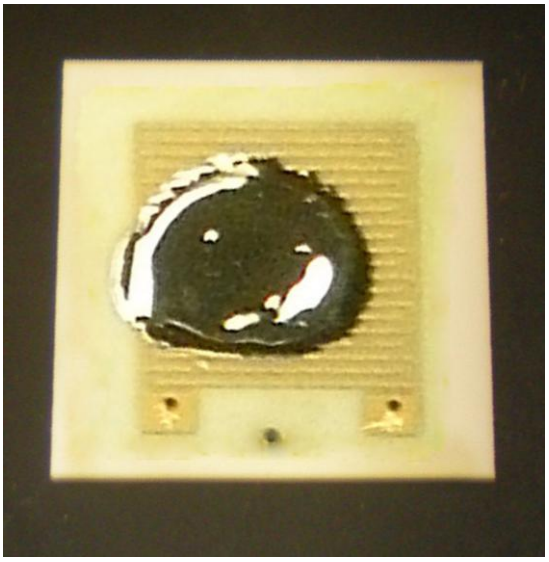

Figure 3.10. Iodine doped film of **poly-15** cast on an interdigitated electrode.

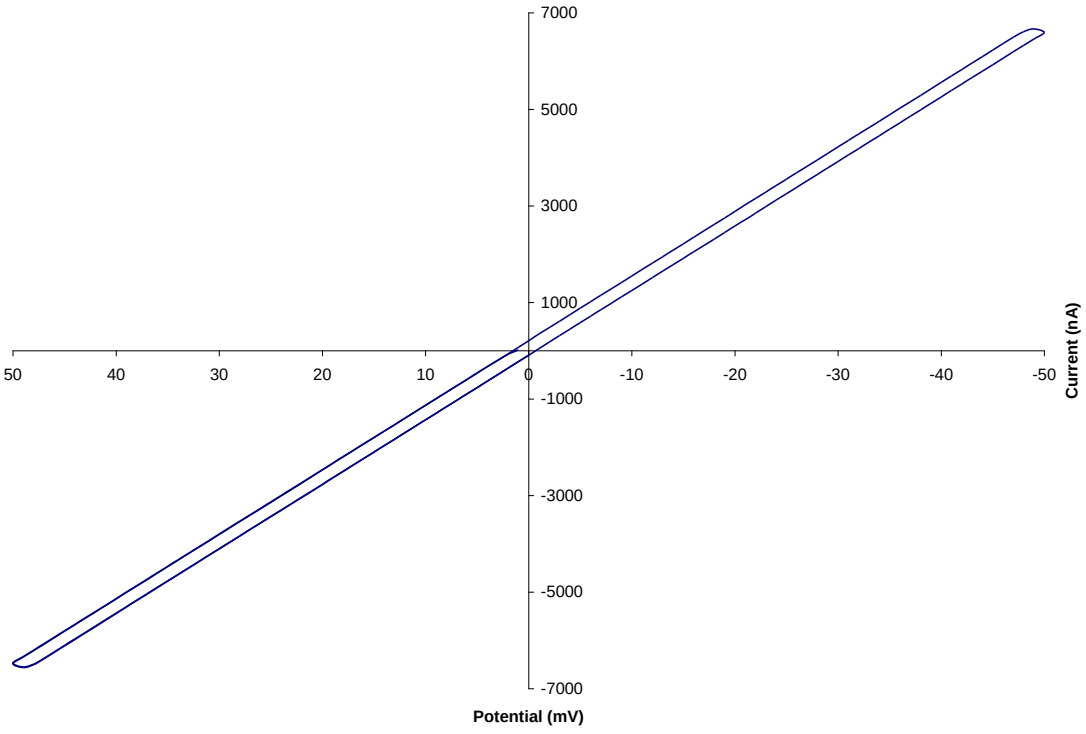

Figure 3.11. Measured conductance of iodine doped **poly-15**.

Cyclic voltammetry (CV) can be a powerful tool when analyzing conjugated polymers.[60] The electrochemical properties of dimeric iridium complexes featuring bridging ligands has been well studied.[61] Cyclic voltammetry scans of **15** and **poly-15** are shown in Figure 3.12; each trace was recorded starting from 0 V (vs. Ag/AgCl) in THF. As depicted in Figure 3.12-top the CV of **15** shows an irreversible oxidation at 0.47 V and reduction at −1.32 V. Given the synthesis of **15**, this is as expected. Bowyer and Geiger have described the change in hapticity as it correlates to the redox cycle in $[Cp^*(C_6Me_6)Ir][PF_6]_2$.[62] They found that Ir^{+1} adopts η^4 hapticity and Ir^{+3} adopts η^6 hapticity. Upon oxidation, the benzene ligand in **15** will likely adopt η^6 coordination as in its synthetic precursor, **21**. This facile chemical change results in an irreversible redox curve. As shown in Figure 3.12-bottom, the CV of **poly-15** exhibits five oxidation peaks at −1.32 V, 0.13 V, 0.64 V, 0.96 V, and 1.22 V. This was followed by five reductions at 0.52 V, −0.03 V, −0.75 V, −1.51 V, and −2.11 V. The CV clearly shows a pattern in **poly-15** indicative of a conjugated molecule with multiple redox sites. This type of correlated redox cycle is in good agreement with studies performed on oligo(*p*-phenylene-vinylene) systems by Heinze and coworkers.[63]

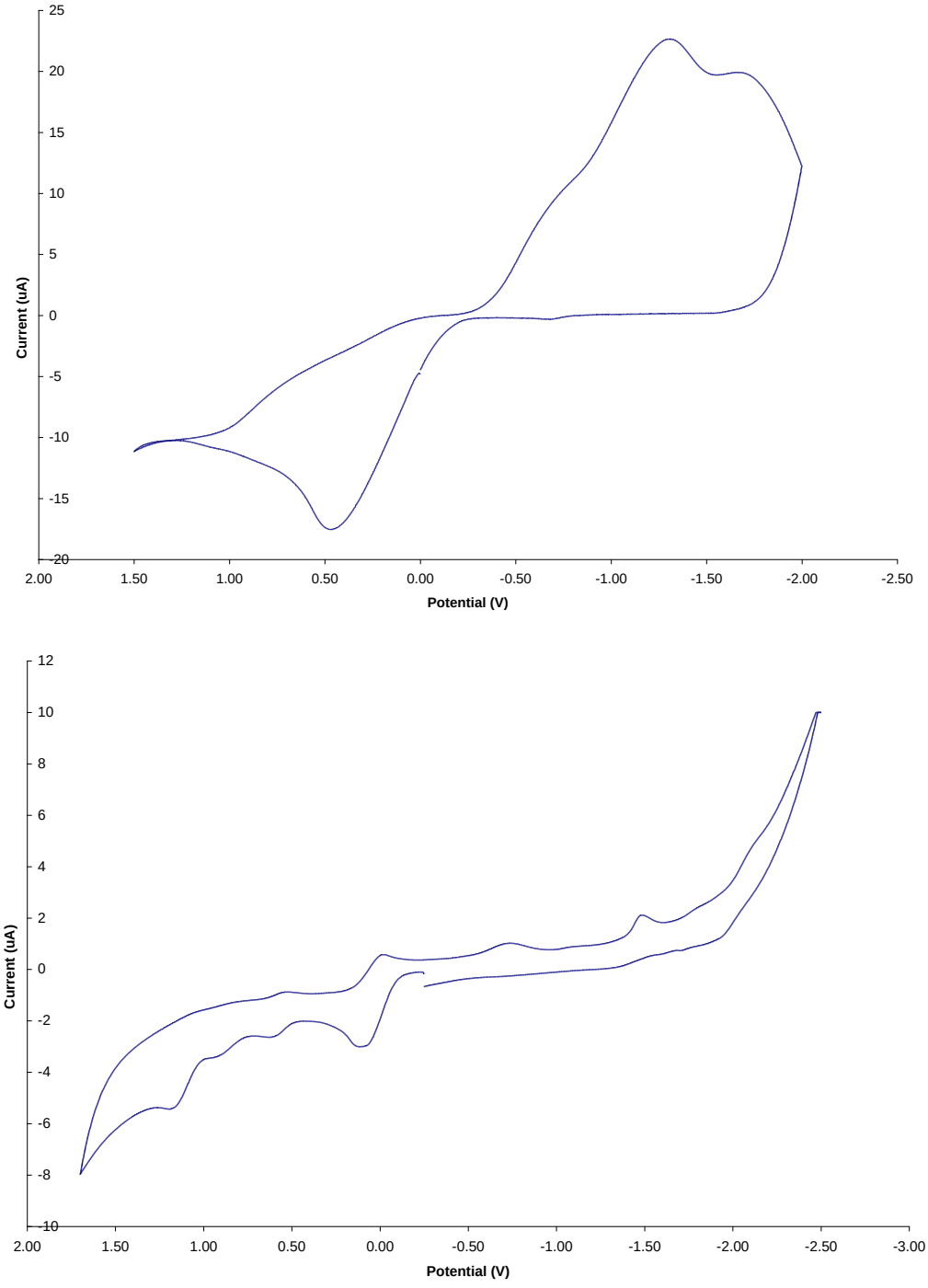

Figure 3.12. Cyclic voltammogram of **15** (1.0 mM), $[NBu_4][BF_4]$ (50 mM), in THF, 0.1 V/s (top), and **poly-15** (1.0 mM), $[NBu_4][BF_4]$ (50 mM), in THF, 0.1 V/s (bottom).

DISCUSSION

This work has explored the use of organometallic substrates as monomers for ROMP to produce PA. Complex **15** was chosen as a literature compound known to show reactivity with the non-coordinated carbon-carbon double bond.[48] The new pentamethylcyclopentadienyl analog **16** has been synthesized and crystallographically characterized. Additionally, the route to **16** developed offers entry into a variety of η^4-(arene)Cp*Ir complexes. Complexes **17** and **18** were chosen for evaluation due to their ease of acquisition.

Unfortunately, the utility of ROMP with COT and benzene organometallic complexes is not general. Although the X-ray crystal structure of **16** confirms a geometric resemblance to norbornadiene, it is not suitable for ROMP. This suggests that there is an underlying electronic influence driving the reactivity of **15**. A steric effect seems less likely since the planar Cp* ligand is in poor proximity of the non-coordinated carbon-carbon double bond (Figure 3.2). However, when ROMP does occur, as with **15**, the polymer thus formed features a regioregular repeat of CpIr π-adducts separated by vinylene linkages. Regioregular polymers often exhibit enhanced crystallinity, which would better facilitate interchain electron transport.[64] The sterics imposed by the CpIr should also prevent potential cross linking which would reduce conjugation.

Contrary to initial expectations, ROMP could not be extended to COT complexes **17** or **18**, even with the same catalyst used for the ROMP of substituted COTs in Scheme 3.4. Although the non-coordinated carbon-carbon double bonds in **18** have been shown to react as a nucleophile, reaction conditions suitable for ROMP of **18** could not be found.[65] Compared to η^4-benzene complexes, the COT ligand in **17** has less ring strain to facilitate ROMP. As discussed in Chapter I, relief of ring strain is typically the driving force in ROMP.

Standard end group analysis, UV-Vis, and electrochemistry of **poly-15** are all consistent with a relatively short conjugated polymer. In particular, the UV-Vis data suggest a short effective conjugation length of 6-7 double bonds (*vide supra*). However, this does not mean the polymer only contains six double bonds (which would be a dimer). As the resonance structure of Scheme 3.6 indicates, η^4 coordination of benzene leads to a loss of planarity. This deviation from planarity remains in the ring-opened polymer about the non-coordinated double bonds as evidenced by the ^{1}H NMR.

For analysis, Scheme 3.10 is recast as Scheme 3.11 with carbon atoms labeled. In the ^{1}H NMR, H_1 in **15** is a triplet with $^3J_{HH}$ = 3.2 Hz at 5.16 ppm. This signal shifted upfield to 4.32 ppm with $^3J_{HH}$ = 2.8 Hz. This suggests that the 1-2 and 3-4 linkages remain in the *cis* configuration, in agreement with an η^4-1,3,5-hexatriene iridium complex from Bianchini and coworkers.[66] Although the configuration about the vinylene linkage could not be definitively assigned, a single vinylene signal was observed in the ^{13}C NMR spectrum (Figure 3.6), suggestive of a single isomer.

Scheme 3.11. ROMP of **15** to form **poly-15** with diagnostic carbon atoms labeled.

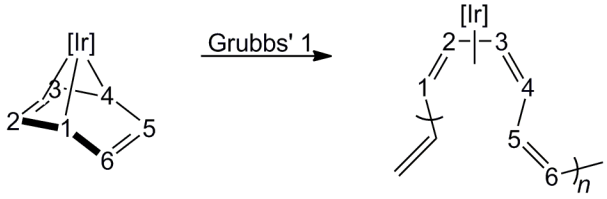

15 **poly-15**

In the probable case of *trans* vinylene linkages, and considering the out of plane bending observed about the C5-C6 bond (Scheme 3.11) and the steric congestion from the CpIr adducts, a coiled helical structure would result as in Figure 3.13 (depicted for clarity with an abbreviated CpIr fragment). Other types of helical PAs have been

engineered.[67] Scanning electron microscopy and polarizing optical microscopy have been used extensively in the literature to evaluate the helical structure in PA.[68] However, the polymer morphology was not investigated in this study.

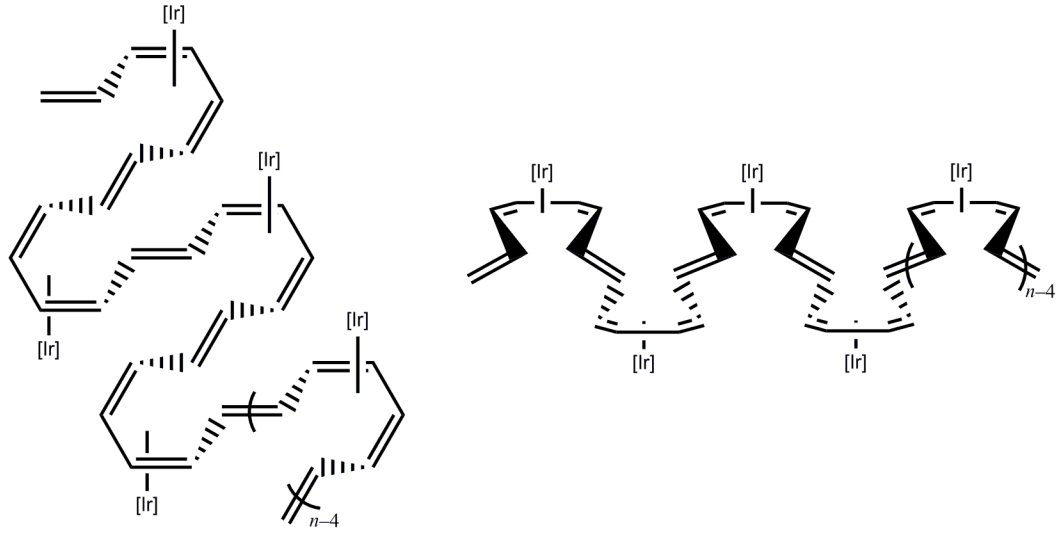

Figure 3.13. Two representations of the helical tertiary structure possibly associated with **poly-15**.

Given the chemical reduction involved in the synthesis of **15** (Scheme 3.7), it was not surprising to observe a non-reversible CV trace (Figure 3.12 top). This synthetic methodology suggests that the η^4-benzene ligand can readily convert to an η^6-benzene ligand upon oxidation. However, in the ring-opened polymer a free carbon-carbon double bond is not readily available to coordinate to the iridium center. As evidenced by the CV of **poly-15** (Figure 3.12 bottom), multiple redox states are accessible. This type of correlated redox curve suggests that intrachain electron transport through correlated sites along the polymer chain is possible.

Iodine doping of **poly-15** introduces several interesting features. First and foremost, doped **poly-15** is a conducting polymer. Since the effective conjugation length is short (*vide supra*), it is evident that the crystalline Cp ligand is adequately suited to

induce effective interchain electron transport. Additionally, the doped polymer has a lustrous metallic like sheen. This surface characteristic is indicative of a uniform layer, which would be advantageous in electronic applications.

CONCLUSION

Poly-15 is a new form of PA employing regioregular CpIr π-adducts and has been developed using ROMP. The synthesis of this new polymer has been optimized, requiring a high catalyst loading of 20 mol% and two days to reach completion in CD_2Cl_2 at 40 °C. UV-Vis analysis of **poly-15** suggests the effective conjugation length is approximately 6-7 double bonds. This new polymer was found to be conductive.

A solid state structural analysis of the closely related monomer **16** shows that the geometry of the benzene ligand does in fact approach that of norbornadiene. However, **16** does not undergo ROMP under a variety of reaction conditions and catalyst variations. Also, polymerization could not be extended to η^4 or η^6-COT complexes.

EXPERIMENTAL

General

All reactions were carried out in an inert atmosphere using standard Schlenk and vacuum line techniques. Chemicals were treated as follows: benzene and pentane were distilled from Na/benzophenone; all other solvents were purified using a Glass Contour solvent purification system; $CDCl_3$ (Cambridge Isotope Laboratories), CD_2Cl_2 (Cambridge Isotope Laboratories), DMSO-d_6 (Aldrich), C_6D_6 (Cambridge Isotope Laboratories), toluene-d_8 (Aldrich), acetonitrile-d_3 (Aldrich), $IrCl_3 \cdot nH_2O$ (Pressure Chemical Company, 52% metal basis), 1,3-cyclohexadiene (Acros, 96%), CpTl (Strem, 95%), Cp*H (Alfa Aesar, 94%), triphenylcarbenium tetrafluoroborate (Alfa Aesar, 98%), Cp_2Co (Alfa Aesar, 98%), $RuCl_3 \cdot 3H_2O$ (Alfa Aesar, 99.9%), $[NH_4][PF_6]$ (Alfa Aesar, 99.5%), COT (Strem, 98%), $[Ag][BF_4]$ (Alfa Aesar, 99%), Grubbs′ first

generation catalyst (**I**) (Aldrich), KO-*t*-Bu (Acros, 98%), ethyl vinyl ether (Alfa Aesar, 99%), WCl_6 (Strem, 99.9%), $SiMe_3OMe$ (Alfa Aesar, 97%), neopentylmagnesium chloride (Rieke Metals Inc., 1.0 M in ether), 1,2-dimethoxyethane (EMD DriSolv®, 99.9%), 2,6-diisopropylaniline (TCI, 90%), chlorotrimethylsilane (Alfa Aesar, 98%), HCl (Aldrich, 2.0 M in ether), $HOC(CF_3)_2(CH_3)$ (Alfa Aesar, 98%), triethylamine (Alfa Aesar, 99%), and *n*-BuLi (Alfa Aesar, 2.85 M in hexanes) were used as received.

NMR spectra were recorded on a Varian NMRS 500 MHz spectrometer at ambient probe temperatures and referenced as follows: ^1H: residual internal $CHCl_3$ (δ, 7.26 ppm), $CDHCl_2$ (δ, 5.32 ppm), DMSO-d_5 (δ, 2.50 ppm), C_6D_5H (δ, 7.15 ppm), toluene-d_7 (δ, 7.09, 7.00, 6.98, and 2.09 ppm) or acetonitrile-d_2 (δ, 1.94 ppm); ^{13}C: internal $CDCl_3$ (δ, 77.2 ppm), CD_2Cl_2 (δ, 54.00 ppm), DMSO-d_6 (δ, 39.51 ppm), C_6D_6 (δ, 128.39 ppm), toluene-d_8 (δ, 129.24, 128.33, 125.49, 20.7 ppm), or acetonitrile-d_3 (δ, 118.69 and 1.39 ppm). Cyclic voltammograms were recorded using a BASi epsilon potentiostat and C-3 cell stand. UV-Vis spectra were recorded on a Shimadsu UV-1800 spectrometer. Melting points were recorded with a Stanford Research Systems (SRS) MPA100 (Opti-Melt) automated melting point system. Microanalyses were conducted by Atlantic Microlab. Interdigitated electrodes were purchased from the Case Western Reserve University Electronics Design Center (item # 102).

$(1,3\text{-}C_6H_8)_2IrCl$ (19)[48]

A round bottom flask was charged with $IrCl_3 \cdot nH_2O$ (4.0013 g, 10.824 mmol), ethanol (60 mL), water (40 mL), and 1,3-cyclohexadiene (9.00 mL, 94.3 mmol). The mixture was refluxed (oil bath) for 8 h, and then cooled in an ice bath. The precipitate was collected by filtration, washed with ethanol (3 × 5 mL), and dried by oil pump vacuum to afford **15** (3.3843 g, 8.7240 mmol, 81%) as an off white solid.

^{1}H NMR ($CDCl_3$): δ 5.12 (m, 4H, C*H*=CHCH$_2$), 4.00 (m, 4H, CH=C*H*CH$_2$), 2.08 and 1.61 (2 m, 2 × 4H, C*H*$_2$).

(1,3-C_6H_8)CpIr (20)[48]

A round bottom flask was charged with CpTl (1.2033 g, 4.4655 mmol), **19** (1.7317 g, 4.4639 mmol), and THF (100 mL) with stirring. After 16 h, the flask was heated to 50 ˚C. After 2 h, the solvent was removed by oil pump vacuum. The residue was extracted with hexanes (150 mL). The extract was filtered, and the solvent removed and residue dried by oil pump vacuum to give **20** (1.4471 g, 4.2885 mmol, 96%) as an off white solid.

^{1}H NMR (C_6D_6): δ 4.58 (s, 5H, Cp), 4.55 (m, 2H, C*H*=CHCH$_2$), 3.23 (m, 2H, CH=C*H*CH$_2$), 1.30 and 1.10 (2 m, 2 × 2H, C*H*$_2$). ^{13}C{^{1}H} NMR (C_6D_6): δ 76.4 (Cp), 66.3 (*C*H=CHCH$_2$), 43.9 (CH=*C*HCH$_2$), 28.8 (*C*H$_2$).

[(η^6-C_6H_6)CpIr][BF_4]$_2$ (21)[48]

A round bottom flask was charged with a solution of **20** (0.8482 g, 2.514 mmol) in dichloromethane (10 mL) and a suspension of triphenylcarbenium tetrafluoroborate (1.6553 g, 5.0604 mmol) in dichloromethane (10 mL) with stirring. After 15 min, ether (140 mL) was added. The precipitate was collected by filtration, washed with ether (2 × 5 mL), and dried by oil pump vacuum to afford **21** (1.2374 g, 2.4309 mmol, 97%) as an off white solid.

(η^4-C_6H_6)CpIr (15)[48]

A round bottom flask was charged with a suspension of Cp_2Co (1.5136 g, 8.0033 mmol) in dichloromethane (20 mL) and a suspension of **21** (2.0441 g, 4.0157 mmol) in dichloromethane (20 mL) with stirring. After 10 min, ether (150 mL) was added. The mixture was filtered and the [Cp_2Co][BF_4] cake washed with ether (2 × 10 mL). The

solvent was removed and the residue dried by oil pump vacuum to give **15** (1.3132 g, 3.9151 mmol, 98%) as a yellow solid.

^{1}H NMR ($CDCl_3$): δ 6.31 (m, 2H, H_5), 5.25 (m, 2H, H_1), 5.16 (s, 5H, Cp), 3.81 (m, 2H, H_2). $^{13}C\{^{1}H\}$ NMR ($CDCl_3$): δ 132.4 (C_5), 76.6 (Cp), 65.7 (C_1), 43.9 (C_2). The ^{1}H and ^{13}C NMR signals are labeled per Scheme 3.11.

$[Cp^*Cl_2Ir]_2$ (22)[49]

A round bottom flask was charged with $IrCl_3 \cdot nH_2O$ (2.5745 g, 6.9646 mmol) and methanol (75 mL). Cp*H (1.51 mL, 9.64 mmol) was then introduced by syringe with stirring. The mixture was refluxed for 2 d, and cooled in an ice bath. The precipitate was collected by filtration, washed with ice cold methanol (2 × 10 mL), and dried by oil pump vacuum to give **22** (2.0670 g, 2.5944 mmol, 75%) as an orange powder.

^{1}H NMR ($CDCl_3$): δ 1.59 (s, 15H, Cp*). $^{13}C\{^{1}H\}$ NMR ($CDCl_3$): δ 86.6 (CCH_3), 9.7 (CH_3). These data agreed with those previously reported.[49]

$[(\eta^6\text{-}C_6H_6)Cp^*Ir][BF_4]_2$ (23)[50]

A scintillation vial was charged with **22** (0.5003 g, 0.6280 mmol), $[Ag][BF_4]$ (0.491 g, 2.522 mmol), and acetone (3 mL) with stirring. After 15 min, the mixture was filtered, and benzene (2.0 mL) was added, with stirring. After 4 h, the precipitate was collected by filtration, washed with benzene (1 mL) and pentane (1 mL), and dried by oil pump vacuum to give **23** (0.4356 g, 0.7521 mmol, 60%) as a colorless solid.

^{1}H NMR (acetonitrile-d_3): δ 7.27 (s, 6H, C_6H_6), 2.32 (s, 15H, CH_3). $^{13}C\{^{1}H\}$ NMR (acetonitrile-d_3): δ 107.5 (CCH_3), 99.4 (C_6H_6), 10.8 (CH_3).

$Cp^*(\eta^4\text{-}C_6H_6)Ir$ (16)

A scintillation vial was charged with **23** (0.3359 g, 0.5800 mmol), Cp_2Co (0.2191 g, 1.159 mmol), and dichloromethane (5 mL) with stirring. After 15 min, the mixture was poured into ether (50 mL) and filtered. The solvent was removed from the

filtrate by oil pump vacuum to afford **16** (0.2326 g, 0.5735 mmol, 99%) as a yellow-brown solid.

^{1}H NMR ($CDCl_3$): δ 5.73 (m, 2H, H_5), 5.09 (m, 2H, H_1), 3.03 (m, 2H, H_2), 1.95 (s, 15H, Cp). $^{13}C\{^{1}H\}$ NMR ($CDCl_3$): δ 130.6 (C_5), 89.7 (CCH_3), 66.3 (C_1), 48.4 (C_2), 10.7 (CH_3). The ^{1}H and ^{13}C NMR spectra are shown in Figure 3.14. The ^{1}H and ^{13}C NMR signals are labeled per Scheme 3.11.

Elemental Analysis: calculated: C, 47.38%; H, 5.22%.

found: C, 45.30%; H, 5.11%.

[(η^6-C_6H_6)$RuCl_2$]$_2$ (24)[54]

A round bottom flask was charged with 1,3-cyclohexadiene (6.20 mL, 65.0 mmol), $RuCl_3 \cdot 3H_2O$ (1.7451 g, 6.6741 mmol), ethanol (90 mL), and water (10 mL) with stirring. The mixture was then heated to 45 ˚C. After 3 h, the mixture was cooled to room temperature and concentrated to 30 mL. The precipitate was collected by filtration, washed with ethanol (2 × 10 mL) and hexanes (4 × 10 mL), and dried by oil pump vacuum to give **24** (1.5032 g, 3.0053 mmol, 90%) as a brown solid.

^{1}H NMR ($CDCl_3$): δ 1.56 (s, 12H, C_6H_6). $^{13}C\{^{1}H\}$ NMR (DMSO-d_6): δ 87.6 (C_6H_6).

[(η^6-C_6H_6)CpRu][Cl] (25)[55]

A round bottom flask was charged with CpTl (0.5398 g, 2.003 mmol), **24** (0.5001 g, 0.9984 mmol), and acetonitrile (150 mL) with stirring. After 1 h, the mixture was filtered and the filter cake rinsed with acetonitrile (2 × 10 mL). The solvent was removed from the filtrate by oil pump vacuum and the residue recrystallized from acetonitrile/ether (30/150 mL). The precipitate was collected by filtration, washed with ether (2 × 10 mL), and dried by oil pump vacuum to give **25** (0.4283 g, 1.531 mmol, 77%) as an off white solid.

^{1}H NMR (DMSO-d_6): δ 6.24 (s, 6H, C_6H_6), 5.48 (s 5H, Cp). ^{13}C{^{1}H} NMR (DMSO-d_6): δ 85.8 (C_6H_6), 80.0 (Cp). These data agreed with those previously reported.[55]

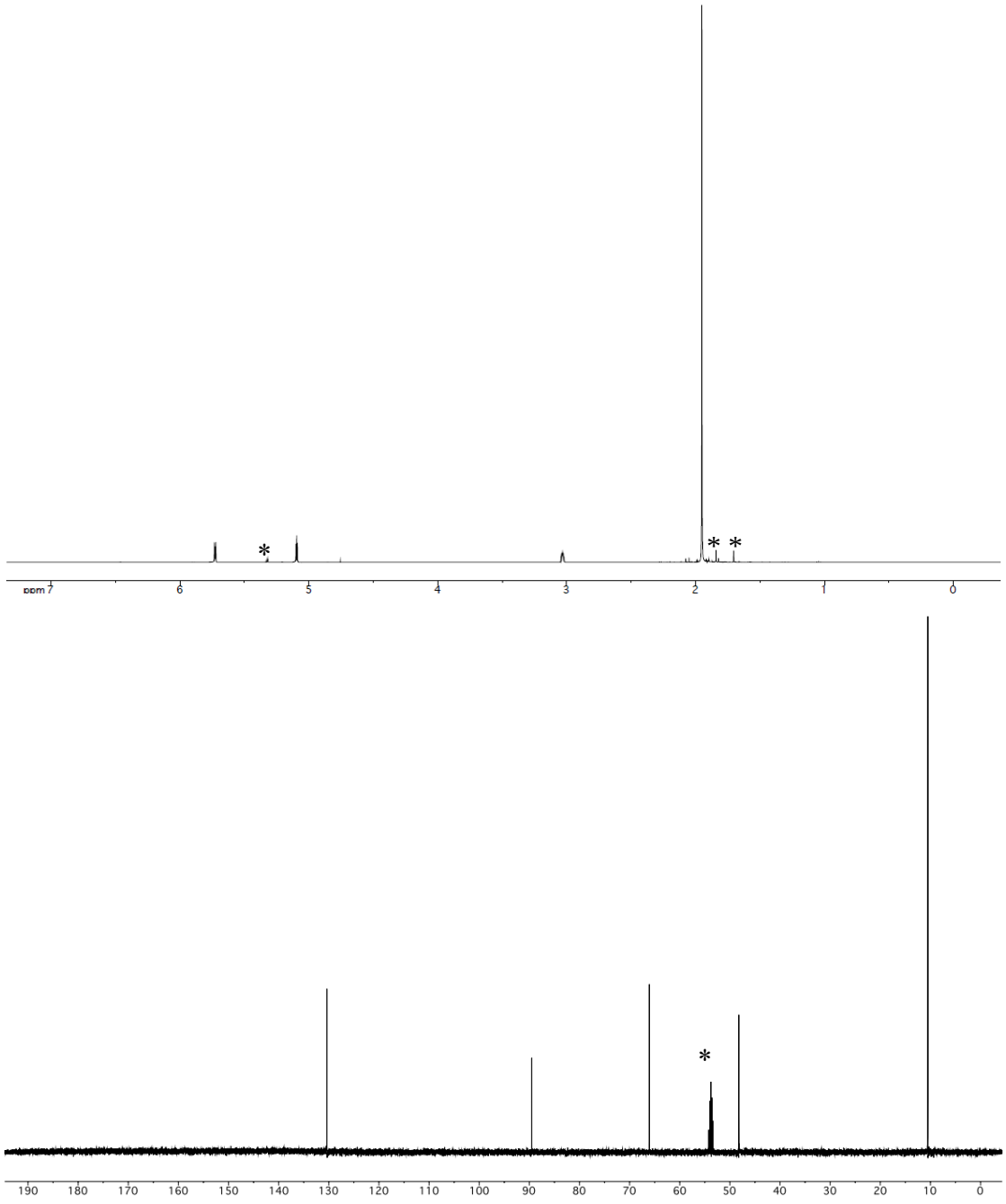

Figure 3.14. NMR spectra of **16** in CD_2Cl_2; ^{1}H (top) and ^{13}C (bottom) (* = solvent peak or impurity).

[(η^6-C_6H_6)CpRu][PF_6] (26)[56]

A round bottom flask was charged with a solution of [NH_4][PF_6] (0.3776 g, 2.317 mmol) in water (10 mL) and a solution of **25** (0.4283 g, 1.531 mmol) in water (40 mL) with stirring. After 5 min, the precipitate was collected by filtration, washed with water (2 × 10 mL), dissolved in acetone (10 mL), reprecipitated with ether (60 mL), recollected by filtration, washed with ether (2 × 10 mL), and dried by oil pump vacuum to give **26** (0.4532 g, 1.164 mmol, 76%) as a colorless solid.

^{1}H NMR (DMSO-d_6): δ 6.24 (s, 6H, C_6H_6), 5.48 (s 5H, Cp). ^{13}C{^{1}H} NMR (DMSO-d_6): δ 85.8 (C_6H_6), 80.0 (Cp). These data agreed with those previously reported.[56]

[Cp(η^6-COT)Ru][PF_6] (17)[56]

A 250 mL quartz immersion photochemical reactor was charged with **26** (0.6689 g, 1.718 mmol) and purged with nitrogen for 20 min. Acetonitrile (200 mL) was then introduced by cannula transfer. The mixture was irradiated with a medium pressure mercury lamp for 5 h, and COT (7.20 mL, 6.39 mmol) was added. The mixture was then stirred for 20 min and the solvent removed by oil pump vacuum. The residue was triturated in hexanes (10 mL). After 3 h, the precipitate was collected by filtration and washed with hexanes (3 × 10 mL). The sample was then dissolved in acetone (10 mL), and ether (100 mL) was added. The precipitate was collected by filtration, washed with ether (3 × 10 mL), and dried by oil pump vacuum to afford **17** (0.6060 g, 1.459 mmol, 85%) as an off white solid.

^{1}H NMR (CD_2Cl_2): δ 6.76 (m, 2H, H_3), 5.88 and 5.83 (2 m, 2 × 2H, H_1 and H_2), 5.52 (s, 5H, Cp), 5.08 (m, 2H, H_7). ^{13}C{^{1}H} NMR (DMSO-d_6): δ 134.1 (C_7), 86.0 (Cp) and 102.5, 92.5, and 81.7 ($C_{1\text{-}3}$). These data agreed with those previously reported.[56] The ^{1}H and ^{13}C NMR signals are labeled per Scheme 3.11.

Grubbs′ second generation catalyst (II)[69]

A Schlenk tube was charged with Grubbs′ first generation catalyst (**I**; 0.9063 g, 1.101 mmol), 1,3-bis(2,4,6-trimethylphenyl)imidazolinium chloride (0.6604 g, 1.926 mmol), KO-*t*-Bu (0.2463 g, 2.195 mmol), and hexanes (15 mL). A septum was wired on and the tube evacuated with stirring for 4 min. The mixture was then heated as a closed system at 60 ˚C. After 24 h, the sample was cooled. A 1:1 v/v mixture of water/isopropanol (25 mL) was added and the mixture stirred in air for 30 min. The precipitate was collected by filtration, washed with 1:1 v/v water/isopropanol (3 × 10 mL) and hexanes (3 × 10 mL), and dried by oil pump vacuum to give **II** (0.5931 g, 0.6986 mmol, 64%) as a peach pink solid.

^{1}H NMR (CD_2Cl_2): δ 19.09 (s, 1H, RuC*H*), 7.38-7.00 (m, 9H, H_{aryl}), 3.97 (s, 4H, NCH_2), 2.8-0.70 (m, 51H). These data agreed with those previously reported.[69]

Grubbs′ third generation catalyst (III)[70]

A round bottom flask was charged with **II** (0.4005 g, 0.4717 mmol), toluene (1.00 mL), and pyridine (3.00 mL) with stirring. After 10 min, pentane (10 mL) was added. The mixture was cooled to −10 ˚C ($CaCl_2$/ice). The precipitate was collected by filtration, washed with pentane (4 × 5 mL), and dried by oil pump vacuum to give **III** (0.2711 g, 0.3730 mmol, 79%) as a green solid.

^{1}H NMR (C_6D_6): δ 19.64 (s, 1H, PhC*H*), 8.65 (br s, 2H, pyr), 8.35 (br s, 2H, pyr), 8.04 (d, 2H, $^3J_{HH}$ = 7.2 Hz, *o*-C*H*), 7.18 (t, 1H, $^3J_{HH}$ = 7.2 Hz, *p*-C*H*), 6.94-6.04 (br, multiple peaks, 6H, pyr, mes C*H*), 3.38 (br d, 4H, CH_2CH_2), 2.84 (br s, 6H, mes CH_3), 2.43 (br s, 6H, mes CH_3), 2.11 (br s, 6H, mes CH_3). These data agreed with those previously reported.[70]

Synthesis of V

$WCl_3(OMe)_3$[71]

A round bottom flask was charged with $SiMe_3OMe$ (21.46 mL, 155.7 mmol) and WCl_6 (20.3161 g, 51.230 mmol) was added in small portions with stirring over 1 h while maintaining a temperature below 5 ˚C. After an additional 15 min, the volatiles were removed by oil pump vacuum. The residue was recrystallized from ether to give $WCl_3(OMe)_3$ (15.8609 g, 41.3780 mmol, 81%) as yellow needles.

^{1}H NMR (C_6D_6): δ 4.94 (s, 6H), 4.49 (s, 3H). $^{13}C\{^1H\}$ NMR (C_6D_6): δ 70.9, 67.6.

$W(\equiv CCMe_3)Np_3$[72]

A round bottom flask was charged with neopentylmagnesium chloride (82.5 mL of a 1.0 M solution in ether, 82.5 mmol). A solution of $WCl_3(OMe)_3$ (5.3505 g, 13.959 mmol) in THF (20 mL) and ether (40 mL) was then added dropwise with stirring over 1 h at −78 ˚C. The mixture was then stirred while the cold bath slowly warmed to room temperature. After 14 h, the mixture was filtered through a pad of celite, which was washed with ether (2 × 50 mL). The volatiles were then removed from the filtrate. The residue was dried by oil pump vacuum, and extracted with pentane (40 mL). The extract was filtered and the insolubles were washed with pentane (2 × 10 mL). The filtrate and washings were concentrated by oil pump vacuum. The product was then distilled from the residue at 80 ˚C and full vacuum. Multiple fractions can be obtained by extracting the distillation residue with pentane, filtering, pumping off the solvent, and distilling the residue. Three crops were combined to give $W(CCMe_3)Np_3$ (2.800 g, 6.004 mmol, 44%) as a yellow solid.

^{1}H NMR (C_6D_6): δ 1.56 (s, 9H, $CC(CH_3)_3$), 1.14 (s, 27H, $CH_2C(CH_3)_3$), 0.98 (s, 6H, CH_2). These data agreed with those previously reported.[72]

W(≡CCMe$_3$)(dme)Cl$_3$[72]

A round bottom flask was charged with W(≡CCMe$_3$)Np$_3$ (1.5512 g, 3.3259 mmol), DME (1.04 mL), and pentane (10 mL). Then HCl (6.45 mL of a 2.0 M solution in ether, 13 mmol) was added dropwise at 0 ˚C, with stirring. After 30 min, the precipitate was collected by filtration, washed with pentane (2 × 5 mL), and dried by oil pump vacuum to give W(≡CCMe$_3$)(dme)Cl$_3$ (0.9821 g, 2.185 mmol, 66%) as a purple solid.

^{1}H NMR (toluene-d$_8$): δ 3.58 and 3.21 (s, 6H, C*H*$_3$O), 2.90 and 2.82 (m, 4H, OC*H*$_2$), 1.25 (s, 9H, C(C*H*$_3$)$_3$). These data agreed with those previously reported.[72]

N(2,6-*i*-Pr$_2$NC$_6$H$_3$)H(TMS)[73]

A round bottom flask was charged with 2,6-diisopropylaniline (4.5229 g, 25.511 mmol) and pentane (30 mL). Then *n*-BuLi (9.00 mL of a 2.85 M solution in hexanes, 25.7 mmol) was added dropwise at 0 ˚C with stirring. After 10 min, the cold bath was removed. After 4 h, the precipitate was collected by filtration, washed with pentane (2 × 10 mL), and dried by oil pump vacuum. A round bottom flask was then charged with the white solid, ether (50 mL), and chlorotrimethylsilane (3.25 mL, 25.6 mmol) with stirring at 0 ˚C. The cold bath was removed. After 14 h, the mixture was filtered through a pad of celite. The pad was washed with ether (2 × 10 mL) and the filtrate concentrated by oil pump vacuum to give N(2,6-*i*-Pr$_2$NC$_6$H$_3$)H(TMS) (6.0196 g, 24.130 mmol, 95%) as a yellow liquid.

^{1}H NMR (CDCl$_3$): δ 7.10-7.00 (m, 3H, *H*$_{aryl}$), 3.39 (sept, 2H, C*H*Me$_2$), 2.31 (s, 1H, N*H*), 1.20 (d, 12H, CH(C*H*$_3$)$_2$), 0.14 (s, 9H, Si(C*H*$_3$)$_3$). These data agreed with those previously reported.[73]

W(≡CCMe$_3$)(NH-2,6-*i*-Pr$_2$NC$_6$H$_3$)(dme)Cl$_2$[74]

A round bottom flask was charged with W(≡CCMe$_3$)(dme)Cl$_3$ (0.9920 g, 2.2207 mmol) and ether (15 mL). A solution of N(2,6-*i*-Pr$_2$NC$_6$H$_3$)H(TMS) (0.5566 g, 2.231 mmol) in ether (3 mL) was then added dropwise at −41 ˚C (acetonitrile/ CO_2(s)) with stirring. The cold bath was then removed. After 30 min, the solvent was removed by oil pump vacuum. The residue was recrystallized from pentane and ether to give W(≡CCMe$_3$)(NH-2,6-*i*-Pr$_2$NC$_6$H$_3$)(dme)Cl$_2$ (0.9409 g, 1.594 mmol, 72%) as a yellow solid.

^{1}H NMR (C_6D_6): δ 10.43 (s, 1H, C*H*CMe$_3$), 7.24-6.98 (m, 3H, H_{aryl}), 4.26 (sept, 2H, C*H*Me$_2$), 3.25 (br s, 6H, CH_3O), 3.08 (s, 4H, OCH_2), 1.60 (br s, 6H, C*H*Me$_2$), 1.25 (br s, 6H, C*H*Me$_2$), 0.94 (s, 9H, C(CH_3)$_3$). These data agreed with those previously reported.[74]

W(=CHCMe$_3$)(N-2,6-*i*-Pr$_2$NC$_6$H$_3$)(dme)Cl$_2$[74]

A round bottom flask was charged with W(≡CCMe$_3$)(NH-2,6-*i*-Pr$_2$NC$_6$H$_3$)(dme)Cl$_2$ (0.9409 g, 1.594 mmol) and ether (40 mL) and cooled to −41 ˚C (acetonitrile/CO_2(s)). A solution of triethylamine (0.15 mL) in ether (1.5 mL) was then added with stirring. After 5 min, the cold bath was removed. After 1 h, the volatiles were removed by oil pump vacuum. The residue was recrystallized from pentane and ether to give W(=CHCMe$_3$)(N-2,6-*i*-Pr$_2$NC$_6$H$_3$)(dme)Cl$_2$ (0.3746 g, 0.6346 mmol, 40%) as an orange solid.

^{1}H NMR (toluene-d_8): δ 9.89 (s, 1H, C*H*CMe$_3$), 7.12-6.98 (m, 3H, H_{aryl}), 4.57 (sept, 2H, C*H*Me$_2$), 3.22 (s, 6H, CH_3O), 3.14 (s, 4H, OCH_2), 1.39 (d, 12H, CH(CH_3)$_2$), 1.33 (s, 9H, C(CH_3)$_3$). These data agreed with those previously reported.[74]

$LiOC(CF_3)_2(CH_3)$

A round bottom flask was charged with *n*-BuLi (10.00 mL of a 2.85 M solution in hexanes, 28.5 mmol) and hexanes (20 mL). Then $HOC(CF_3)_2(CH_3)$ (3.85 mL, 31.4 mmol) was added dropwise at 0 ˚C with stirring. After 20 min, the cold bath was removed. After 4 h, the volatiles were removed by oil pump vacuum to afford $LiOC(CF_3)_2(CH_3)$ (4.8147 g, 25.610 mmol, 90%) as a white solid.

$W(=CHCMe_3)(N\text{-}2,6\text{-}i\text{-}Pr_2NC_6H_3)(OCMe(CF_3)_2)_2$ (V)[74]

A scintillation vial was charged with solutions of $W(=CHCMe_3)(N\text{-}2,6\text{-}i\text{-}Pr_2NC_6H_3)(dme)Cl_2$ (0.3746 g, 0.6478 mmol) and $LiOC(CF_3)_2(CH_3)$ each in 5 mL of ether at −35 ˚C with stirring. After 30 min, the mixture was filtered though a pad of celite. The pad was washed with ether (3 × 2 mL) and the filtrate concentrated by oil pump vacuum. The residue was dried by oil pump vacuum for 30 h, treated with pentane (8 mL) and ether (2 mL), and cooled to −35 ˚C. After 14 h, a small amount of yellow-brown solid precipitated. The supernatant was decanted and the solvent removed by oil pump vacuum to afford **V** (0.3716 g, 0.4696 mmol, 73%) as a yellow solid.

^1H NMR (C_6D_6): δ 8.83 (s, 1H, C*H*CMe_3), 7.02 (m, 3H, H_{aryl}), 3.34 (sept, 2H, C*H*Me_2), 1.35 (s, 6H, $OC(CH_3)(CF_3)_2$), 1.20 (d, 12H, $CH(CH_2)_2$), 1.06 (s, 9H, $C(CH_3)_3$). These data agreed with those previously reported.[74]

Poly-15

Method A: A J. Young NMR tube was charged with **15** (0.0320 g, 0.0954 mmol), **I** (0.0076 g, 0.0092 mmol), and CD_2Cl_2 (1 mL). The reaction was monitored by ^1H NMR at room temperature. Analogous experiments were conducted with **II** and **IV** (10 mol%) at room temperature and 40 °C.

Method B: A tube was charged with **15** (0.2347 g, 0.6997 mmol), **I** (0.1150 g, 0.1397 mmol), and dichloromethane (10 mL) and sealed with a threaded stopper. The

mixture was heated to 40 °C with stirring as a closed system. After 3 d, the mixture was cooled and ethyl vinyl ether (0.750 mL) was added. After 10 min, the volatiles were removed by oil pump vacuum to give **poly-15** (0.3402 g) as a red-brown solid.

Other polymerization reactions

A J. Young NMR tube was charged with **16**, **17**, or **18** (0.1 mmol), **I**, **II**, **III**, **IV**, or **V** (10 mol%), and CD_2Cl_2 (1 mL). The reactions (see text) were monitored by ^1H NMR at room temperature and then 40 °C.

Conductivity Measurement

A 0.025 mL aliquot of a solution of **poly-15** (0.0100 g) in CH_2Cl_2 (0.0679 mL) was dropped onto the interdigitated electrode in an argon glove box. The sample was dried for 1 h under ambient conditions in the glove box, followed by vacuum drying for 14 h. The electrode and one crystal of I_2 were then sealed in a vial for 24 h under static vacuum. The remaining I_2 was then removed and the electrode sample left under dynamic vacuum for 24 h. Employing the potentiostat from a cyclic voltammetry instrument, a potential was then applied across the film and the current measured. A two electrode connection was made by combining the red (auxiliary lead) and white (reference lead) together as one electrode and the black lead (working lead) as the other electrode.

Crystallography

A single crystal X-ray diffraction study was performed on 1**6**. A summary of crystal and refinement data are presented below.

Single crystals of **16** suitable for X-ray diffraction were grown by slow evaporation of a saturated pentane solution. After one day, the yellow plates were taken directly to an APEXII BRUKER X-ray diffractometer for data collection as outlined in Table 3.5. Cell parameters were obtained from 36 frames using a 5° scan and refined with 16005 reflections. A suitable cell was found and refined by nonlinear least squares and Bravais lattice procedures. No super-cell or erroneous reflections were observed. Integrated intensity information for each reflection was obtained by reduction of the data frames with the program APEX2.[35] Lorentz, polarization, and absorption corrections[36] were applied. The space group, P−1, was determined from systematic reflection conditions and statistical tests. The structure was solved by direct methods using SHELXTL (SHELXS).[37] All non-hydrogen atoms were refined with anisotropic thermal parameters. The hydrogen atoms were placed in idealized positions. The parameters were refined by weighted least squares refinement on F^2 to convergence.[37] Two independent molecules were found in the unit cell.

Table 3.5. Summary of crystal and refinement data for **16**.

Empirical formula	$C_{16}H_{21}Ir$
Formula weight	405.53
Temperature	120(2) K
Wavelength	0.71073 Å
Crystal system	Triclinic
Space group	P−1
Unit cell dimensions	a = 8.371(3) Å
	b = 11.414(4) Å
	c = 14.760(5) Å
	α = 87.652(4)°
	β = 88.522(4)°
	γ = 79.837(4)°
Volume	1386.8(8) $Å^3$
Z	4
Density (calculated)	1.942 Mg/m^3
Absorption coefficient	9.604 mm^{-1}
F (000)	776
Crystal size	0.42 × 0.34 × 0.09 mm^3
Theta range for data collection	1.81 to 27.97°
Index range (h, k, l)	−11, 10; −14, 15; −19, 19
Reflections collected	16005
Independent reflections	6511 [R(int) = 0.0476]
Completeness to theta = 27.97°	97.8%
Absorption correction	Semi-empirical from equivalents
Max. and min. transmission	0.4786 and 0.1073
Refinement method	Full-matrix least-squares on F^2
Data / restraints / parameters	6511 / 0 / 317
Goodness-of-fit on F^2	1.045
Final R indices [I>2sigma(I)]	R1 = 0.0342, wR2 = 0.0855
R indices (all data)	R1 = 0.0445, wR2 = 0.0981
Largest diff. peak and hole	2.679 and −2.643 $eÅ^{-3}$

CHAPTER IV

ORGANOMETALLIC Π-ADDUCTS OF POLY(PHENYLENE-VINYLENE) FROM ACYCLIC DIENE METATHESIS POLYMERIZATION

INTRODUCTION

Poly(phenylene-vinylene) (PPV) has been one of the most thoroughly studied conjugated polymers reported to date.[75] In part, this interest spawned from Burroughes and coworkers′ 1990 discovery of electroluminescence in PPV.[76] Photoluminescence and conductivity as high as 5×10^3 S/cm has also been observed in PPVs.[75,77] As a conducting polymer, the broad photophysical properties of PPVs have found extensive applications with organic electronics, particularly with light-emitting diodes and photovoltaics.[75]

An early synthesis of PPV by Campbell and McDonald utilized a Wittig reaction between *p*-xylylene-bis(triphenylphosphonium chloride) and terephthalaldehyde as shown in Scheme 4.1.[78] A lack of solubility in the resulting polymer led to a low DP of 10.

Scheme 4.1. Campbell and McDonald′s Wittig synthesis of PPV.

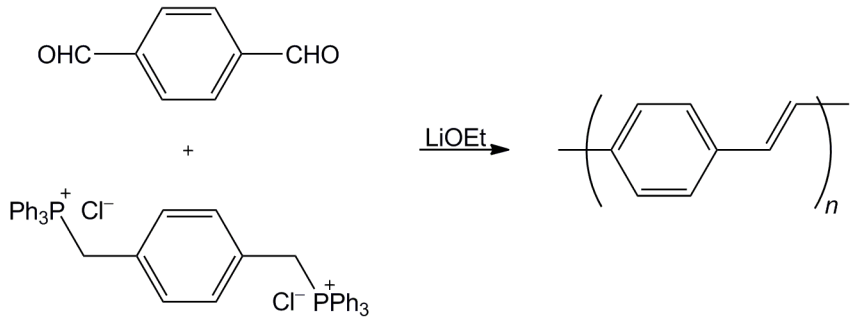

Alternatively, Schrock and coworkers have explored ADMET with the well defined catalyst **IV** (Figure 1.1) as a route to PPV (Scheme 4.2).[79] Again, solubility was a limiting factor. In pentane they found the dimer (DP = 2) to dominate and in dichloromethane the tetramer (DP = 4) was prevalent. Additionally, in a brief report by Thorn-Csányi and Pflug, a DP of > 20 was claimed from a tungsten catalyst.[80]

Scheme 4.2. ADMET synthesis of PPV.

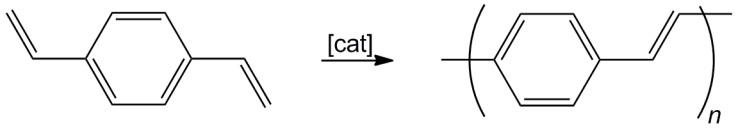

To circumvent the solubility problems associated with PPV, Wessling and Zimmerman developed a precursor route as shown in Scheme 4.3.[81] In this method, an anionic polymerization is used to generate a soluble sulphonium polymer. Pyrolysis is then employed to generate a PPV film.

Scheme 4.3. Wessling and Zimmerman′s precursor synthesis of PPV.

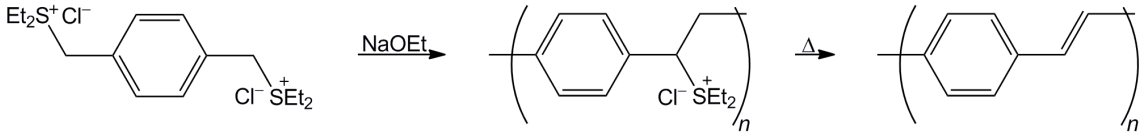

As another approach to increasing the solubility of PPV, Wudl and Srdanov utilized alkyl substituents on the phenylene spacers as shown in Scheme 4.4.[82] Their protocol again uses an anionic polymerization to form poly(2-methoxy-5-(2′-ethyl-hexyloxy)-*p*-phenylene-vinylene) (MEH-PPV). The advantageous solubility of MEH-PPV has lead to a breadth of research, particularly with photovoltaics.[76] Additionally,

MEH-PPV has become somewhat of a standard in conjugated polymers and is commercially available from Aldrich.

Scheme 4.4. Wudl and Srdanov′s synthesis of MEH-PPV.

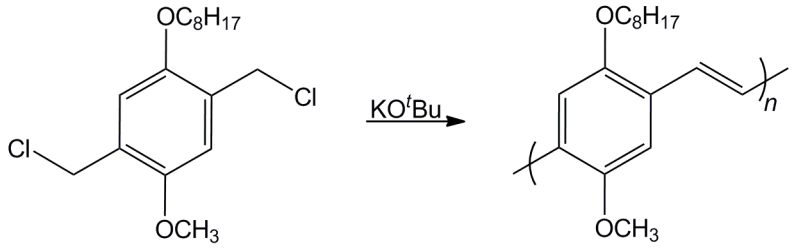

In a conjugated polymer related to PPV, poly(*p*-phenylene) (PPP), Eyring and coworkers have explored the utility of transition metal arene complexes along the polymer backbone (Scheme 4.5).[83] This work focused on a post polymerization modification leading to a regiorandom distribution of metal adducts. The Eyring synthesis reacted chromium and molybdenum complexes of the type $M(CO)_3(NCCH_3)_3$ with PPP to produce a polymer with metal adducts on 25% of the phenylene linkages. The resultant metal containing polymer exhibited partial doping with an increase in conductivity of 10^4.

Scheme 4.5. Eyring′s synthesis of PPP-$M(CO)_3$.

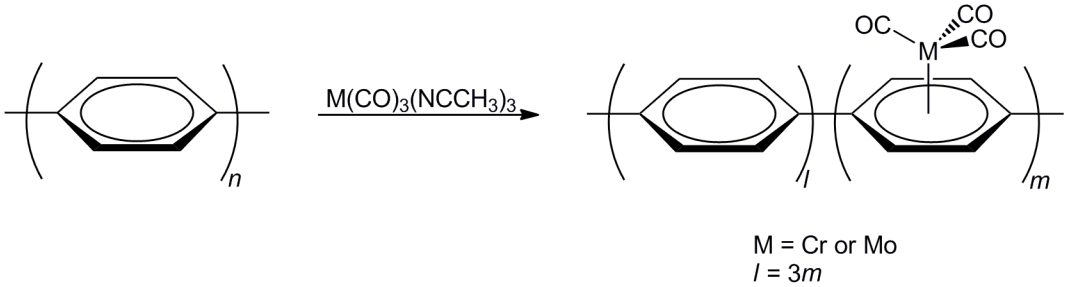

Nishihara and coworkers have subsequently investigated metal adducts of poly-(*n*-hexylphenylene) (PHP) (Scheme 4.6).[84,85] This hexyl group greatly increases the solubility of the conjugated polymer. First, they used a route analogous to Eyring to install $M(CO)_3$ (M = Cr or Mo) adducts (Scheme 4.6 top).[84] With this method, they were able to complex approximately 20% of the phenylene linkages. Although specific values were not given, they report an increase in conductivity relative to pristine PHP. Additionally, they reacted PHP with ferrocene, aluminum, and aluminum chloride followed by quenching with $[NH_4][PF_6]$ to install $[FeCp][PF_6]$ fragments on 38% of the phenylene linkages (Scheme 4.6 bottom). This derivative of PHP is also of interest since it is a polyelectrolyte. Although not fully characterized, Nishihara and coworkers also reported the synthesis of PBP-$Cr(CO)_3$ (PBP = poly(*n*-butylphenylene)).[84]

Scheme 4.6. Nishihara's syntheses of PHP-$M(CO)_3$ (top) and PHP-$[FeCp][PF_6]$ (bottom).

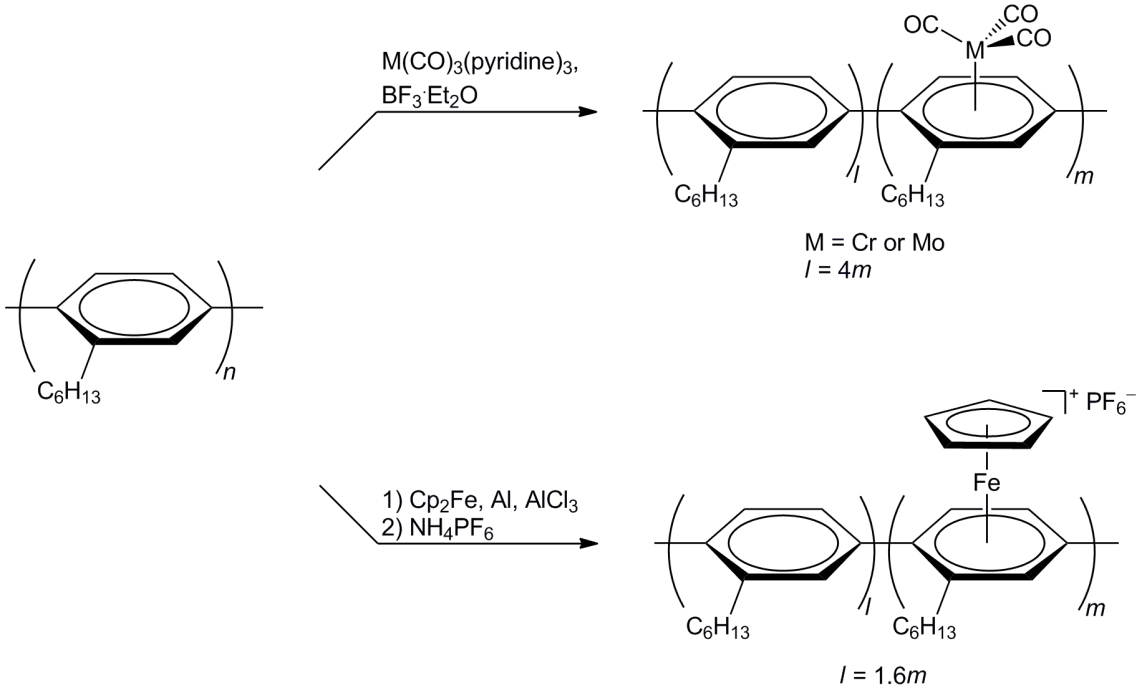

As a new approach to PPV, this chapter focuses on ADMET of divinylbenzene metal complexes (Scheme 4.7). Theoretically, any metal arene complex in which the arene is divinyl benzene can be used with ADMET to produce a polymer with a PPV backbone. In this method, the organometallic species bound to the arene acts as a solubilizing group to prevent precipitation during the polymerization.

Scheme 4.7. Aim of this work: ADMET of organometallic divinyl benzene complexes.

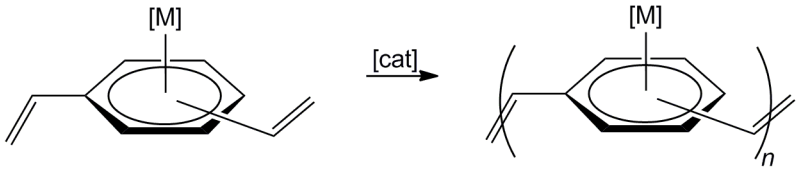

RESULTS

Monomers investigated in this work are depicted in Figure 4.1. These two substrates were chosen due to their facile synthesis and Cp* ligands that would be capable of π-π stacking in crystals. In general, divinyl benzene is a reactive liquid that can spontaneously polymerize. Hence, syntheses of divinyl benzene metal complexes should be carried out under mild reaction conditions. Additionally, divinyl benzene has been employed as a mixture of isomers as it is considerably more cost effective than a single isomer.

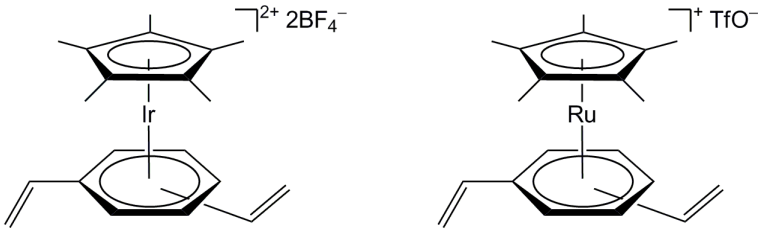

Figure 4.1. Divinyl benzene complexes investigated with ADMET.

The synthesis of the new iridium divinyl benzene complex monomer **27** is shown in Scheme 4.8. The precursor, **22**, was synthesized as described in the literature and Chapter III.[49] Complex **27** was then prepared following standard iridium arene chemistry, analogous to the synthesis of **23**, in 71% yield.[50] As a mixture of isomers, the NMR spectrum was not assigned. However, an expanded view of the ^{1}H NMR clearly shows a shift upon coordination to iridium (Figure 4.2). The structural assignment of **27** was also supported by the mass spectrum with m/z = 229 (ESI^{+}, $[\mathbf{27} - 2BF_4]^{2+}$, 100%) and m/z = 87 (ESI^{-}, $[BF_4]^{-}$, 100%).

Scheme 4.8. Synthesis of the iridium divinyl benzene complex **27**.

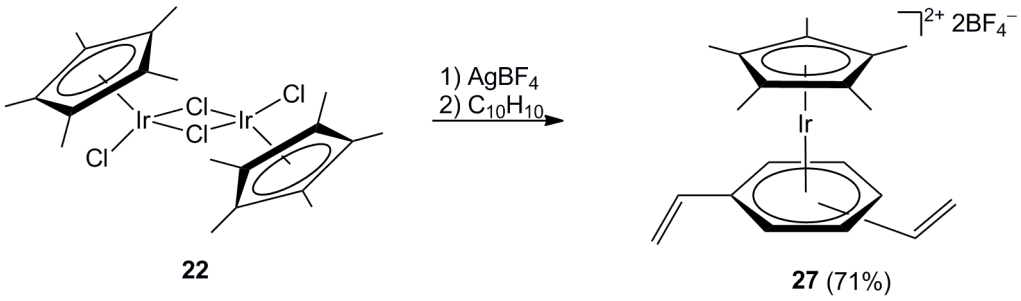

22 **27** (71%)

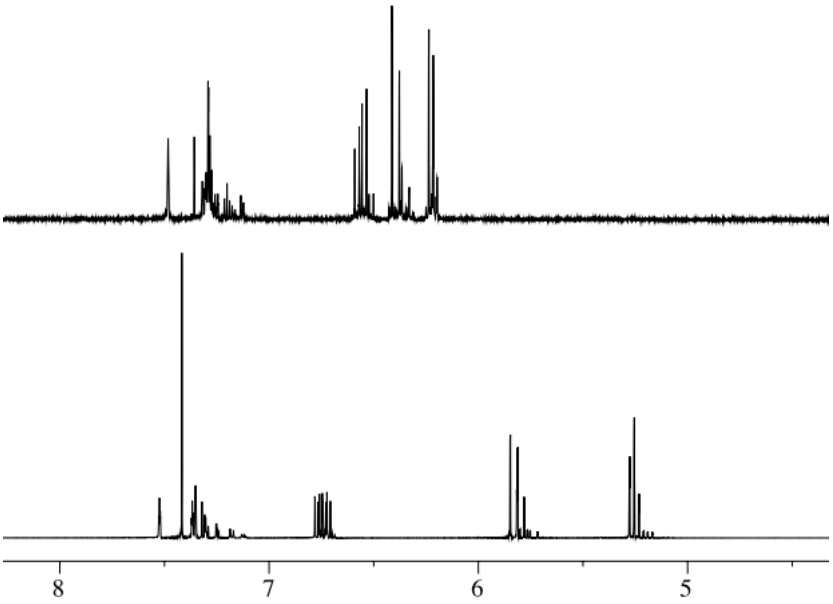

Figure 4.2. Expanded ^{1}H NMR view; divinyl benzene mixture of isomers (bottom) and **27** (top).

The complete synthesis of the new ruthenium divinyl benzene complex monomer **28** is shown in Scheme 4.9. The synthesis of complexes **29-31** follow literature precedent.[86,87] Standard conditions for synthesizing ruthenium arene complexes[87] then afforded the target monomer **28** in 62% yield. As a mixture of isomers, the NMR spectrum was not assigned. However, an expanded view of the ^{1}H NMR clearly shows a shift upon coordination to ruthenium (Figure 4.3). The structural assignment of **28** was also supported by the mass spectrum with m/z = 367 (ESI^{+}, [**28** − $OTf]^{+}$, 100%) and m/z = 149 (ESI^{-}, $[OTf]^{-}$, 100%).

Scheme 4.9. Synthesis of the ruthenium divinyl benzene complex **28**.

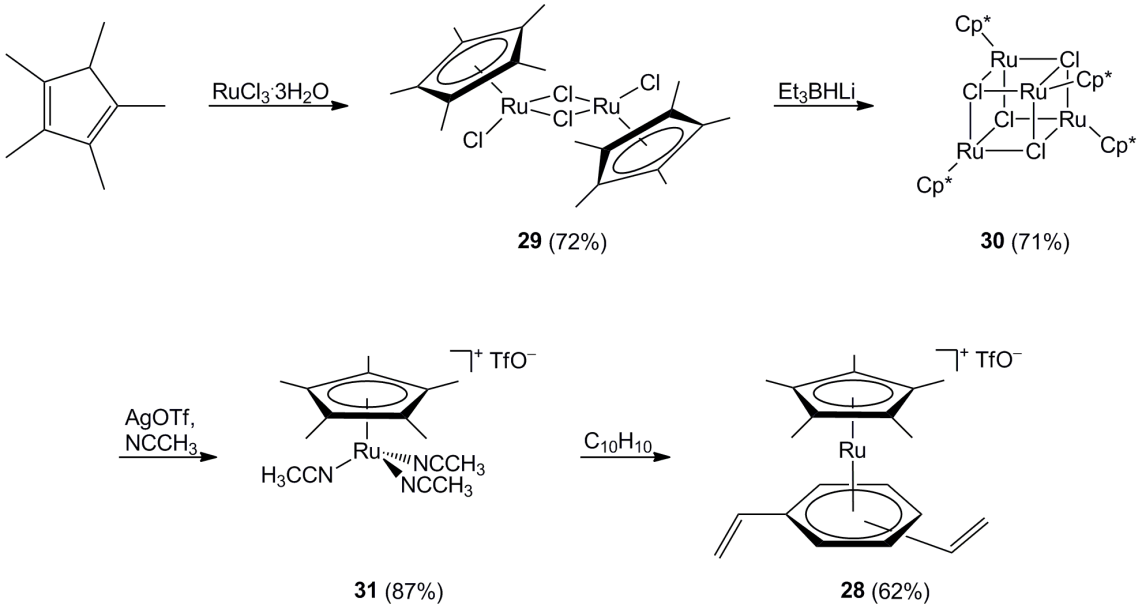

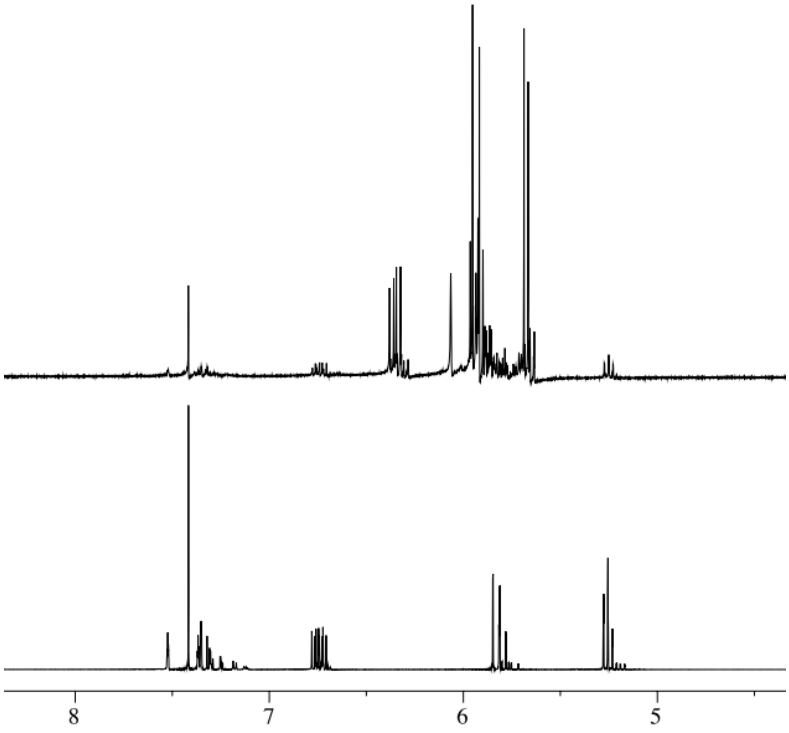

Figure 4.3. Expanded ^{1}H NMR view; divinyl benzene mixture of isomers (bottom) and **28** (top).

Monomers **27** and **28** (Figure 4.1) were then evaluated in ADMET using Grubbs′ second generation catalyst (**II**; Figure 1.1). As shown in Scheme 4.10, ADMET affords PPV with metal-arene complexes along the polymer backbone. In this polymerization route, Cp*M adducts would be coordinated to the PPV backbone on every phenylene linkage (regioregular). This is in contrast to the regiorandom metal adducts shown in Schemes 4.5-4.6. Since both precursors are cationic, a polar solvent was sought. Optimal conditions for the polymerization of **27** were found with refluxing methanol. Since the monocation **28** exhibited better solubility in less polar solvents, optimal polymerization conditions involved refluxing in a 1:1 v/v mixture of CH_2Cl_2/methanol. In both cases, the reaction mixtures started as pink suspensions. Upon heating, they became homogeneous and yellow. Since both monomers are colorless, the yellow in the polymers can be attributed to the PPV backbone.

Scheme 4.10. Syntheses of organometallic PPVs **poly-27** and **poly-28** *via* ADMET.

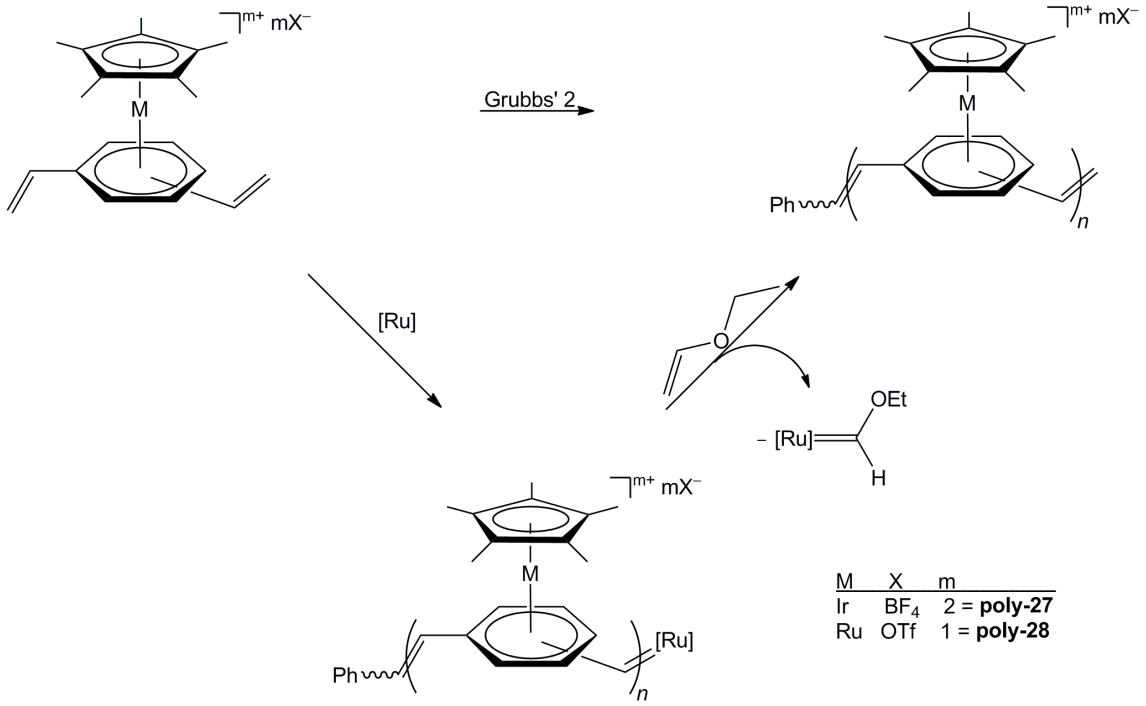

The UV-Vis spectra of **27** and **poly-27** are shown in Figure 4.4. That of **poly-27** shows a new absorption with λ_{max} = 414 nm. This signal is considerably blue-shifted from MEH-PPV (λ_{max} = 489 nm).[88] As shown in Figure 4.5, an acetone solution of **27** is colorless while an acetone solution of **poly-27** is yellow, consistent with a conjugated backbone. However, no photoluminescence was observed with **poly-27**.

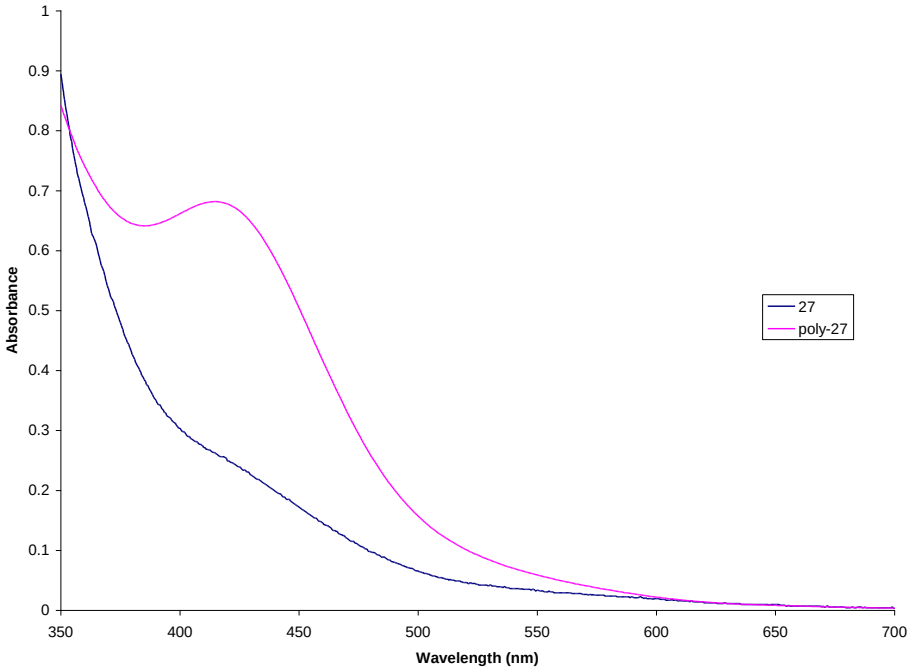

Figure 4.4. UV-Vis spectra of **27** (4.97×10^{-4} M or 0.314 g/L in acetone) and **poly-27** (0.447 g/L in acetone).

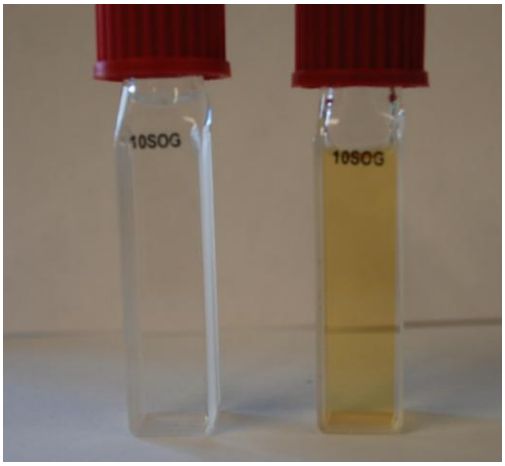

Figure 4.5. Solutions of **27** (4.97×10^{-4} M or 0.314 g/L in acetone, left) and **poly-27** (0.447 g/L in acetone, right).

The UV-Vis spectra of **28** and **poly-28** are shown in Figure 4.6. While **poly-28** is faint yellow in solution (Figure 4.7), only a slight red-shift is observed in the absorption spectrum, relative to **28**.

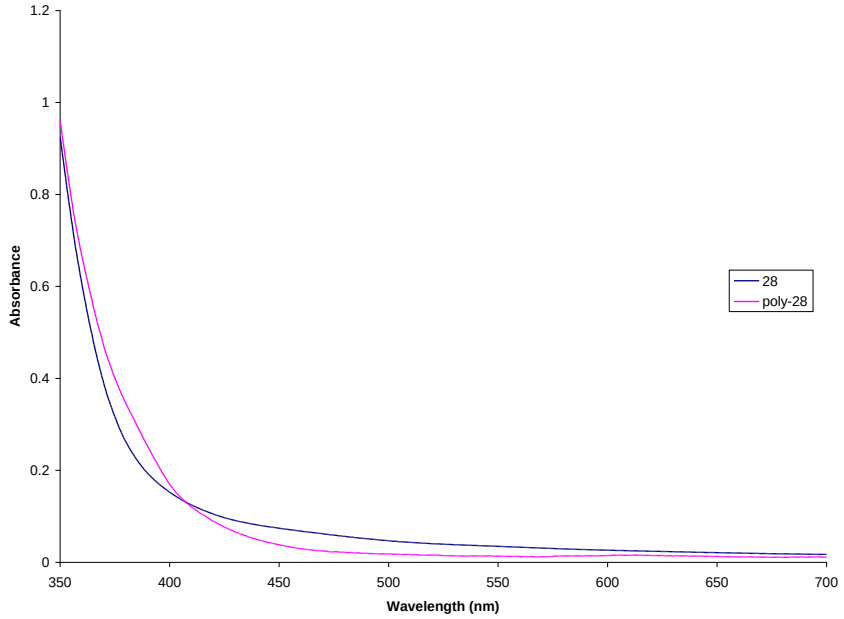

Figure 4.6. UV-Vis spectra of **28** (2.31×10^{-4} M or 0.119 g/L in acetone) and **poly-28** (0.378 g/L in acetone).

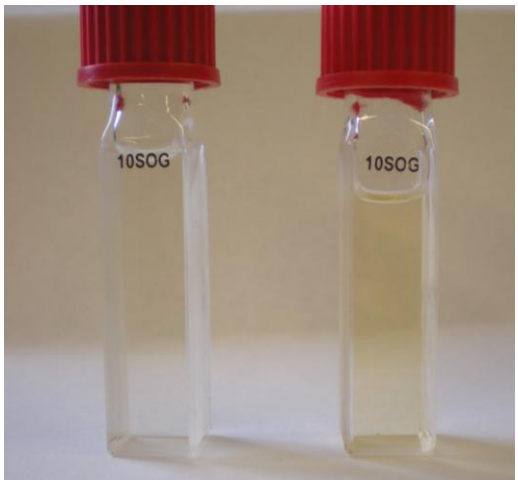

Figure 4.7. Solutions of **28** (2.31×10^{-4} M or 0.119 g/L in acetone, left) and **poly-28** (0.378 g/L in acetone, right).

The photoluminescence excitation and emission spectra of **poly-28** are shown in Figure 4.8. The excitation spectrum exhibits a λ_{max} of 350 nm, at this excitation wavelength the emission spectrum shows a λ_{max} of 413 nm. A solution of **poly-28** (0.378 g/L in acetone) under 365 nm irradiation is shown in Figure 4.9.

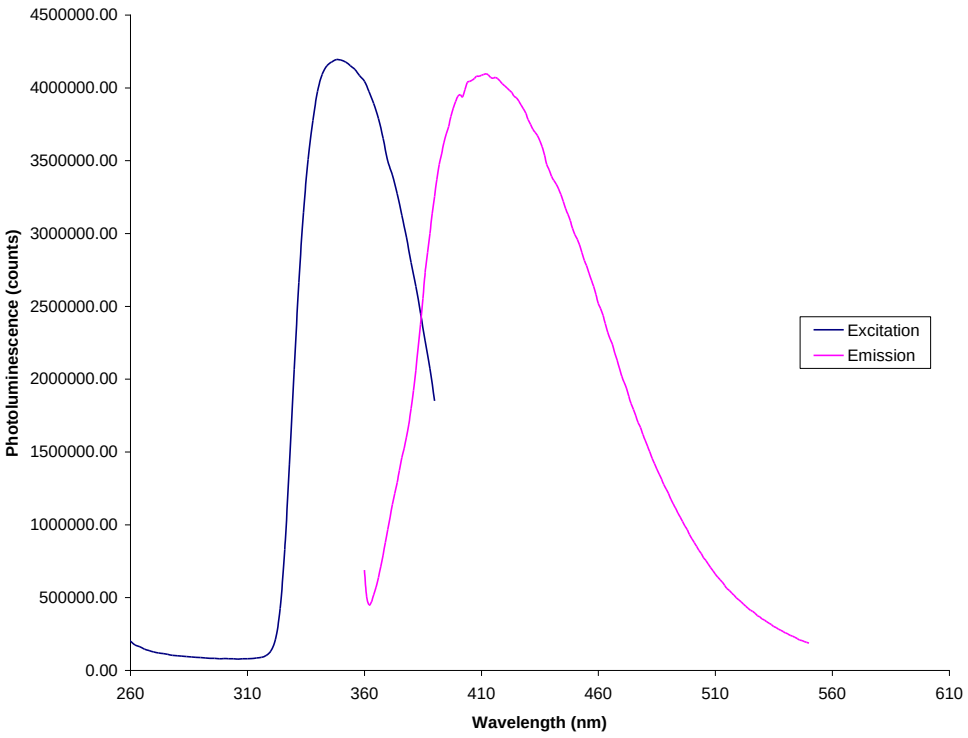

Figure 4.8. Photoluminescence excitation and emission spectra of **poly-28** (0.108 g/L in acetone).

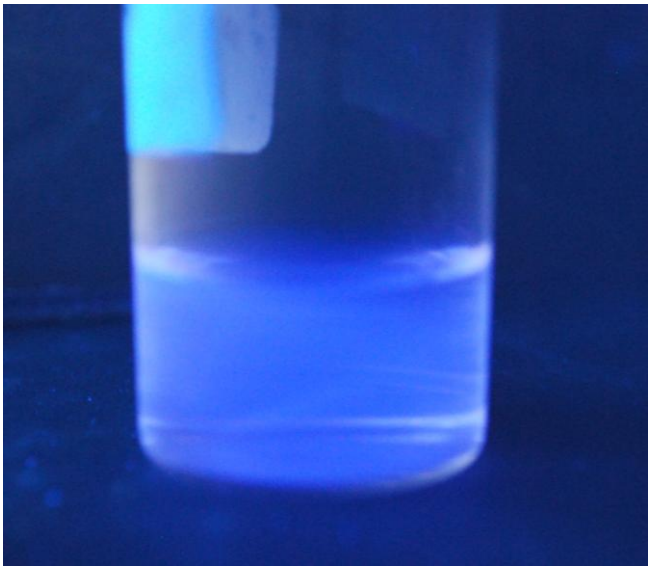

Figure 4.9. Solution of **poly-28** (0.108 g/L in acetone) under 365 nm irradiation.

The conductivity of **poly-27** and **poly-28** was evaluated using gold interdigitated electrode arrays.[89] It was found that acetone solutions of **poly-27** and **poly-28** readily gave films upon evaporation. Iodine doping of a drop-cast film of **poly-27** afforded a lustrous brown film (Figure 4.10 left). Iodine doping of a drop-cast film of **poly-28** afforded a copper colored film (Figure 4.10 right). Upon applying a potential, current was measured through each film as shown in Figure 4.11. While this method is a convenient way to test for and confirm conductivity, it does not allow for the determination of specific conductance values.

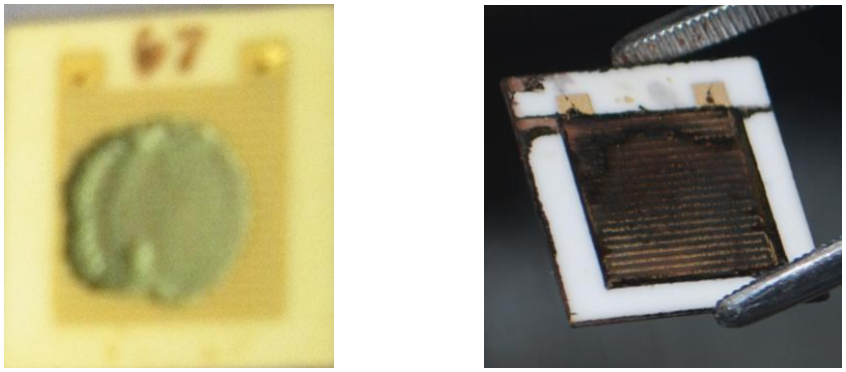

Figure 4.10. Iodine doped films of **poly-27** (left) and **poly-28** (right).

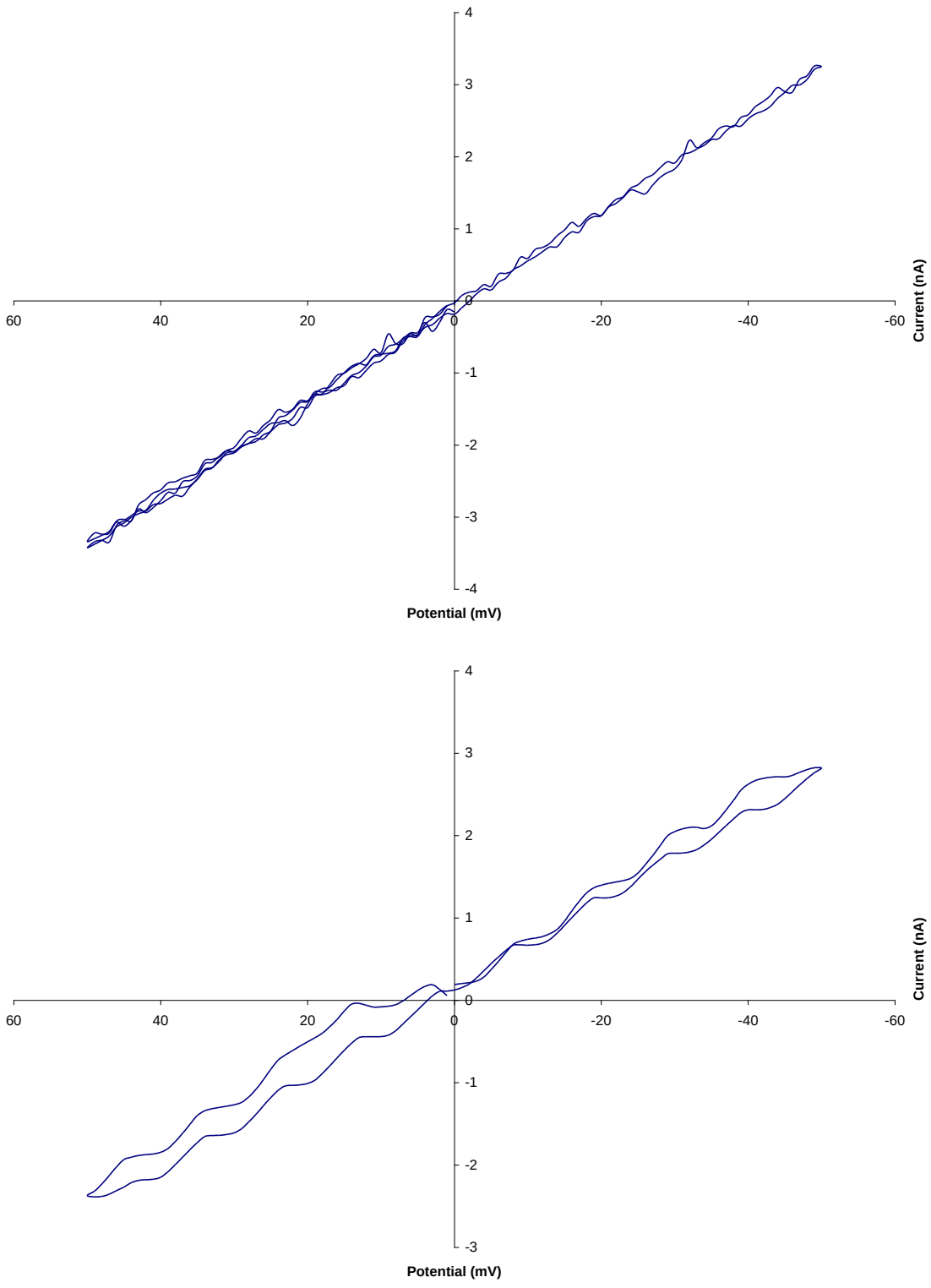

Figure 4.11. Measured conductance of iodine doped **poly-27** (top) and **poly-28** (bottom).

DISCUSSION

This work has explored the use of organometallic substrates as monomers for ADMET to produce PPV. Divinyl benzene complexes **27** and **28** were chosen for evaluation with ADMET due to the mild reaction conditions under which they can be synthesized, thereby avoiding free radical or other polymerization of the free or coordinated ligand.

Complexes **27** and **28** were both found to readily undergo ADMET polymerization to form regioregular organometallic π-adducts of conjugated polyelectrolytes. In each polymer, the backbone is PPV with each phenylene group existing as an η^6-arene moiety.

Table 4.1 focuses in on the photophysical properties associated with organometallic π-adducts of phenylene based conjugated polymers. Previous work with organometallic π-adducts has focused on poly(phenylene)s (entries 3-6).[84,85] In one case (entry 3), a red-shift is observed for the cationic polymer PHP-[FeCp][PF_6], relative to the parent PHP. In two cases (entries 4 and 5), metal adducts cause blue-shifts relative to the parent polymers. This work has focused on the development of organometallic π-adducts of poly(phenylene-vinylene)s (entries 1, 2, and 7). As shown in Figure 4.5 above, ADMET of the colorless monomer **27** affords a yellow PPV. The UV-Vis spectrum of **poly-27** (Figure 4.4 above) shows a new absorption with λ_{max} = 414 nm. This signal is considerably blue-shifted from MEH-PPV (λ_{max} = 489 nm), suggesting a larger HOMO-LUMO gap.[88] As shown in Figure 4.6 above, ADMET of the colorless monomer **28** affords a faint yellow PPV. The color change upon polymerization is not as strong as observed in **poly-27**, showing only a slight red-shift in the UV-Vis spectrum (Figure 4.7 above). Interestingly, a smaller coordination shift is observed in the ^{1}H NMR

spectrum for a benzene ligand in $[Cp^*Ir(C_6H_6)][BF_4]_2$ (0.04 ppm) as compared to the shift in $[Cp^*Ru(C_6H_6)][OTf]$ (-1.30 ppm).[90]

Table 4.1. Photophysical properties of **poly-27**, **poly-28**, and literature examples.

Entry (Scheme)	Polymer	$\lambda_{UV\text{-}Vis}$	$\lambda_{Excitation}$	$\lambda_{Emission}$
1 (4.10)	**poly-27**[a]	<350, 414	-	-
2 (4.10)	**poly-28**[a]	<350	350	413
3 (4.6)	PHP-$[FeCp][PF_6]$[b]	400, 450[85]	520[85]	518, 571[85]
4 (4.6)	PHP-$Mo(CO)_3$[b]	290[84]	340[85]	479[85]
5	PBP-$Cr(CO)_3$[b]	320[84]	-	-
6	PHP[b]	236, 324[85]	400[85]	511[85]
7 (4.4)	MEH-PPV[c]	489[88]	550[88]	565[88]

[a] Acetone solution. [b] CH_2Cl_2 solution. [c] $CHCl_3$ solution.

As shown in Table 4.1, photoluminescence in phenylene based polymers is also important. Photoluminescence was observed in **poly-28** (Figure 4.8 above). The excitation spectrum shows a λ_{max} of 350 nm and the emission spectrum shows a λ_{max} of 413 nm. Both values are considerably blue-shifted relative to MEH-PPV (excitation λ_{max} = 550 nm, emission λ_{max} = 565).[88] Photoluminescence was not observed in **poly-27**.

While **poly-27** and **poly-28** exhibit photophysical properties characteristic of PPVs not seen in the parent monomers, they also retain strong UV absorption due to

their organometallic nature. This strong absorption of high energy photons should have a unique application in photovoltaic devices for high energy output.[91] Materials for photovoltaic applications that only absorb low energy visible light focus on collecting a lot of photons. By contrast, collecting higher energy UV light would require fewer photons for the same power output. By this analysis, a significant size reduction could be employed in solar panels featuring **poly-27** or **poly-28**.

As shown in Figure 4.11, iodine doped **poly-27** and **poly-28** were found to be conductive. The conductivities shown in Figure 4.11 are somewhat noisy as this data is near the detection limit. Low conductivities in **poly-27** and **poly-28** are attributable to thin films formed from poor solubility of the polymers.

CONCLUSION

Poly-27 and **poly-28** are new forms of PPV that feature π-Cp*M fragments that have been arrayed in a regioregular manner using ADMET. The new polymers are also polyelectrolytes. The photophysical properties of the new polymers have been evaluated and show characteristics typical of PPVs while retaining the strong UV absorption from their organometallic heritage. Films of **poly-27** and **poly-28** were found to be conductive on gold interdigitated electrodes.

EXPERIMENTAL

General

All reactions were carried out in inert atmospheres using standard Schlenk and vacuum line techniques. Chemicals were treated as follows: pentane was distilled from Na/benzophenone, acetonitrile was distilled from CaH_2, and methanol was sparged with nitrogen for 1 h immediately before use; all other solvents were purified using a Glass Contour solvent purification system; $CDCl_3$ (Cambridge Isotope Laboratories), CD_2Cl_2 (Cambridge Isotope Laboratories), $IrCl_3 \cdot nH_2O$ (Pressure Chemical Company, 52%

metal basis), $RuCl_3 \cdot 3H_2O$ (Alfa Aesar, 99.9%), Cp*H (Alfa Aesar, 94%), ethyl vinyl ether (Alfa Aesar, 99%), divinyl benzene (Alfa Aesar, mixture of isomers, 80%), $[Ag][BF_4]$ (Alfa Aesar, 99%), [Ag][OTf] (Alfa Aesar, 98%), and lithium triethylborohydride (Alfa Aesar, 1.0 M in hexanes) were used as received; $[Cp^*Cl_2Ir]_2$ (22) and Grubbs′ second generation catalyst (**II**) were prepared as described in Chapter III.

NMR spectra were recorded on a Varian NMRS 500 MHz spectrometer at ambient probe temperatures and referenced as follows: ^1H: residual internal $CHCl_3$ (δ, 7.26 ppm), $CDHCl_2$ (δ, 5.32 ppm) or acetonitrile-d_2 (δ, 1.94 ppm); ^{13}C: internal $CDCl_3$ (δ, 77.2 ppm), CD_2Cl_2 (δ, 54.00 ppm), or acetonitrile-d_3 (δ, 118.69 and 1.39 ppm). Cyclic voltammograms were recorded using a BASi epsilon potentiostat and C-3 cell stand. UV-Vis spectra were recorded on a Shimadsu UV-1800 spectrometer. Fluorescence spectra were recorded on a Cary Eclipse spectrometer. Melting points were recorded with a Stanford Research Systems (SRS) MPA100 (Opti-Melt) automated melting point system. Microanalyses were conducted by Atlantic Microlab.

$[Cp^*Ir(C_6H_4(CH{=}CH_2)_2)][BF_4]_2$ (27)

A round bottom flask was charged with $[Cp^*IrCl_2]_2$ (0.5090 g, 0.6389 mmol), $[Ag][BF_4]$ (0.4961 g, 2.525 mmol), and acetone (3.0 mL) with stirring. After 10 min, the mixture was filtered and divinylbenzene (2.00 mL) added to the filtrate. The yellow solution rapidly turned brown and a cream colored precipitate began to form. After 4 h, the precipitate was collected by filtration, washed with ether (2 × 10 mL), and dried by oil pump vacuum to give **27** (0.5726 g, 0.9071 mmol, 71.0%) as a cream colored solid.

^1H NMR (acetonitrile-d_3): δ 7.32-7.18 (m, 4H, C_6H_4), 6.60-6.50 (m, 2H, $CH{=}CH_2$), 6.42-6.19 (m, 4H, $CH{=}CH_2$), 2.15 and 2.10 (2 s, 15H, $C_5(CH_3)_5$) (Figure 4.2).

MS: ESI^+, 229 ([**27** − $2BF_4$]$^{2+}$, 100%); ESI^-, 87 ($[BF_4]^-$, 100%).[92]

Elemental Analysis: calculated: C, 38.05%; H, 3.99%.

found: C, 37.60%; H, 3.95%.

[Cp*RuCl$_2$]$_2$ (29)[86]

A round bottom flask was charged with $RuCl_3 \cdot 3H_2O$ (4.0057 g, 15.061 mmol) and methanol (200 mL). Cp*H (6.00 mL, 38.3 mmol) was then introduced by syringe with stirring. The mixture was refluxed for 3 h, and cooled to room temperature. The mixture was then concentrated to 100 mL. The precipitate was collected by filtration, washed with methanol (2 × 5 mL) and hexanes (2 × 5 mL), and dried by oil pump vacuum to give **29** (3.3154 g, 5.3962 mmol, 72%) as a brown solid.

^{1}H NMR ($CDCl_3$): δ 4.51 (s, 15H).

[Cp*Ru-μ$_3$-Cl]$_4$ (30)[87]

A round bottom flask was charged with **29** (2.0001 g, 3.2553 mmol) and THF (10 mL). A solution of lithium triethylborohydride (6.60 mL, 1.0 M in THF, 6.60 mmol) was then introduced by syringe with stirring. After stirring 1 h, the precipitate was collected by filtration, washed with THF (2 × 2 mL), and dried by oil pump vacuum to give **30** (1.2613 g, 1.1603 mmol, 71%) as a dark orange-red solid.

^{1}H NMR (CD_2Cl_2): δ 1.54 (s, 15H).

[Cp*Ru(NCCH$_3$)$_3$][OTf] (31)[87]

A round bottom flask was charged with **30** (0.8928 g, 0.8213 mmol) and acetonitrile (10 mL) with stirring. The mixture was then refluxed 1 h to dissolve **30**. After cooling to room temperature, [Ag][OTf] (0.8480 g, 3.300 mmol) was added. After 45 min, the mixture was filtered and the volatiles removed by oil pump vacuum. The residue was treated with ether (10 mL). The precipitate was collected by filtration,

washed with ether (5 mL), and dried by oil pump vacuum to give **31** (1.4555 g, 2.8622 mmol, 87%) as an orange-yellow solid.

^{1}H NMR ($CDCl_3$): δ 2.35 (br s, 9H, NCCH_3), 1.59 (s, 15H, $C_5(CH_3)_5$).

[Cp*Ru(C_6H_4(CH=CH_2)$_2$)][OTf] (28)

A round bottom flask was charged with **31** (0.5031 g, 0.9895 mmol), dichloromethane (30 mL), and an excess of divinyl benzene (2.00 mL) with stirring. After 5 h, the mixture was concentrated to 10 mL by oil pump vacuum and ether (90 mL) added. The supernatant was decanted from the viscous oil that forms. The oil residue was then dried by oil pump vacuum to give **28** (0.3172 g, 0.6153 mmol, 62%) as a cream colored solid.

^{1}H NMR (acetonitrile-d_3): δ 6.39-6.32 (m, 2H, CH=CH_2), 5.97-5.65 (m, 8H, C_6H_4 and CH=CH_2), 1.82 and 1.79 (2 s, 15H, $C_5(CH_3)_5$) (Figure 4.3).

MS: ESI^+, 367 ([**28** − OTf]$^+$, 100%); ESI^-, 149 ([OTf]$^-$, 100%).[92]

Elemental Analysis: calculated: C, 48.92%; H, 4.89%; S, 6.22.

found: C, 50.61%; H, 4.92%; S, 5.89.

Poly-27

A round bottom flask was charged with **27** (0.2524 g, 0.3998 mmol), Grubbs′ second generation catalyst (0.0172 g, 0.0203 mmol), and methanol (10 mL) with stirring. The mixture was then refluxed while maintaining a flow of nitrogen orthogonal to the top of the condenser. After 5 h, the mixture was cooled and ethyl vinyl ether (0.1 mL) added. After 10 min, the volatiles were removed and the residue dried by oil pump vacuum to give **poly-27** (0.2465 g) as a yellow solid.

Poly-28

A round bottom flask was charged with **28** (0.1282 g, 0.2487 mmol), Grubbs′ second generation catalyst (0.0103 g, 0.0121 mmol), dichloromethane (4 mL), and

methanol (4 mL) with stirring. The mixture was then refluxed while maintaining a flow of nitrogen orthogonal to the top of the condenser. After 5 h, the mixture was cooled and ethyl vinyl ether (0.1 mL) added. After 10 min, the volatiles were removed and the residue dried by oil pump vacuum to give **poly-28** (0.1305 g) as a yellow-brown solid.

Conductivity Measurement

A 0.025 mL aliquot of a solution of **poly-27** (0.0010 g) in acetone (0.1252 mL) was dropped onto the interdigitated electrode in an argon glove box. The sample was dried for 1 h under ambient conditions in the glove box, followed by vacuum drying for 14 h. The electrode and one crystal of I_2 were then sealed in a vial for 24 h under static vacuum. The remaining I_2 was then removed and the electrode sample left under dynamic vacuum for 24 h. Employing the potentiostat from a cyclic voltammetry instrument, a potential was then applied across the film and the current measured. A two electrode connection was made by combining the red (auxiliary lead) and white (reference lead) together as one electrode and the black lead (working lead) as the other electrode.

A 0.100 mL aliquot of a solution of **poly-28** (0.0020 g) in acetone (0.1239 mL) was dropped onto the interdigitated electrode (with a barrier of 0.0025 inch Kapton tape around the electrodes) in an argon glove box. The sample was dried for 1 h under ambient conditions in the glove box, followed by vacuum drying for 14 h. The electrode and one crystal of I_2 were then sealed in a vial for 24 h under static vacuum. The remaining I_2 was then removed and the electrode sample left under dynamic vacuum for 24 h. A potential was then applied across the film and the current measured.

CHAPTER V

CONCLUSIONS

As outlined in Chapter I, olefin metathesis is a powerful carbon-carbon bond forming reaction which can be used in a diverse range of metal coordination spheres. This work has focused on ring-closing metathesis, ring-opening metathesis polymerization, and acyclic diene metathesis to form novel molecular machines and conjugated polymers.

Ring-closing metathesis has been employed with a variety of alkene containing pyridines to synthesize and elaborate on novel *trans*-bis(pyridine)platinum complexes. Subsequently, these complexes have undergone ring-closing metatheses and hydrogenations to afford new single spoke molecular rotors featuring macrocycles of 13, 15, 21, 29, and 31 atoms, as well as a giant two spoke molecular rotor featuring a macrocycle of 29 atoms. The syntheses of the single spoke molecular rotors proceed much more readily than their two spoke counterparts.

It has also been shown that systems with 3-substituted pyridine ligands exhibit much less congestion about the metal center. Substitution reactions become facile, allowing the rotator to be desymmetrized – i.e., the exchange of a single chloride ligand for a methyl ligand. Even with the smallest 3-substituted macrocycle, rotation of the resulting chloride methyl complex remains rapid on the NMR time scale to −120 ˚C.

Ring-opening metathesis polymerization has been employed to develop a new form of PA (**poly-15**) employing regioregular CpIr π-adducts. The synthesis of this new polymer has been optimized, requiring a high catalyst loading of 20 mol% and two days to reach completion in CD_2Cl_2 at 40 °C. UV-Vis analysis of **poly-15** suggests the

effective conjugation length is approximately 6-7 double bonds. This new polymer was found to be conductive.

A solid state structural analysis of the closely related monomer **16** shows that the geometry of the benzene ligand does in fact approach that of norbornadiene. However, **16** does not undergo ring-opening metathesis polymerization under a variety of reaction conditions and catalyst variations. Also, polymerization could not be extended to η^4 or η^6-COT complexes.

Acyclic diene metathesis polymerization has been employed to develop two new forms of PPV (**poly-27** and **poly-28**) that feature π-Cp*M fragments that have been arrayed in a regioregular manner. The new polymers are also polyelectrolytes. The photophysical properties of the new polymers have been evaluated and show characteristics typical of PPVs while retaining the strong UV absorption from their organometallic heritage. Films of **poly-27** and **poly-28** were found to be conductive on gold interdigitated electrodes.

REFERENCES

(1) Handbook of Metathesis, 1st ed.; Grubbs, R. H., Ed.; Wiley-VCH, Weinheim, Germany, 2003; Vols 1-3.

(2) (a) Ziegler, K.; Holzkamp, E.; Breil, H.; Martin, H. *Angew. Chem.* **1955**, *67*, 541-547. (b) Truett, W. L.; Johnson, D. R.; Robinson, I. M.; Montague, B. A. *J. Am. Chem. Soc.* **1960**, *82*, 2337-2338.

(3) (a) Ruwwe, J.; Martín-Alvarez, J. M.; Horn, C. R.; Bauer, E. B.; Szafert, S.; Lis, T.; Hampel, F.; Cagle, P. C.; Gladysz, J. A. *Chem. Eur. J.* **2001**, *7*, 3931-3950.

(4) (a) de Quadras, L.; Bauer, E. B.; Mohr, W.; Bohling, J. C.; Peters, T. B.; Martín-Alva-rez, J. M.; Hampel, F.; Gladysz, J. A. *J. Am. Chem. Soc.* **2007**, *129*, 8296-8309. (b) de Quadras, L.; Bauer, E. B.; Stahl, J.; Zhuravlev, F.; Hampel, F.; Gladysz, J. A. *New. J. Chem.* **2007**, *31*, 1594-1604.

(5) (a) Shima, T.; Hampel, F.; Gladysz, J. A. *Angew. Chem., Int. Ed.* **2004**, *43*, 5537-5540; *Angew. Chem.* **2004**, *116*, 5653-5656. (b) Nawara, A. J.; Shima, T.; Hampel, F.; Gladysz, J. A. *J. Am. Chem. Soc.* **2006**, *128*, 4962-4963. (c) Wang, L.; Hampel, F.; Gladysz, J. A. *Angew. Chem., Int. Ed.* **2006**, *45*, 4372-4375; *Angew. Chem.* **2006**, *118*, 4479-4482. (d) Wang, L.; Shima, T.; Hampel, F.; Gladysz, J. A. *Chem. Commun.* **2006**, 4075-4077. (f) Hess, G. D.; Hampel, F.; Gladysz, J. A. *Organometallics* **2007**, *26*, 5129-5131. (e) Skopek, K.; Barbasiewicz, M.; Hampel, F. Gladysz, J. A. *Inorg. Chem.* **2008**, *47*, 3474-3476. (f) Stollenz, M.; Barbasiewicz, M.; Nawara-Hultzsch, A. J.; Fiedler, T.; Laddusaw, R.; Bhuvanesh, N.; Gladysz, J. A. *Angew. Chem., Int. Ed.* **2011**, *50*, 6647-6651; *Angew. Chem.* **2011**, *123*, 6777-6781.

(6) Toledano, C. A.; Parlier, A.; Rudler, H.; Daran, J. -C.; Jeannin, Y. *J. Chem. Soc., Chem. Commun.* **1984**, 576-578.

(7) (a) Yasuda, T.; Abe, J.; Iyoda, T.; Kawai, T. *Chem. Lett.* **2001**, 812-813. (b) Yasuda, T.; Abe, J.; Yoshida, H.; Iyoda, T.; Kawai, T. *Adv. Synth. Catal.* **2002**, *344*, 705-711.

(8) Buretea, M. A.; Tilley, T. D. *Organometallics* **1997**, *16*, 1507-1510.

(9) Heo, R. W.; Somoza, F. B.; Lee, T. R. *J. Am. Chem. Soc.* **1998**, *120*, 1621-1622.

(10) Shultz, G. V.; Zemke, J. M.; Tyler, D. R. *Macromolecules* **2009**, *42*, 7644-7649.

(11) Schalley, C. A. *Angew. Chem. Int. Ed.* **2002**, *41*, 1513-1515.

(12) Kottas, G. S.; Clarke, L. I.; Horinek, D.; Michl, J. *Chem. Rev.* **2005**, *105*, 1281-1376.

(13) Vögtle, F.; Mew, P. K. T. *Angew. Chem., Int. Ed. Engl.* **1978**, *17*, 60-62; *Angew. Chem.* **1978**, *90*, 58-60.

(14) Bedard, T. C.; Moore, J. S. *J. Am. Chem. Soc.* **1995**, *117*, 10662-10671.

(15) Fiedler, T. Syntheses of Gyroscope-like Osmium Complexes and Cage-like Diphosphines. Ph.D. Dissertation, Friedrich-Alexander-Universität Erlangen-Nürnberg, Erlangen, Germany, June 2011.

(16) Ng, P. L.; Lambert, J. N. *Synlett* **1999**, 1749-1750.

(17) (a) Reed, M. A.; Zhou, C.; Muller, C. J.; Burgin, T. P.; Tour, J. M. *Science* **1997**, *278*, 252-254. (b) Reichert, J.; Ochs, R.; Beckmann, D.; Weber, H. B.; Mayor, M.; Löhneysen, H. v. *Phys. Rev. Lett.* **2002**, *88*, 176804-1-176804-4. (c) Weber, H. B.; Reichert, J.; Weigend, F.; Ochs, R.; Beckmann, D.; Mayor, M.; Ahlrichs, R.; Löhneysen, H. v. *Chem. Phys.* **2002**, 113-125.

(18) (a) Dominguez, Z.; Khoung, T-A. V.; Dang, H.; Sanrame, C. N.; Nuñez, J. E.; Garcia-Garibay, M. A. *J. Am. Chem. Soc.* **2003**, *125*, 8827-8837. (b) Jarowski, P.

D.; Houk, K. N.; Garcia-Garibay, M. A. *J. Am. Chem. Soc.* **2007**, *129*, 3110-3117.

(19) Rachiero, G. P. Alkene Metathesis: Applications in the Synthesis of Novel Organometallic Complexes, and Mechanistic Investigations. Ph.D. Dissertation, Friedrich-Alexander-Universität Erlangen-Nürnberg, Erlangen, Germany, October 2008.

(20) Bondi, A. *J. Phys. Chem.* **1964**, *68*, 441-451.

(21) (a) Lockemeyer, J. R.; Rheingold, A. L.; Bulkowski, J. E. *Organometallics* **1993**, *12*, 256-258. (b) Dijkstra, H. P.; Chuchuryukin, A.; Suijkerbuijk, B. M. J. M.; van Klink, G. P. M.; Mills, A. M.; Spek, A. L.; van Koten, G. *Adv. Synth. Catal.* **2002**, *344*, 771-780.

(22) (a) Cattalini, L.; Guidi, F.; Tobe, M. *J. Chem. Soc., Dalton Trans.* **1993**, 233-236. (b) Chatt, J.; Shaw, B. L. *J. Chem. Soc.* **1959**, 705-716. (c) Chatt, J.; Shaw, B. L. *J. Chem. Soc.* **1959**, 4020-4033.

(23) Adams, C. J.; James, S. L.; Raithby, P. R. *Chem. Commun.* **1997**, 2155-2156.

(24) Capriati, V.; Florio, S.; Ingrosso, G.; Granito, C.; Troisi, L. *Eur. J. Org. Chem.* **2002**, 478-484.

(25) Westwell, A. D.; Williams, J. M. J. *Tetrahedron* **1997**, *53*, 13063-13078.

(26) (a) Rochon, F. D.; Beauchamp, A. L.; Bensimon, C. *Can. J. Chem.* **1996**, *74*, 2121-2130. (b) Tessier, C.; Rochon, F. D. *Inorg. Chim. Acta* **1999**, *295*, 25-38.

(27) Silverstein, R. M.; Bassler, G. C.; Morrill, T. *Sprectrometric Identification of Organic Compounds*, 5th ed.; John Wiley and Sons, New York, 1991, pp. 239-241.

(28) Siegel, J. S.; Anet, F. A. L. *J. Org. Chem.* **1988**, *53*, 2629-2630.

(29) Hartmann, C. E.; Nolan, S. P.; Cazin, C. S. J. *Organometallics*, **2009**, *28*, 2915-2919.

(30) Tamao, K.; Kodama, S.; Nakajima, I.; Kumada, M. *Tetrahedron* **1982**, *38*, 3347-3354.

(31) (a) Tagat, J. R.; McCombie, S. W.; Barton, B. E.; Jackson, J.; Shortail, J. *Bioorg. Med. Chem. Lett.* **1995**, 5, 2143-2146. (b) Jacquemard, U.; Routier, S.; Dias, N.; Lansiaux, A.; Goossens, J.; Bailly, C.; Mérour, J. *Eur. J. Med. Chem.* **2005**, *40*, 1087-1095.

(32) Krasovskiy, A.; Knochel, P. *Synthesis* **2006**, *5*, 890-891.

(33) *Dynamic NMR Spectroscopy,* Sandström, J. Academic Press, New York, 1982.

(34) Chuang, T. -H.; Chen, Y. -C.; Pola, S. *J. Org. Chem.* **2010**, *75*, 6625-6630.

(35) APEX2 "Program for Data Collection on Area Detectors" BRUKER AXS Inc., 5465 East Cheryl Parkway, Madison, WI 53711-5373 USA.

(36) SADABS, Sheldrick, G.M. "Program for Absorption Correction of Area Detector Frames", BRUKER AXS Inc., 5465 East Cheryl Parkway, Madison, WI 53711-5373 USA.

(37) Sheldrick, G.M. *Acta Cryst*. **2008**, *A64*, 112-122.

(38) Natta. G.; Mazzanti, G.; Corradini, P. *Att. Acad. Nazl. Lincei Rend. Classe Sci. Fis. Mat. Nat.* **1958**, *25*, 3-12.

(39) Shirikawa, H.; Louis, E. J.; MacDiarmid, A. G.; Chiang, C. K.; Heeger, A. J. *Chem. Commun.* **1977**, 578-580.

(40) (a) Burroughes, J. H.; Jones, C. A.; Friend, R. H. *Nature* **1988**, *335*, 137-141. (b) Marder, S. R.; Perry, J. W.; Klavetter, F. L.; Grubbs, R. H. *Chem. Mater.* **1989**, *1*, 171-173. (c) Garnier, F.; Horowitz, G. *Makromol. Chem. Macromol. Symp.* **1987**, *8*, 159-170. (d) Kanicki, J. In *Handbook on Conjugated Electrically*

Conducting Polymers, Skotheim, T. A. Ed.; Dekker, New York, 1986; pp 609-613. Vannikov, A. V.; Zhuravleva, T. S. *J. Mol. Electron.* **1989**, *5*, 63-70. (e) Shirakawa, H. *Angew. Chem., Int. Ed.* **2001**, *40*, 2574-2580. (f) MacDiarmid, A. G. *Angew. Chem., Int. Ed.* **2001**, *40*, 2581-2590. (g) Heeger, A. J. *Angew. Chem., Int. Ed.* **2001**, *40*, 2591-2611.

(41) Freund, M. S.; Deore, B. Intrinsically Conducting Polymers. In *Self–Doped Conducting Polymers*; John Wiley and Sons: West Sussex, 2007; pp 6-9.

(42) (a) Zeigler, J. M.; U.S. patent 760,433 (filed July 30, 1985); *Chem. Abstr.* **1986**, *20*, 157042. (b) Zeigler, J. M. *Polym. Prep.* **1984**, *25*, 223-224. (c) Okano, Y.; Masuda, T.; Higashimura, T. *J. Polym. Sci.: Polym. Chem. Ed.* **1984**, *22*, 1603-1610.

(43) Edwards, J. H.; Feast, W. J.; Bott, D. C.; *Polymer* **1984**, *25*, 395-398.

(44) Schrock, R. R.; Krouse, S. A.; Knoll, K.; Feldman, J.; Murdzek, J. S.; Yang, D. C. *J. Mol. Cat.* **1988**, *46*, 243-253.

(45) Gorman, C. B.; Ginsburg, E. J.; Sailor, M. J.; Moore, J. S.; Jozefiak, T. H.; Lewis, N. S.; Grubbs, R. H. *Synth. Met.* **1991**, *41*, 1033-1038.

(46) Muetterties, E. L.; Bleeke, J. R.; Wucherer, E. J.; Albright, T. A. *Chem. Rev.* **1982**, *82*, 499-525, and references therein.

(47) Bianchini, C.; Caulton, K. G.; Chardon, C.; Eisenstein, O.; Folting, K.; Johnson, T. J.; Meli, A.; Peruzzini, M.; Rauscher, D. J.; Streib, W. E.; Vizza, F. *J. Am. Chem. Soc.* **1991**, *113*, 5127-5129.

(48) Müller, J.; Gaede, P. E.; Qiao, K. *J. Organomet. Chem.* **1994**, *480*, 213-220.

(49) White, C.; Yates, A.; Maitlis, P. M. *Inorg. Syn.* **1992**, *29*, 228-234.

(50) Grundy, S. L.; Maitlis, P. M. *J. Organomet. Chem.* **1984**, *272*, 265-282.

(51) Min, J.; Benet-Buchholz, J.; Boese, R. *Chem. Commun.* **1998**, 2751-2752.

(52) Benet-Buchholz, J.; Haumann, T.; Boese, R. *Chem. Commun.* **1998**, 2003-2004.

(53) Huttner, G.; Lange, S. *Acta Cryst.* **1972**, *B28*, 2049-2060.

(54) Zelonka, R. A.; Baird, M. C. *Can. J. Chem.* **1972**, *50*, 3063-3072.

(55) Zelonka, R. A.; Baird, M. C. *J. Organomet. Chem.* **1972**, *44*, 383-389.

(56) Gill, T. P.; Mann, K. R. *Organometallics* **1982**, *1*, 485-488.

(57) Wu, Z.; Nguyen, S. T.; Grubbs, R. H.; Ziller, J. W. *J. Am. Chem. Soc.* **1995**, *117*, 5503-5511.

(58) Case Western Reserve University, Electronics Design Center online catalog. http://www.engineering.case.edu/edc/pdfs/Electrodes.pdf (accessed August 19, 2011).

(59) (a) Sheppard, N. F., Jr.; Tucker, R. C.; Wu, C. *Anal. Chem.* **1993**, *65*, 1199-1202. (b) Sakamoto, K.; Nishihara, H.; Aramaki, K. *J. Chem. Soc. Dalton Trans.* **1992**, 1877-1881. (c) Chidsey, C. E.; Feldman, B. J.; Lundgren, C.; Murray, R. W. *Anal. Chem.* **1986**, *58*, 601-607. (d) Sakamoto, K.; Aramaki, K.; Nishihara, H. *Chem. Lett.* **1993**, 659-662.

(60) Heinze, J.; Frontana-Uribe, B. A.; Ludwigs, S. *Chem. Rev.* **2010**, *110*, 4724-4771, and references therein.

(61) (a) Bertini, F.; Calucci, L.; Cicogna, F.; Gaddi, B.; Ingrosso, G.; Marcaccio, M.; Marchetti, F.; Paolucci, D.; Paolucci, F.; Pinzino, C. *J. Organomet. Chem.* **2006**, *691*, 2987-3002. (b) Cicogna, F.; Gaddi, B.; Ingrosso, G.; Marcaccio, M.; Marchetti, F.; Paolucci, D.; Paolucci, F.; Pinzino, C.; Viglione, R. *Inorg. Chim. Acta* **2004**, *357*, 2915-2932. (c) Kaim, W.; Berger, S.; Greulich, S.; Reinhardt, R.; Fiedler, J. *J. Organomet. Chem.* **1999**, *582*, 153-159.

(62) Bowyer, W. J.; Geiger, W. E. *J. Am. Chem. Soc.* **1985**, *107*, 5657-5663.

(63) Meerholz, K.; Gregorius, H.; Müllen, K.; Heinze, J. *Adv. Mater* **1994**, *6*, 671-674.

(64) Mas-Torrent, M.; Rovira, C. *Chem. Rev.* [Online early access]. DOI: 10.1021/cr100142w. Published online March 18, 2011. http://pubs.acs.org/doi/pdf/10.1021/cr100142w (accessed July 8, 2011).

(65) Wallock, N. J.; Donaldson, W. A. *J. Org. Chem.* **2004**, *69*, 2997-3007.

(66) Bianchini, C.; Caulton, K. G.; Johnson, T. J.; Meli, A.; Peruzzini, M.; Vizza, F. *Organometallics* **1995**, *14*, 933-943.

(67) Ohsawa, S.; Sakurai, S.; Nagai, K.; Banno, M.; Maeda, K.; Kumaki, J.; Yashima, E. *J. Am. Chem. Soc.* **2011**, *133*, 108-114.

(68) Akagi, K. *Chem. Rev.* **2009**, *109*, 5354-5401.

(69) Trnka, T. M.; Morgan, J. P.; Sanford, M. S.; Wilhelm, T. E.; Scholl, M.; Choi, T. -L.; Ding, S.; Day, M. W.; Grubbs, R. H. *J. Am. Chem. Soc.* **2003**, *125*, 2546-2558.

(70) Sanford, M. S.; Love, J. A.; Grubbs, R. H. *Organometallics* **2001**, *20*, 5314-5318.

(71) Handy, L. B.; Sharp, K. G.; Brinckman, F. F. *Inorg. Chem.* **1972**, *11*, 523-531.

(72) Schrock, R. R.; Clark, D. N.; Sancho, J.; Wengrovius, J. H.; Rocklage, S. M.; Pedersen, S. F. *Organometallics* **1982**, *1*, 1645-1651.

(73) Chao, Y. -W.; Wexler, P. A.; Wigley, D. E. *Inorg. Chem.* **1989**, *28*, 3860-3868.

(74) Schrock, R. R.; DePue, R. T.; Feldman, J.; Schaverien, C. J.; Dewan, J. C.; Liu, A. H. *J. Am. Chem. Soc.* **1988**, *110*, 1423-1435.

(75) (a) Grimsdale, A. C.; Chan, K. L.; Martin, R. E.; Jokisz, P. G.; Holmes, A. B. *Chem. Rev.* **2009**, *109*, 897-1091. (b) Facchetti, A. *Chem. Mater.* **2011**, *23*, 733-758. (c) Cheng, Y.-J.; Yang, S.-H.; Hsu, C.-S. *Chem. Rev.* **2009**, *109*, 5868-5923.

(76) Burroughes, J. H.; Bradley, D. D. C.; Brown, A. R.; Marks, R. N.; Mackay, K.; Friend, R. H.; Burns, P. L.; Holmes, A. B. *Nature* **1990**, *347*, 539-541.

(77) Clery, D. *Science* **1994**, *263*, 1700-1702.

(78) McDonald, R. N.; Campbell, T. W. *J. Am. Chem. Soc.* **1960**, *82*, 4669-4671.

(79) Fox, H. H.; Schrock, R. R.; O'Dell, R. *Organometallics* **1994**, *13*, 635-639.

(80) Thorn-Csányi, E.; Pflug, K. P. *J. Mol. Cat.* **1994**, *90*, 69-74.

(81) (a) Wessling, R. A.; Zimmerman, R. G. U.S. patent 3,401,152 (filed Nov. 3, 1966); *Chem. Abstr.* **1968**, *69*, 87735. (b) Wessling, R. A.; Zimmerman, R. G. U.S. patent 3,532,643 (filed Feb. 23, 1967); *Chem. Abstr.* **1971**, *74*, 3994.

(82) (a) Wudl, F.; Srdanov, G. U.S. patent 5,189,136 (filed Dec. 12, 1990); *Chem. Abstr.* **1993**, *118*, 255575. (b) Voss, K. F.; Foster, C. M.; Smilowitz, L.; Mihailović, D.; Askari, S.; Srdanov, G.; Ni, Z.; Shi, S.; Heeger, A. J.; Wudl, F. *Phys. Rev. B* **1991**, *43*, 5109-5118.

(83) Yaniger, S. I.; Rose, D. J.; McKenna, W. P.; Eyring, E. M. *Macromolecules* **1984**, *17*, 2579-2583.

(84) Nishihara, H.; Funaki, H.; Shimura, T.; Aramaki, K. *Synth. Met.* **1993**, *55-57*, 942-947.

(85) Funaki, H.; Aramaki, K.; Nishihara, H. *Synth. Met.* **1995**, *74*, 59-64.

(86) Koelle, U.; Kossakowski, J. *Inorg. Syn.* **1992**, *29*, 225-228.

(87) Fagan, P. J.; Ward, M. D.; Calabrese, J. C. *J. Am. Chem. Soc.* **1989**, *111*, 1698-1719.

(88) Lü, X.; He, Y.; Lü, C. *Polym. Sci., Ser. A* **2011**, *53*, 403-408.

(89) The use of interdigitated electrodes has been described in chapter III, as well as in references 58 and 59.

(90) (a) White, C.; Maitlis, P. M. *J. Chem. Soc. A* **1971**, 3322-3326. (b) Koelle, U.; Kossakowski, J. *J. Organomet. Chem.* **1989**, *362*, 383-398.

(91) Li, C.; Liu, M.; Pschirer, N. G.; Baumgarten, M.; Müllen, K. *Chem. Rev.* **2010**, *110*, 6817-6855.

(92) The most intense peak of the isotope envelope is given; *m/z* (relative intensity, %).

VITA

Paul David Zeits

Texas A&M university
Department of Chemistry
P.O. Box 30012
College Station, TX 77842-30127

paul.zeits@gmail.com

B.S.; Chemistry, Michigan State University, East Lansing, MI, 2005

Ph.D.; Chemistry, Texas A&M University, College Station, TX, 2011